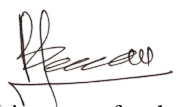




FACULTY OF SCIENCE AND TECHNOLOGY

MASTER'S THESIS

Study programme/specialisation: Marine and Offshore Technology	Spring semester, 2019 Open
Author: Pulkit Dewan	 (signature of author)
Programme coordinator: Prof. Muk Chen Ong Supervisor(s): Prof. Muk Chen Ong Dr. Lin Li Dr. Karl Gunnar Aarsæther	
Title of master's thesis: Dynamic analysis of flexible gravity-based fish cages under accidental failures in the mooring system	
Credits (ECTS): 30	
Keywords: <ul style="list-style-type: none">– Accidental failure– Conventional frame-mooring– Dynamic response– Gravity-based fish cage– Marine aquaculture– Numerical analysis– Waves and currents	Number of pages: 93 + supplemental material/other: 0 Stavanger, June 15. 2019

Dynamic analysis of flexible gravity-based fish cages under accidental failures in the mooring system

Pulkit Dewan

MASTER'S THESIS

Spring 2019

Department of Mechanical and Structural Engineering and
Materials Science

University of Stavanger

Supervisor: Prof. Muk Chen Ong

Co-supervisors: Dr. Lin Li (University of Stavanger)

Dr. Karl Gunnar Aarsæther (SINTEF Ocean AS)

Abstract

A growing population needs an increasing amount of high-protein and nutritious food. Having acknowledged that, there is a substantial increase in seafood production in the world today. Due to spatial and environmental concerns, the marine aquaculture is moving further towards more exposed seas, motivating a lot of research in this field. An accidental failure of a critically loaded cable in the mooring frame would contribute to additional loads in one of the mooring lines which might affect the overall structural integrity of the fish farm.

In this thesis, a conventional gravity-based fish cage is analysed using a numerical tool called FhSim, which is an in-house software developed by SINTEF Ocean AS. The focus is on the effect of accidental failures on the mooring line loads, which represent the global loads acting on the system. These structures are built for farming the fish. Therefore, its welfare should be the primary concern. Thus, this thesis also focuses on the extent of volume reduction in the net structures caused due to deformations under severe environmental loading. The sensitivity of the mooring loads and net deformations of the cages to the environmental parameters and net solidities is also presented in this thesis.

Two different models of the fish cages are numerically analysed. Firstly, a preliminary study is performed to understand the response of a single cage configuration exposed to the environmental loads. The same net structure is then used to develop the second model with multiple cages in a 1x3 configuration, representing a fully functional fish farm. The response of this model is studied in detail under different currents and waves approaching from different directions. For both of these models, the critically loaded mooring lines and cables are identified. The loading condition is defined corresponding to an accidental failure in a particular cable.

It is found that the failure in the critical frame cables and bridles does not significantly affect the mooring line loads for the model with a single cage. The loads are instead transferred onto the neighbouring cables which may trigger the rupture of other cables if not designed to withstand these additional loads. This could start a chain of failures in these cables which would eventually lead to adverse consequences. For the second model, the accidental failure in one of the critically loaded frame cables leads to a momentous increase in the mooring line loads. Therefore, the design and dimensioning of the critical mooring line will depend on this frame cable of the first fish cage in the direction of the currents.

Acknowledgements

I am very thankful to my supervisor, Prof. Muk Chen Ong for his continuous guidance and consultation throughout this semester.

I would like to express my gratitude to my co-supervisor, Dr. Lin Li, for all the valuable discussions and her unparalleled mentoring all these months. I extend my vote of thanks to Dr. Karl Gunnar Aarsæther from SINTEF Ocean AS for granting access to their in-house software FhSim for my work. His introductory sessions to the software were of great help. I am indebted to his technical support to all my queries and feedback, in general. Both of my co-supervisors have invested a great amount of their time in this thesis.

A special mention for Ph.D. candidate Hui Cheng for his efforts and swift responses whenever I sought help with the numerical tool.

Finally, I want to thank my family and friends for their belief and unlimited support that has kept me going with confidence through these stressful times.

Contents

Abstract	i
Acknowledgement	ii
List of Figures	vi
List of Tables	x
1 Introduction	1
1.1 Background and motivation	1
1.1.1 Background of Norwegian aquaculture industry	1
1.1.2 Motivation behind the thesis	2
1.2 An overview of a sea-based fish farm	3
1.2.1 Cage system	4
1.2.2 Feeding system	7
1.3 Scope and structure of the thesis	8
2 Theory	10
2.1 Literature review	10
2.2 Forces on a submerged cylinder	11
2.2.1 Morison equation	12
2.2.2 Wake effect	14
2.3 Hydrodynamics of a fish cage	15
2.3.1 Forces acting on a floating collar	16
2.3.2 Forces acting on a net structure	16
2.4 Parameters affecting cage hydrodynamics	18
2.4.1 Solidity ratio	18
2.4.2 Reynolds number	19
2.4.3 Angle of attack	20
2.5 Linear wave theory	21
2.5.1 Potential function	22
2.5.2 Dispersion relation	23
3 Numerical Analysis	25

3.1	Overview of a gravity-based fish cage	25
3.1.1	Floating collar	25
3.1.2	Net structure	26
3.1.3	Sinker tube	27
3.1.4	Buoy system	27
3.1.5	Mooring system	28
3.2	Introduction of the numerical tool	29
3.2.1	A general overview of FhSim architecture	29
3.2.2	Fish cage model realization in FhSim	30
3.3	Numerical models implemented in FhSim	31
3.3.1	Structural model of the floating collar	32
3.3.2	Response calculation of the floating collar	33
3.3.3	Structural model of the net structure	34
3.3.4	Hydrodynamic model of the net structure	35
3.3.5	Mooring system	35
3.4	Model parameters	36
3.4.1	Time-domain analysis	37
3.4.2	Method of calculating volume of the net structure	38
4	Analysis of a single-cage system	40
4.1	Model set-up	40
4.2	Simulation set-up	41
4.2.1	Loading conditions	41
4.2.2	Environmental loading	43
4.3	Results and discussions	44
4.3.1	Responses of a single-cage model under intact condition	44
4.3.2	Responses of a single-cage model under different loading conditions	52
5	Analysis of a multiple-cage system	58
5.1	Model set-up	58
5.2	Simulation set-up	59
5.2.1	Loading conditions	59
5.2.2	Environmental loading	63
5.3	Results and discussions	63
5.3.1	Responses of a multiple-cage model under intact condition	64

5.3.2	Responses of a multiple-cage model under different loading conditions	73
5.3.3	Sensitivity study on net solidities	78
6	Conclusions and future work	87
6.1	Conclusions	87
6.2	Future work	88
	References	93

List of Figures

1.1	Comparison of world capture fisheries and aquaculture production (Source: Food and Agriculture Organization)	1
1.2	A typical marine aquaculture site (Source: AKVA Group)	3
1.3	Different types of floating fish cages	4
1.4	Sinking operation of a submersible fish cage (Source: Badinotti Group) . . .	5
1.5	Different types of submersible fish cages	6
1.6	New concepts of fish cage systems in Norway	7
1.7	A typical feeding system in a fish farm (Source: AKVA Group)	7
2.1	Lift and drag forces on a submerged slender cylinder	13
2.2	Boundary layer separation over a cylinder leading to generation of wake effect (Source: Aerospace Engineering Blog)	15
2.3	Different approaches used for hydrodynamic force calculation for net structures	17
2.4	Parameters affecting solidity ratio of the net structure of a fish cage	18
2.5	Drag coefficient of a smooth sphere and cylinder (Source: H.Schlichting's "Boundary Layer Theory")	20
2.6	Sinusoidal wave profile	21
3.1	Schematic overview of a conventional flexible gravity-based fish cage (Reproduced from Grue [1])	25
3.2	Double-pipe floating collar of a gravity-based fish cage (Source: Aqualine AS)	26
3.3	Net structure and sinker tube of a gravity-based fish cage	27
3.4	Buoy system of a fully functional fish farm	28
3.5	Mooring system of a fully functional fish farm (Source: AKVA Group)	28
3.6	Flow-chart showing architecture of FhSim (Source: SINTEF Ocean AS) . . .	29
3.7	Visualization of a gravity-based fish cage model realised in FhVis	30
3.8	Transfer of variables across interconnected SimObjects during numerical analysis in FhSim (Source: SINTEF Ocean AS)	31
3.9	Single torus model representing the floating collar (Reproduced from Endresen [2])	32
3.10	Priour's triangular element for numerical modelling of net structures	34
4.1	Plan view of the single-case system with a single fish cell as realized in FhVis	40
4.2	Response of the single-case system when the currents are flowing 0° to the model	42

4.3	Time-series response of the single-cage system when the currents are flowing with a 0° heading	44
4.4	Time-series of the tension forces in the critical cables of the single-cage system when the currents are flowing with a 0° heading	45
4.5	Effect of regular waves on the volume-remaining coefficient of the net of the single-cage model subjected to 600 seconds of prior loading under pure currents	47
4.6	Effect of regular waves on the tension force in the mooring line 3 of the single-cage model subjected to 600 seconds of prior current loading	48
4.7	Effect of regular waves on the tension force in the frame cable FC2 of the single-cage model subjected to 600 seconds of prior current loading	49
4.8	Effect of regular waves on the tension force in the bridle B4 of the single-cage model subjected to 600 seconds of prior current loading	49
4.9	Effect of regular wave on the tension force in the bridle B5 of the single-cage model subjected to 600 seconds of prior current loading	50
4.10	Effect of regular waves on the tension force in the bridle B6 of the single cage model subjected to 600 seconds of prior current loading	51
4.11	Effect of accidental failures in cables defined by the loading conditions on the responses of the single-cage model (pure current condition)	52
4.12	Effect of accidental failures in cables defined by the loading conditions on the mean tension forces in the critical cables of the single-cage model (pure current condition)	54
4.13	Effect of accidental failures in cables defined by the loading conditions on the responses of the single-cage model (combined wave-current condition)	55
4.14	Effect of accidental failures in cables defined by the loading conditions on the mean tension forces in the critical cables of the single-cage model (combined wave-current condition)	57
5.1	Plan view of the multiple-cage system in a 1x3 cell configuration as realised in FhVis	58
5.2	Time series of the volume-remaining coefficient of the net structure of cell 1 of the multiple- cage system under pure currents condition	60
5.3	Mean tension forces in mooring lines of the multiple-cage system ($U=0.40$ m/s)	61
5.4	Mean tension forces in frame cables of the multiple-cage system ($U=0.40$ m/s)	62
5.5	Time-series response of the multiple-cage system when the currents are flowing with a 0° heading	64

5.6	Time-series response of the multiple-cage system when the currents are flowing with a 90° heading	65
5.7	Geometry of the multiple-cage model at different time intervals when the current is flowing with a 0° heading (U=0.40 m/s)	66
5.8	Geometry of the multiple-cage model at different time intervals when the current is flowing with a 90° heading (U=0.40 m/s)	67
5.9	Effect of regular waves on the response of the multiple-cage model subjected to 600 seconds of prior current loading (0° current-wave heading)	68
5.10	Effect of regular waves on the response of the multiple-cage model subjected to 600 seconds of prior current loading (90° current-wave heading)	69
5.11	Effect of regular waves on the steady state geometry of the multiple-cage model for 0° current heading (Case C0.40H2WL50)	70
5.12	Effect of regular waves on the steady state geometry of the multiple-cage model for 90° current heading (Case C0.40H2WL50)	71
5.13	Effect of accidental failures in cables defined by the loading conditions on the volume- remaining coefficient of the net structure of cell 1 under pure currents condition	74
5.14	Effect of accidental failures in cables defined by the loading conditions on the critical mooring lines of the multiple-cage model under pure currents condition	74
5.15	Effect of loading conditions on volume-remaining coefficients of the net structure of cell 1 under combined wave-current condition	76
5.16	Effect of accidental failures in cables defined by the loading conditions on the critical mooring lines of the multiple-cage model under combined wave-current condition	77
5.17	Effect of net solidities on the volume-remaining coefficient of the net structure of cell 1 of the multiple-cage model under pure currents condition (0° heading)	79
5.18	Effect of net solidities on the volume-remaining coefficient of the net structure of cell 1 of the multiple-cage model under pure currents condition (90° heading)	80
5.19	Effect of net solidities on the mean tension forces in mooring line 1 of the multiple-cage model under pure currents condition (0° heading)	81
5.20	Effect of net solidities on the mean tension forces in mooring line 3 of the multiple-cage model under pure currents condition (90° heading)	82

5.21	Effect of loading conditions on the volume-remaining coefficient of the net structure of cell 1 with different solidities under combined wave-current condition (0° heading)	83
5.22	Effect of loading conditions on the volume-remaining coefficient of the net structure of cell 1 with different solidities under combined wave-current condition (90° heading)	84
5.23	Effect of loading conditions on the mean tension forces in mooring line 1 of the multiple-cage system under combined wave-current condition (0° heading)	85
5.24	Effect of loading conditions on the mean tension forces in mooring line 3 of the multiple-cage system under combined wave-current condition (90° heading)	86

List of Tables

3.1	Specifications of a typical Norwegian fish cage used for developing the numerical models	36
3.2	Parameters for time-domain numerical analysis in FhSim	37
4.1	Environmental parameters for the single-cage model under pure currents condition	41
4.2	Loading conditions for the single-cage model	43
4.3	Environmental parameters for the single-cage model under combined wave-current condition	44
4.4	Mean values of volume-remaining coefficient and tension forces for net and critical cables respectively of the intact model of single-cage system subjected to different environmental loads	51
5.1	Environmental parameters for the multiple-cage model under pure currents condition	59
5.2	Loading conditions for the multiple-cage model	62
5.3	Environmental parameters for the multiple-cage model under pure currents condition	63
5.4	Mean values of volume-remaining coefficient of the net structure of cell 1, and tension forces in the mooring line 1 and critical cables of multiple-cage system subjected to different environmental loads (0° heading)	72
5.5	Mean values of volume-remaining coefficient of the net structure of cell 1, and tension forces in the mooring line 3 and critical cables of multiple-cage system subjected to different environmental loads (90° heading)	73
5.6	Environmental parameters for the sensitivity study on net solidity of the multiple-cage system under combined wave-current condition	78

1 Introduction

In this chapter, a brief background of aquaculture in Norway is presented followed by the motivation behind the research. A general overview of a sea-based fish farm is given. The scope and structure of this thesis have been outlined.

1.1 Background and motivation

1.1.1 Background of Norwegian aquaculture industry

According to DNV GL's Energy Transition Outlook 2018, there will be about 9.2 billion people on Earth in 2050, some 1.5 billion more than today [3]. It is obvious that there shall be a requirement for more food to feed such a growing population. The key challenge, however, would be the production of the food that serves this need without affecting the environment. Studies reflect that seafood production is more sustainable than meat production [4]. Salmon has a climate footprint of 2.5 Kg CO₂ per kilogram of production, which is 50% of pork and 8% of beef. Norwegian salmon production is monthly cultivated under controlled conditions, a practice known as "Aquaculture".

Figure 1.1 shows the comparison of capture fisheries and aquaculture production in the world as of 2016. With the former being relatively stable since 2000, aquaculture production showed continuing and impressive growth in the seafood supply for human consumption [5].

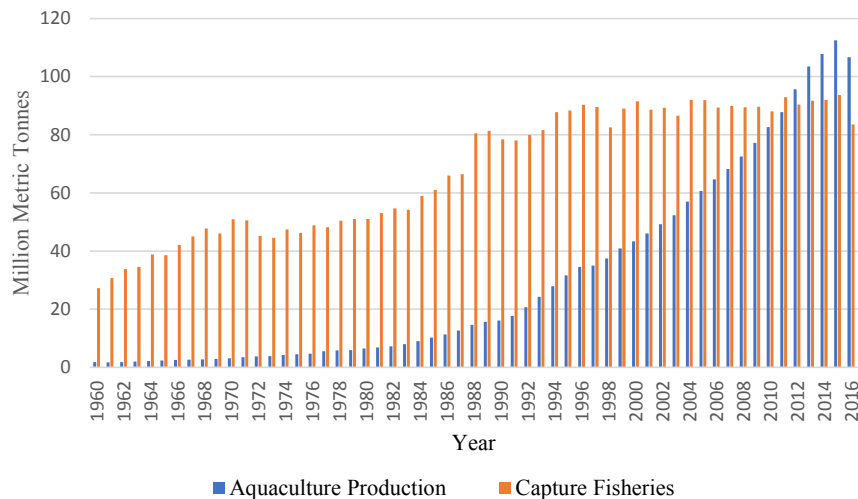


Figure 1.1: Comparison of world capture fisheries and aquaculture production (Source: Food and Agriculture Organization)

Fish farming is a huge and fast-growing industry in Norway and is also expanding rapidly worldwide. Norway alone contributes more than 50% of the global salmon production and is expected to maintain this leading market position in the years to come [6]. Marine fish farming had some major technological advances in recent years and has become an emerging alternative to the conventional inland fresh water fish farming and hatcheries. In aquaculture, the rearing environment is the natural environment of the fish. There are interactions between cages and the environment in both the directions – cages affect the environment, and vice-versa.

Choosing a site in any fish farming operation is crucial because of the exposure to the number of waves and currents. An offshore location will mean higher investments for cages and mooring system, higher cost of maintenance and greater risks, resulting in greater production cost. On the other hand, an exposed site will have better water exchange resulting in a lower environmental impact, better fish welfare and a better product quality [7].

As per statistics for 2018 from Norwegian Directorate of Fisheries, there are a total of 1207 aquaculture sites in sea water out of which 84% are for Atlantic salmon and rainbow trout. The remaining are for other fish species and molluscs, crustaceans and echinoderms [8]. With an increasing number of activities every year, there is a requirement for stricter standards and rules to be adhered to while practising marine aquaculture.

Regulations for certification and inspection of fish farms point to technical standards like NS 9415 for specific technical requirements. The Norwegian standard NS9415 released in 2003 and revised in 2009 as NYTEK, defines the technical requirements for site survey, risk analysis, dimensioning, design, construction, installation and operations of floating fish farms [9]. DNV GL rule DNV-GL-RU- OU-0503 was introduced in 2017 to provide aid for designs of fish farming units and installations in more exposed sites with swell seas that might not be sufficiently covered by the NS9415:2009 in terms of responses in such a harsh environment. Normally, the DNV GL rule does not cover fish farming units with floating collars typically made up of polymers, net pens and associated equipment, and fish escapes [10].

1.1.2 Motivation behind the thesis

There are several challenges faced by the conventional frame moored gravity-based flexible fish cages today. There exists risk of fish escapes and physical damages due to wave and current loads. Studies indicate that the stress responses in fishes are quite similar to other vertebrates [11] and farmed fish may be exposed to stress during the production cycle

in the sea. Monitoring fish welfare has recently gained a lot of focus in the aquaculture industry. Another major concern in a fish farming unit is maintaining its overall structural integrity. Wave loads increase global loads which eventually get transferred to mooring system. Furthermore, additional loads from accidental failures of critically loaded cables in the mooring frame and bridles can concentrate larger loads in parts of the mooring lines.

A lot of research and analysis have been carried out in the past to overcome these problems and there is still a lot of ongoing research and development. The aforementioned challenges are the primary source of motivation in investing efforts for further study of the responses of flexible gravity-based fish cages under accidental failures. The author of this thesis acknowledges the importance of this industry and keeps a keen interest to gain valuable knowledge in this area.

1.2 An overview of a sea-based fish farm

Two major systems that complete an offshore fish farm are the cage system and the feeding system. A lot of advances has been achieved in the design of the cage systems in the past and there are still ongoing researches on new types of cage systems.

A typical fish farming unit is illustrated in figure 1.2 below. It consists of about six to ten cages moored in a suitable configuration connected to a feeding barge via feeding pipes. A 50 metre wide and 30 metre deep cage can hold upto 200,000 Salmon with a maximum stocking density of $25\text{Kg}/\text{m}^3$.



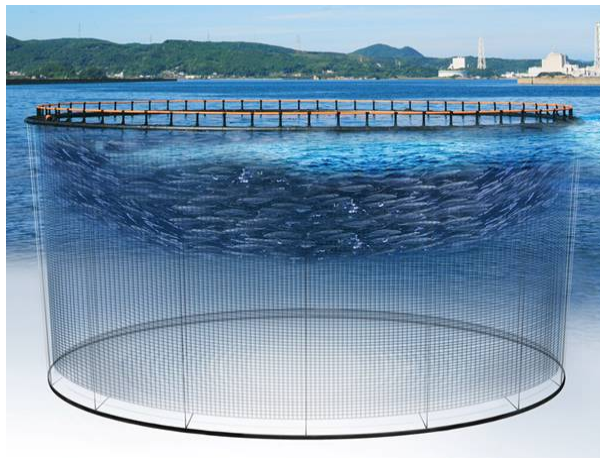
Figure 1.2: A typical marine aquaculture site (Source: AKVA Group)

1.2.1 Cage system

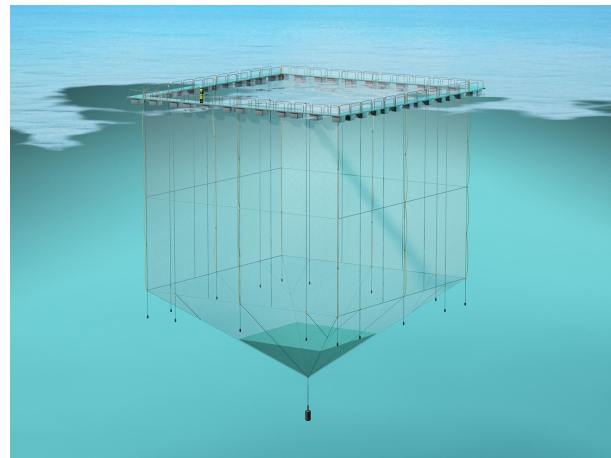
The cage system is an essential part of a fish farm as it serves as the backbone of the farm and contributes to the entire durability of the system. It is designed so that it can withstand both static and dynamic loading. The forces affecting the net structure and its corresponding motions are transferred to the mooring frame and eventually to the mooring lines. The cage system can be further classified on the basis of its operation and configurations as presented below.

- **Floating cage system:**

These cage systems are designed to stay afloat with the floating collar partially submerged in water. The most conventional example is a flexible gravity-based fish cage. It is cylindrical in shape with usually two or three collars made of extruded high density polyethylene (HDPE) pipes as shown in figure 1.3a. They mainly rely on the gravitational force due to the attached weight system and the buoyancy of the floating collar to maintain a certain volume. The net is tensioned with either ropes or chains connected to a ring at the bottom of the cylindrical part called a “Sinker tube”. These cages are very advantageous due to high flexibility and bear a reduced risk of failure due to fatigue. Today, several manufactures also supply custom-made square or rectangular net solutions for steel-based installations as shown in figure 1.3b.



(a) Conventional circular flexible gravity-based fish cage (Source: Badinotti Group)



(b) Square nets for steel-based pen installations (Source: Egersund Net)

Figure 1.3: Different types of floating fish cages

- Submersible cage system:

These cage systems are designed to stay submerged below the water surface for a certain period and thus, incur far less exposure to the strong waves at the surface during harsh sea conditions. This feature adds safety and simplicity in design, however, the potential risk and complexity cannot be neglected as they operate in two modes, surface and sub-surface. This operation is illustrated in figure 1.4. These cages are known to be relatively cost effective as the design combines the features of conventional operation with storm protection. The feeding must be done subsurface due to the limited access on the surface [12].

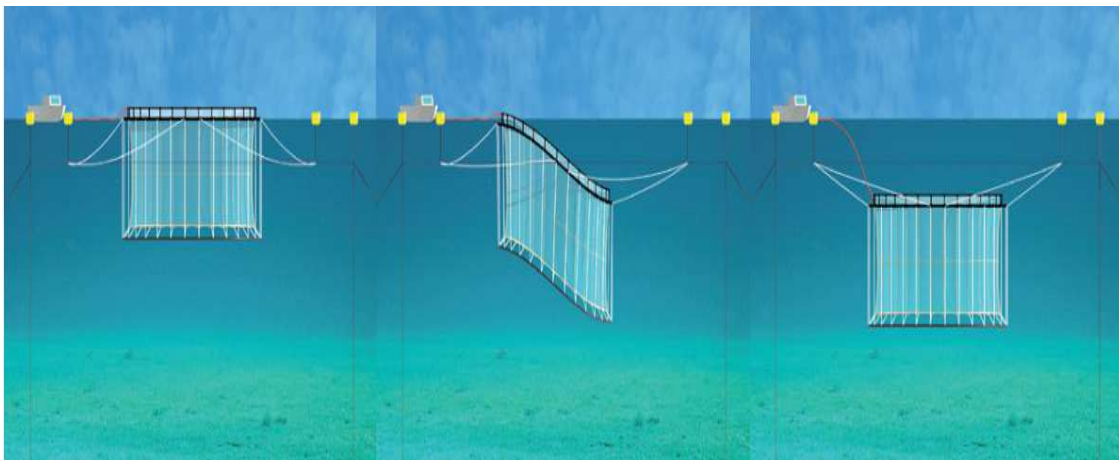
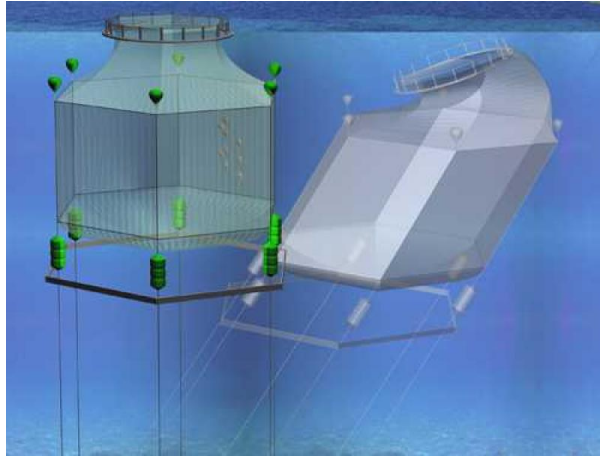


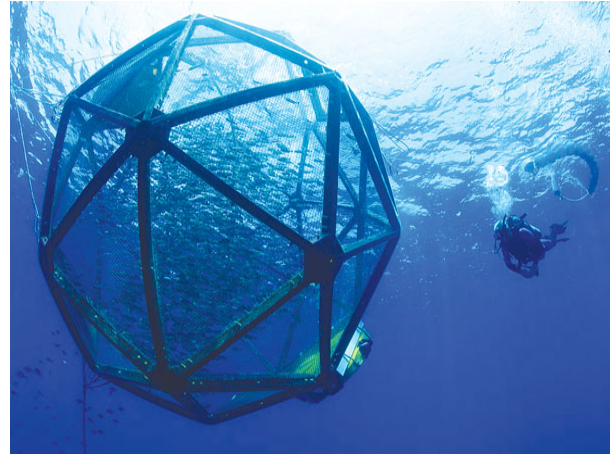
Figure 1.4: Sinking operation of a submersible fish cage (Source: Badinotti Group)

Some other concepts of submersible cages id the Tension Leg Cage (TLC) and a spherical underwater habitat termed as “Aquapod” as shown in figure 1.5. These designs are based on the dynamics of wave energy dispersion in the ocean. At a water depth equivalent to half of the wavelength of a regular wave, the wave particle velocity reduces to about 4% of its highest value at the water surface. When submerged at such water depths, they can avoid the intense wave loading to a great extent. These cages move in synergy with the waves and currents instead of opposing these environmental forces. This allows the fishes to move around as they would generally behave in the wild.

Each TLC is an independent free-floating unit that is tension moored to minimize any heave motions in the unit. The aquapods can be single point moored and are able to change locations in line with the current direction.



(a) A tension leg cage submerging under environmental loads(Source: REFAMED)



(b) An aquapod drifting in deep ocean currents (Source: The Valella Mariculture Project)

Figure 1.5: Different types of submersible fish cages

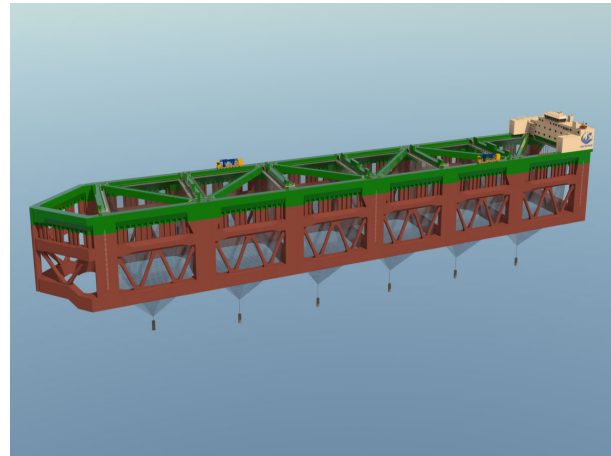
The floating cages has several advantages over the submersible cages. These are inexpensive compared to submersible cages but experience large deformations in high sea states. They are advantageous for farming salmon and trout because these fish species need access to water surface to replenish swim bladder. While the submersible cages complicate the traditional frame moored fish farm consisting of several cages, they can avoid intense wave loads during harsh weather conditions.

- **Some new concepts:** In recent past, the Norwegian government proposed development concessions and licenses for grant to the promising concepts of fish cage systems. This led to a high rate of investment and innovation of several concepts.

Figure 1.6 below shows two of these approved concepts. Hauge Aqua's concept called "The Egg" is an egg-shaped closed-containment fish cage. It is a large and designed as semi-flexible tank as shown in figure 1.6a constructed from composite materials which gives a great impact strength to the structure [13]. Nordlaks AS' concept called "Havfarm" is a vessel-shaped fish farm with several hanging net pens as seen in figure 1.6b. The vessel is single point moored and is designed to reduce environmental loading by station keeping [14].



(a) Egg-shaped fish cage concept (Source: Hauge Aqua)



(b) Vessel-shaped fish farm concept (Source: Nordlaks AS)

Figure 1.6: New concepts of fish cage systems in Norway

1.2.2 Feeding system

Initially, there might be some natural feed in the fish cage but to maximise the fish production, a well-balanced feed needs to be supplied at regular time intervals. Therefore, the feeding system is also considered a vital part of a fish farm. A feeding system is comprised of several reliable components that help to transport the feed stored in the feeding barges to the fish cages via feeding tubes as illustrated in figure 1.7.



Figure 1.7: A typical feeding system in a fish farm (Source: AKVA Group)

Most advanced feed systems today are fully automated and integrated with several controls

allowing 24x7 monitoring of the fish cages. The feeding is achieved with the help of a control system operated by skilled and trained personnel. The blower located in the upstream circuit of the feed storage generates the required amount of air pressure to transport the feed in the form of pellets.

The transport air is compressed from ambient pressure and the required pressure depends on the feeding tube length and feeding regime. Compressed air generates heat and requires to be cooled down to a certain temperature before it reaches the dosers. The feed dosers are supplying the pellets into the incoming air flow. Next in line is the selector valve which is the connection point for several HDPE feeding tubes. The feed will finally flow through the main pipe in the distribution chamber into the feeding tubes connected to the respective fish cages.

1.3 Scope and structure of the thesis

Gravity-based fish cages are dominant today in aquaculture industry worldwide. This thesis focuses on the effect of accidental failures in the mooring frame on the response of a conventional flexible gravity-based fish cage. Two models developed using the same net structures are considered for numerical analysis in FhSim, a numerical tool developed by SINTEF Ocean AS. The accidental failures in the cables are defined by the different loading conditions. The models are subjected to different environmental loading - pure currents condition and a combined wave-current condition. For these loading and environmental conditions, the net deformations and mean tension force in the mooring lines are investigated.

Chapter 2 entitled “Theory” presents the literature review on the studies conducted on gravity-based fish cages. The different loads acting on a fish cage and the basic theories behind the hydrodynamic force computations are presented. It includes brief excerpts on the different models used in numerical analysis of the cages and further details out the relevant parameters defining these net structures.

Chapter 3 entitled “Numerical analysis” begins with an overview of a flexible gravity-based cage net and its interaction with other components in a fish farm. It outlines the framework of the FhSim software used for the simulations in this thesis. The realization of a fish cage in this numerical tool is presented along with the implementation of the models for the different components. The parametric description of a typical Norwegian fish cage used in this thesis is given.

Chapter 4 entitled “Analysis of a single-cage system” presents the set-up for a preliminary study of a model with a single cell cage. The loading conditions are defined based on the critical cables in the model. This is followed by formulation of the simulation matrix defining the environmental parameters for each case. Several results are presented and discussed throughout this chapter.

Chapter 5 entitled “Analysis of a multiple-cage system” presents the set-up of a model with multiple fish cells in a 1x3 configuration representing a fully functional fish farm. On the outline of the previous chapter, this chapter also includes formulation of the simulation matrices for different loading and environmental conditions. The net deformations and the mean tension force in the critically loaded mooring line are discussed in this chapter. The sensitivity studies on three different net solidities are also investigated for this model.

Final chapter, 6 entitled “Conclusions and future work” presents a summary of the discussions and findings from the two models. The probable sources of error encountered in the numerical analysis of the two models are construed. The limitations of the thesis and the possible scope of future work are stated.

2 Theory

In this chapter, the basic theories related to the hydrodynamics of the fish cage are presented. This is followed by a detailed description of the models implemented in the numerical tool for the different cage components.

2.1 Literature review

In the past decades, many researches have focused on both the experimental work and numerical studies on marine aquaculture in order to have a better understanding of the hydrodynamic responses of fish cages exposed to currents and waves.

Estimation of drag forces and cage deformations using the Morison equation requires selection of a reasonable drag coefficient. In 2010, Decew et al. [15] investigated the dynamics of a single-point moored submersible fish cage under currents and proposed analytical formulas to describe the drag coefficient as a function of Reynolds Number. This approximation over predicts the loads at high current velocities but shows good results for lower velocities and thus, is widely implemented in several numerical tools today.

Back in 1990, Aarsnes et al. [16] worked on the calculation of drag and lift forces over net panels. The study included calculation of current forces and deformations in nets based on their geometry and angle of attack of flow with respect to the net panel. They performed sensitivity studies with different solidity ratios and derived a formula for reduced velocity downstream of the net. Three years later in 1993, Løland [17] presented an empirical formulation for reduced velocity experienced by subsequent cages to the first cage in the direction of the current in multiple-cage configurations. This effect is referred to as “shielding effect”.

The advancement in numerical modelling techniques started with Priour’s [18] introduction of triangular element for the modelling of the net. The hypothesis of constant twine orientation in each triangular element showed quite good results on comparison with a model with twines described as elastic bars. Later in 2003, Tsukrov et al. [19] proposed a consistent finite element over simple truss element to model the hydrodynamic response of net panels to environmental loading. Lee et al presented a model for modelling the net where it was assumed to be a network of masses and springs. This mass-spring model offered quite low computational times with stable solutions.

Later in 2012, Kristiansen and Faltinsen [20] proposed a screen model for the calculation of viscous hydrodynamic loads on nets. The net structure was assumed to be divided into number of flat panels called “screens”. They documented satisfactory agreement between the numerical predictions and experimental work. In 2015, Moe-Føre et al. [21] compared and evaluated the performance of numerical methods based on these three different elements called spring, truss and triangular elements. They concluded that each method showed a few strengths and weaknesses. While truss and spring elements are computationally very effective, the triangular elements are promising due to introduction of local wake effects.

These methods have been validated with experimental work and physical model tests under current and wave loading. In 2005, Lader and Enerhaug [22] tested a scaled down model of a flexible circular net with three different bottom weights subjected to uniform current velocities in a flume tank. One of their findings showed that the hydrodynamic forces acting on the net and its deformation were mutually dependent and suggested that this dependency shall be taken into account in numerical modelling. Two years later in 2007, Lader et al. [23] presented experimental measurements of forces on net panels with three different solidities exposed to five regular wave cases. Their studies clearly indicated that the forces increased with an increase in solidity ratio of the net. These measurements were compared with equivalent numerical models and were reasonably justified.

Such extensive research work conducted in all these years have improved the understanding of the different forces acting on the cage systems in marine aquaculture. Although, it provides collectible and beneficial information for further studying the dynamics of flexible gravity-based fish cages under currents and waves, there has not been much research on the effect of accidental failures on the responses of fish cages. This thesis, thus, aims to focus on the dynamics of cages post accidental failures in fish farming units.

2.2 Forces on a submerged cylinder

Ropes made up of different fibre material are twisted or braided and knitted in a grid-like structure to make a net. The forces acting on submerged cylinders are applicable to the net as its twines can be treated as thin cylinders.

2.2.1 Morison equation

Morison et al. 2.1 introduced a semi-empirical expression for calculation of in-line force on a slender cylindrical body submerged in an oscillatory flow. The hydrodynamic force, $F(t)$ acting on a unit length of the body is a combination of inertial and drag forces as shown in equation.

$$F(t) = \rho C_M V \cdot \dot{u}(t) + \frac{1}{2} \rho C_D A \cdot u(t) |u(t)| \quad (2.1)$$

where

C_M is the mass coefficient of the inertial term

C_D is the drag coefficient of the drag term

ρ is the density of water

A is the reference area of the body

V is the volume of the body

u is the velocity of the flow

\dot{u} is the acceleration of the flow

For a cylinder with diameter D , the reference area A is the diameter itself and the volume V is $\frac{\pi}{4} D^2$ and thus, equation 2.1 can be re-written as

$$F(t) = \frac{\pi}{4} \rho C_M D^2 \cdot \dot{u}(t) + \frac{1}{2} \rho C_D D \cdot u(t) |u(t)| \quad (2.2)$$

Equation 2.2 is a general form of Morison equation when the cylindrical body is stationary. However, it will not stay still any more when it is exposed to wave loads. Therefore, when this vertical cylinder is moving with a certain velocity $v(t)$ in a fluid with velocity $u(t)$, the Morison equation becomes

$$F(t) = \underbrace{\frac{\pi}{4} \rho C_M D^2 \cdot \dot{u}(t)}_{\text{I}} - \underbrace{\frac{\pi}{4} \rho C_A D^2 \cdot \dot{v}(t)}_{\text{II}} + \underbrace{\frac{1}{2} \rho C_D D \cdot (u(t) - v(t)) |u(t) - v(t)|}_{\text{III}} \quad (2.3)$$

where

I is the Froude-Krylov and diffraction force

II is the hydrodynamic mass force

\mathbf{III} is the drag force

$\mathbf{C_A}$ is the added mass coefficient and is equivalent to $(C_m - 1)$

$\dot{\mathbf{v}}(\mathbf{t})$ is the acceleration of the body

This expression is applied to calculate the force on the cage simulated in this thesis. When the model is subjected to a steady current, the inertial term is zero. Therefore, only drag term contributes to the hydrodynamic forces. For combined wave-current loading, the model will also experience accelerations and thus, both the terms will contribute to the hydrodynamic response.

The flow separation force on a submerged slender cylinder under pure currents is a combination of a drag force acting in-line with the flow direction and lift force acting normal to the body as shown in figure 2.1. A body is considered to be slender when its length to diameter ratio is large.

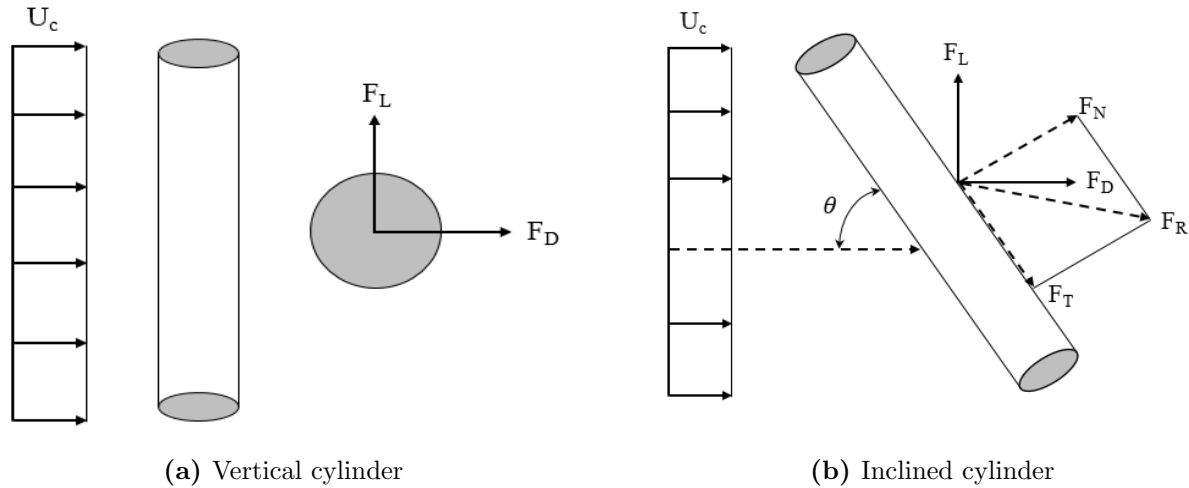


Figure 2.1: Lift and drag forces on a submerged slender cylinder

For a non-inclined or vertical cylinder as shown in figure 2.1a, the lift force F_L and drag force F_D are given by the following equations

$$\begin{aligned} F_L &= \frac{1}{2} \rho C_L A \cdot U_\infty^2 \\ F_D &= \frac{1}{2} \rho C_D A \cdot U_\infty^2 \end{aligned} \tag{2.4}$$

where

C_D and C_L are the lift and drag coefficients

U_∞ is the velocity of the ambient current

In case this cylinder is inclined at an angle θ as shown in figure 2.1b, the following expressions can be used to determine the normal force F_N and tangential force F_T per unit length

$$\begin{aligned} F_N &= \frac{1}{2} \rho C_D A \cdot U_N^2 \\ F_T &= \frac{1}{2} \rho C_F \pi A \cdot U_T^2 \end{aligned} \tag{2.5}$$

where

C_D and C_F are the normal and tangential drag coefficients

U_N is the normal component of the inflow velocity

U_T is the tangential component of the inflow velocity

For a velocity vector $U(u, v, w)$, these two components are given by

$$\begin{aligned} U_N &= \sqrt{u^2 + v^2} \\ U_T &= w \end{aligned} \tag{2.6}$$

The velocity vector components used in equation 2.6 represent a coordinate system with Z-axis parallel to the cylinder axis. Since the drag results from the flow tangential to the cylinder, the frictional coefficient C_F is used for the tangential force. The resultant force, F_R can then be determined from the equation 2.5 which is a good approximation for θ upto 60° [24].

2.2.2 Wake effect

When a fluid particle flows within the boundary layer around a circular cylinder, boundary layer separation may occur leading to formation of a wake behind the cylinder. The pressure reaches a maximum value at a stagnation point upstream of the cylinder as illustrated in the figure 2.2. It gradually decreases along the front half of the cylinder until it reaches $\frac{\pi}{2}$ and the flow remains attached to the surface. As it enters the second half, the pressure starts to increase leading to a significant pressure gradient experienced by the particle. This is the reason the flow separates from the body surface and leads to a turbulent region downstream of the cylinder called the “wake”. The pressure remains low inside this region and a pressure drag is generated.

These wake effects are experienced by the aft half of the netting due to blockage cause by the first half that lies upstream of the flow [25]. The velocity of the flow is reduced after it passes through the net panels by a velocity reduction factor [21]. The reduced velocity leads to a significant effect on the the deformations of the subsequent cages and consequential forces. This reduction has been found to be dependent on the net solidities and the angle of attack discussed in the next section.

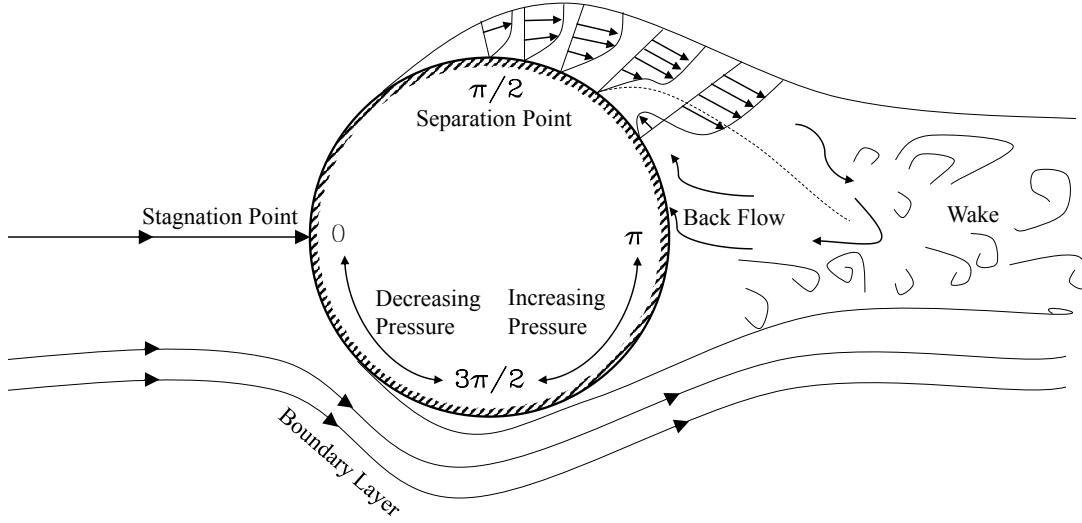


Figure 2.2: Boundary layer separation over a cylinder leading to generation of wake effect
(Source: Aerospace Engineering Blog)

This wake effect is implemented locally within the net structure used for the numerical study in this thesis. This shielding effect is based on Blevins wake formulation for a circular cylinder [26]. This method was further developed by Endresen et al to obtain the total effect for a net panel [25].

2.3 Hydrodynamics of a fish cage

Mooring system in a fish farm is designed to carry the global loads. The major contributions to these loads are due to the forces acting on the floating collar and net structure.

2.3.1 Forces acting on a floating collar

The hydrodynamic force acting on the floating collar in radial and vertical directions is equal to the sum of the external forces acting on it [1]. It can be written as

$$F_{R,Z}^{Total} = F_{R,Z}^{FK} + F_{R,Z}^{diffraction} + F_{R,Z}^{addedmass} + F_{R,Z}^{drag} + F_{R,Z}^{netcage} + F_{R,Z}^{mooring} \quad (2.7)$$

where

$\mathbf{F}_{r,z}^{FK}$ is the Froude-Krylov Force

$\mathbf{F}_{r,z}^{diffraction}$ is the diffraction force

$\mathbf{F}_{r,z}^{addedmass}$ is the added mass force

$\mathbf{F}_{r,z}^{netcage}$ is the force transferred by net structure

$\mathbf{F}_{r,z}^{mooring}$ is the force transferred by mooring lines

2.3.2 Forces acting on a net structure

The hydrodynamic force acting on the net is equal to the sum of the forces acting on each twine. The dynamic motion equation of a net structure can be written as

$$[M][\ddot{X}] + [C][\dot{X}] + [K][X] = [F_D] + [F_M] + [F_B] + [W] \quad (2.8)$$

where

$[M]$ is the mass matrix

$[C]$ is the damping matrix

$[K]$ is the stiffness matrix

$[F_D]$ is the drag force matrix

$[F_M]$ is the inertia force matrix

$[F_B]$ is the buoyant force matrix

$[W]$ is the gravity matrix

The two widely used models used to calculate the drag forces in a net structure are described below.

- **Morison model:**

In this approach, the total drag forces in a net structure is computed by summing the drag and lift forces on the individual twines and knots as shown in figure 2.3a. The drag coefficient is determined from the Reynolds number (R_e) at the twine as shown in equation 2.9. This model usually does not account for the interaction between the two adjacent twines. It was developed by Lader and Fredheim in 2006 [27] and is implemented in FhSim software used in this thesis.

$$\begin{aligned} F_L &= \frac{1}{2} \rho C_L(R_e) A \cdot U_{rel}^2 \\ F_D &= \frac{1}{2} \rho C_D(R_e) A \cdot U_{rel}^2 \end{aligned} \quad (2.9)$$

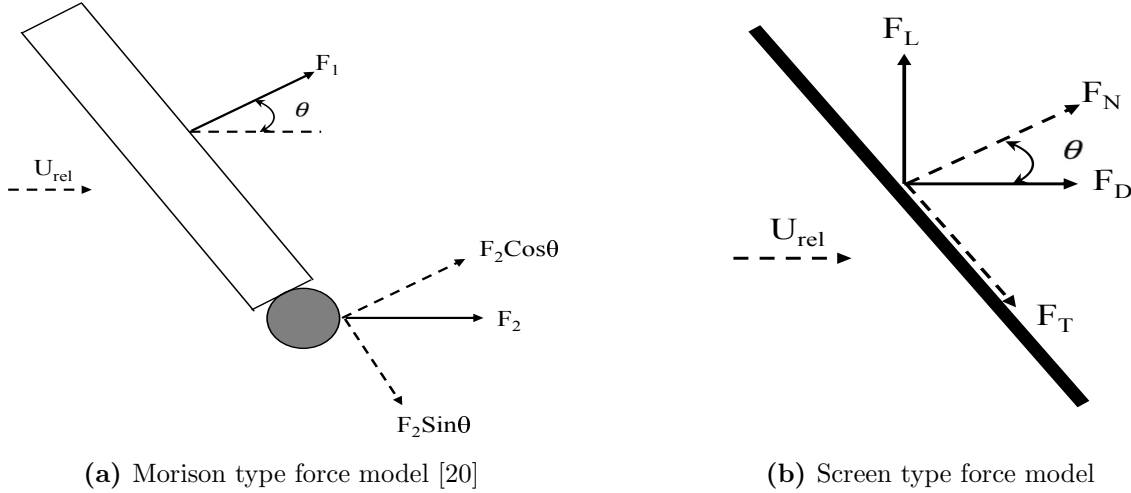


Figure 2.3: Different approaches used for hydrodynamic force calculation for net structures

- **Screen model:** In this approach, the total drag forces in a net structure is computed by summing drag and lift forces on the individual net panels as shown in figure 2.3b. The drag coefficient is determined from the Reynolds number (R_e), solidity ratio (S_n) and the angle of attack (θ) at the panel as shown in equation 2.10. This model is developed by Kristiansen and Faltinsen in 2012 [20].

$$\begin{aligned} F_L &= \frac{1}{2} \rho C_L(R_e, S_n, \theta) A \cdot U_{rel}^2 \\ F_D &= \frac{1}{2} \rho C_D(R_e, S_n, \theta) A \cdot U_{rel}^2 \end{aligned} \quad (2.10)$$

They differ in the way they compute viscous loads on the net panels. While the Morison model determines the drag coefficient based on the twine diameter and the Reynolds number, the screen model determines the drag coefficient based on the area's solidity, angle of attack in addition to the Reynolds number at the twines [1].

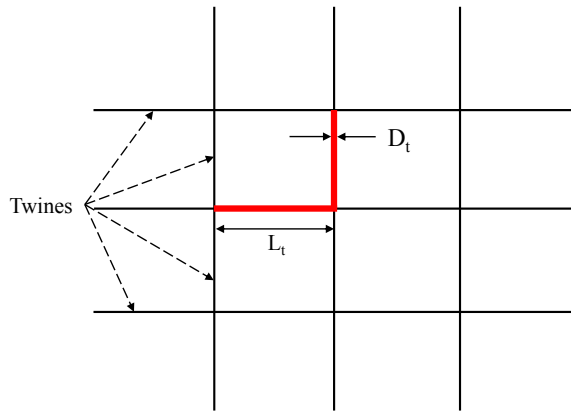
The hydrodynamic model implemented in FhSim is a Morison type force model and takes into account only the local shielding in each element. A screen model will have local shielding incorporated if there are drag/lift coefficients which are angle dependent while Morison model fails to capture such effects since they consider a number of twines in flow.

2.4 Parameters affecting cage hydrodynamics

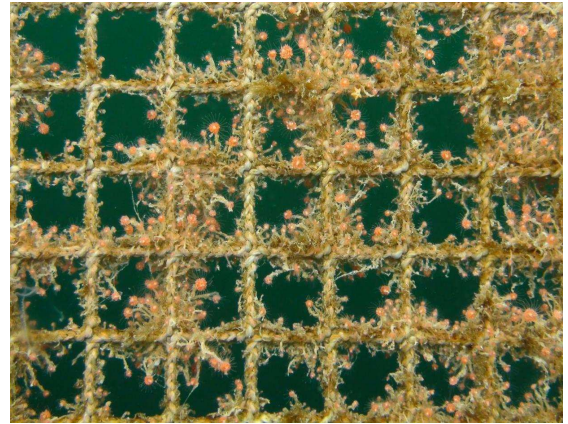
In the previous sections, several parameters that affect the hydrodynamics of the cage have been mentioned. These are discussed further below.

2.4.1 Solidity ratio

Solidity ratio, S_n of a net is the ratio of the projected area to the total area of the netting when laid out in a 2-Dimensional plane. It is a dimensionless quantity with a value between 0 to 1 with 1 representing a solid fabric [21]. The solidity ratio is dependent on the twine length L_t and diameter D_t as shown in figure 2.4a.



(a) Sketch of an enlarged section of a square-woven net



(b) Biofouling on a cage net (Source: SINTEF Ocean AS)

Figure 2.4: Parameters affecting solidity ratio of the net structure of a fish cage

For a square woven net, net solidity can be expressed by equation 2.11.

$$S_n = 2 \cdot \frac{D_t}{L_t} - \left(\frac{D_t}{L_t} \right)^2 \quad (2.11)$$

In marine aquaculture, net solidity needs to be adjusted during the production cycle. A finer mesh is used during early stages of the farming cycle. If the solidity ratio is high enough, the young and smaller fishes in the cage might escape. Netting with lower solidity is required during final stages of the fish farming because large fishes require a better water flow through the cage. A typical Norwegian fish cage has a net solidity between 0.10-0.30. In this thesis, net with three different solidity ratios 0.19, 0.24 and 0.29 are used for sensitivity studies.

One of the primary reasons of an increase in the net solidity is the marine biofouling. Certain organisms in the sea have a tendency to accumulate on submerged artificial surfaces and this build-up is called as “Biofouling”. This leads to a decrease in the mesh size of the net as shown in figure 2.4b. This might increase the weight of the net structure to a significant extent. It is harmful for the fish health because sufficient amount of clean water would not flow across the net structure. Moreover, an increase in the solidity ratio will increase the hydrodynamic drag acting on the net because the water will naturally flow around the structure instead of flowing through it. These increased forces acting on the net are eventually transferred onto the mooring system of the fish farm.

2.4.2 Reynolds number

Reynolds number, Re is defined as the ratio of the inertial forces to the viscous forces. It is expressed by equation 2.12.

$$Re = \frac{U_{rel} D_t}{\nu} \quad (2.12)$$

where

U_{rel} is the velocity of the water relative to the twine

D_t is the diameter of twine

ν is the kinematic viscosity of water

The net cage wake effect implemented in FhSim software is based on Morison’s approach to calculate forces and accounts for Reynolds number dependent drag coefficient. Figure 2.5 shows the effect of Reynolds number on the drag coefficient of a smooth sphere and cylinder.

C_D decreases with increase in Reynolds number and experiences a sudden drop when the separation switches from laminar to turbulent flow.

There is a requirement of a detailed representation of the affect of the variations in the incident water velocity on the drag coefficients. The net model used in this thesis is expanded with a Reynolds dependent drag coefficient for the twines.

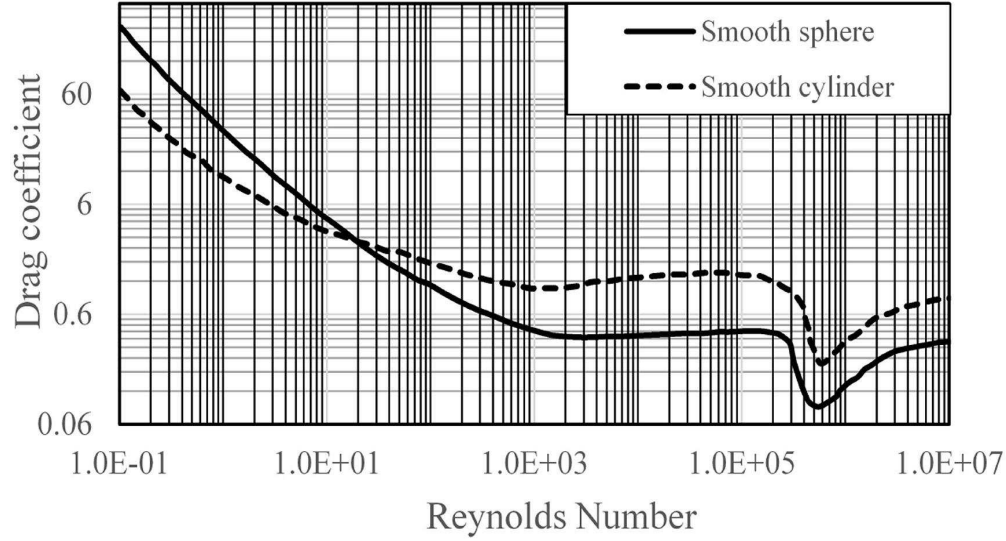


Figure 2.5: Drag coefficient of a smooth sphere and cylinder (Source: H.Schlichting’s “Boundary Layer Theory”)

2.4.3 Angle of attack

Angle of attack, θ is the angle made by the flow vector and the cylindrical axis as shown in figure 2.1b and changes in this angle may lead to changes in forces acting on the cylinder. A small angle of attack ($\theta \approx 0^\circ$) induces almost a zero drag and this is observed by the horizontal twines in the net structure. The drag is maximum for the vertical twines which are at an angle of 90° to the incoming flow. It can be inferred from equation 2.5 that the drag coefficient C_D is dependent on the normal component of the inflow velocity, U_N and thus is independent of the angle of attack, θ . This is called as the “Independence principle” [28].

Based on flow-visualization experiments by Kozakiewicz et al, the critical value of θ is known to be approximately 35° [28]. This implies that for $\theta \leq 35^\circ$, the streamlines do not bend any more unlike for higher angles where the streamlines in the vicinity of the cylinder bend as

if the cylinder is at an angle of about 90° . Therefore, the C_D is dependent on θ and there is a violation of the independence principle. For lift forces, the principle in discussion is valid for the range $45^\circ \leq \theta \leq 90^\circ$.

2.5 Linear wave theory

The two models simulated in the thesis are exposed to regular waves based on the linear wave theory. Published by George Biddell Airy, it is often referred to as the “Airy wave theory”. It gives a linearised description of the gravity wave propagation on the surface of a potential flow. The generated wave profile is sinusoidal in nature as sketched in figure 2.6 where H is the wave height, ζ is the surface elevation and λ is the wavelength. At the surface, the Z coordinate is 0 and extends until $-d$ at the seabed where d is the water depth.

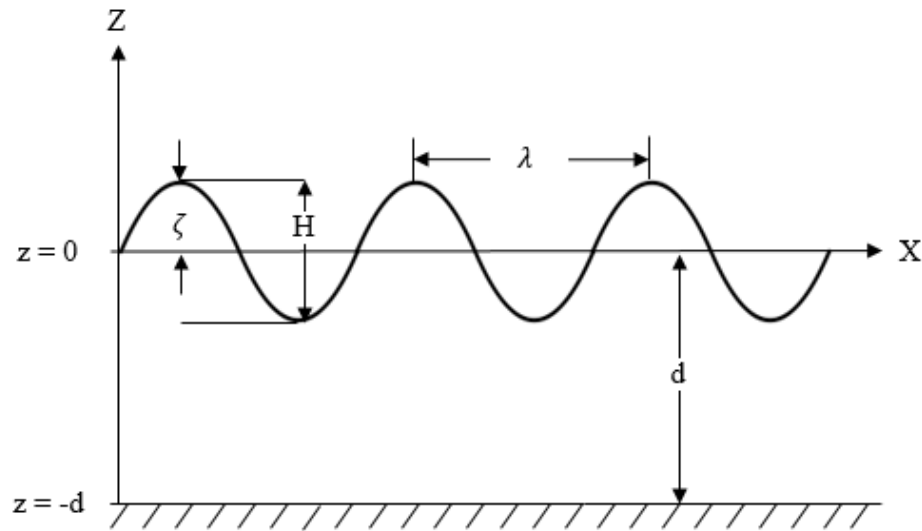


Figure 2.6: Sinusoidal wave profile

The free surface elevation, ζ is expressed as a function of horizontal position x and time t as given by equation 2.13.

$$\zeta(x, t) = a \cos(kx - \omega t) \quad (2.13)$$

where

a is the wave amplitude

k is the wavenumber

ω is the angular frequency of the wave

The theory is based on assumptions that the propagating medium is incompressible and irrotational. In continuum mechanics, incompressible flow refers to a flow where the density of fluid, ρ remains constant within an infinitesimal volume. It is expressed by a zero divergence of the flow velocity vector $\vec{U}(u, v, w)$ as given by the equation 2.16.

$$\frac{D\rho}{Dt} + \rho \left(\frac{\partial u}{\partial x} + \frac{\partial v}{\partial y} + \frac{\partial w}{\partial z} \right) = 0 \quad (2.14)$$

$$\frac{D\rho}{Dt} + \rho \nabla \cdot \vec{U} = 0 \quad (2.15)$$

$$\nabla \cdot \vec{U} = 0 \quad (2.16)$$

Further, an irrotational flow refers to a flow where there is no rotation in the fluid elements with respect to each other. There is no shear forces acting between the layers making it frictionless. It is expressed by a zero cross gradient of the flow velocity vector $\vec{U}(u, v, w)$ as given by the equation 2.17.

$$\nabla \times \vec{U} = 0 \quad (2.17)$$

2.5.1 Potential function

The velocity potential, $\phi(x, z, t)$ related to the flow components u_x and u_z in the horizontal and vertical directions respectively is given by equation 2.18.

$$u_x = \frac{\partial \phi}{\partial x} \quad \text{and} \quad u_z = \frac{\partial \phi}{\partial z} \quad (2.18)$$

The potential ϕ has to satisfy the Laplace equation 2.19 due to the assumption that the flow is incompressible.

$$\frac{\partial^2 \phi}{\partial x^2} + \frac{\partial^2 \phi}{\partial z^2} = 0 \quad (2.19)$$

In order to find the solutions, boundary conditions must be established at the free surface and seabed. It is important to specify a zeroth-order solution for the formulation of this theory. The base state is assumed at rest which implies that the mean flow velocities are zero.

- Kinematic bed boundary condition (KBBC):

No water can flow through an impervious boundary such as the seabed. For a flat bottom, this boundary condition is expressed by equation 2.20.

$$\left. \frac{\partial \phi}{\partial z} = 0 \right|_{z=-d} \quad (2.20)$$

- **Kinematic free surface boundary condition (KFSBC):**

For infinitesimal waves, the vertical velocity of the particle on the free surface follows the vertical velocity of the surface itself. In other words, once a particle on the free surface, always a particle on the free surface. This boundary condition is expressed by equation 2.21.

$$w = u \frac{\partial \zeta}{\partial x} + \frac{\partial \zeta}{\partial t} \quad \left|_{z=\zeta(x,t)} \quad (2.21)$$

An additional boundary condition is needed as the surface elevation ζ is also an unknown. It is given by Bernoulli's equation for an unsteady potential flow.

- **Dynamic free surface boundary condition (DFSBC):**

The pressure across the free surface interface is constant and equal to the atmospheric pressure. This pressure boundary condition is expressed by equation 2.22.

$$\rho \left\{ \frac{\partial \phi}{\partial t} + \frac{1}{2} u^2 + g\zeta \right\} = 0 \quad \left|_{z=\zeta(x,t)} \quad (2.22)$$

The solution for velocity potential ϕ satisfying Laplace equation 2.19 as well as the boundary conditions in equations 2.20, 2.21 and 2.22 is a 2D linearised function given by equation 2.23.

$$\phi(x, y, z, t) = \frac{\omega}{k} a \frac{\cosh(k(z+d))}{\sin(kh)} \sin(kx - \omega t) \quad (2.23)$$

2.5.2 Dispersion relation

On substituting the first order velocity potential into the combined free surface boundary condition, an expression given below is derived [29].

$$\omega^2 = gk \tanh(kd) \quad (2.24)$$

Wave number, k and wave frequency, ω can be expressed as

$$k = \frac{2\pi}{T} \quad \text{and} \quad \omega = \frac{2\pi}{\lambda} \quad (2.25)$$

The equation 2.24 can thus be manipulated to achieve a relation between wave length, λ and wave period, T as given below by equation 2.26. This is known as “Dispersion relation” and is used to define the airy wave used for time-domain simulations in this thesis.

$$\lambda = \frac{g}{2\pi} T^2 \tanh(kd) \quad (2.26)$$

3 Numerical Analysis

Two models are simulated numerically in this thesis and are described later in chapters 4 and 5. First, a single-cage system was analysed to study the response of one fish cell and the same fish cell was then used to develop a 1x3 matrix to study the response of the multiple-cage system representing a fully functional fish farm. The two models differ in the number of fish cells and the mooring system configuration.

3.1 Overview of a gravity-based fish cage

The schematic of a conventional flexible gravity-based fish cage is shown below in figure 3.1. It is made up of a floating collar, net structure, bottom ring called “sinker tube” and chains that keep it under tension. The cage interacts with the mooring system via bridles and frame cables of the mooring frame while the buoys help keeping it afloat on the water surface. All of these components help in maintaining the shape and position of the fish cage at all times, especially when it is exposed to severe environmental loading.

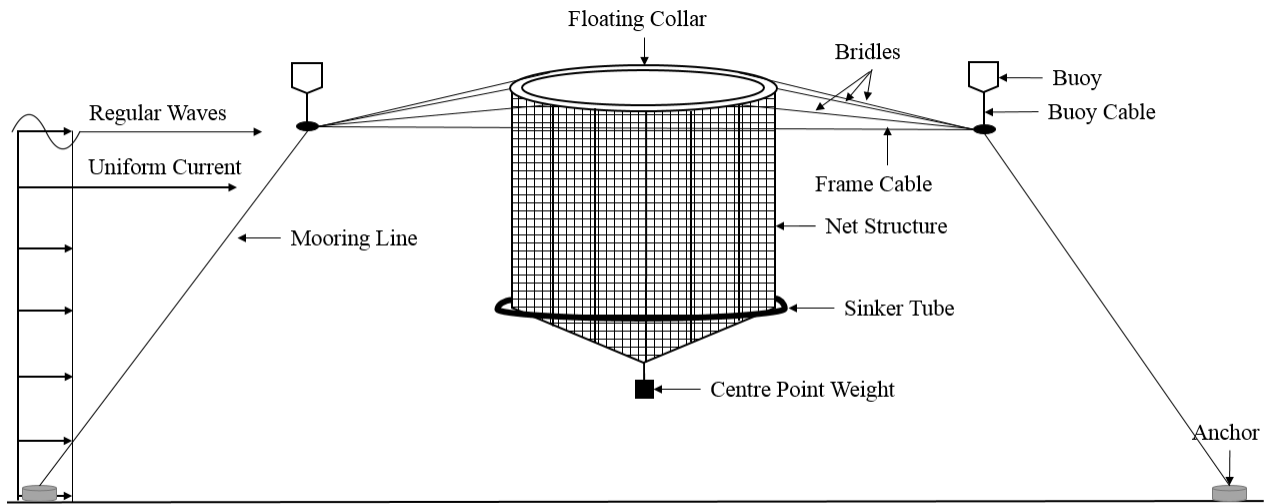


Figure 3.1: Schematic overview of a conventional flexible gravity-based fish cage (Reproduced from Grue [1])

3.1.1 Floating collar

Floating collar is one of the primary components of a fish cage and is basically a high density polyethylene (HDPE) pipe. It serves as the hang-off point for the net structure containing

fish and the connection point for the bridles for fastening purposes. The pipe is hollow to provide sufficient buoyancy to the partially submerged net structure in order to prevent fish escapes from the top. It may be connected to the sinker tube suspended at the bottom of the net structure via chains. It is designed such that it can follow the wave motion rather than resisting it when subjected to large wave conditions [30].

Typical cage systems consist of double-pipe collar and these two pipes are connected with brackets. The grating on these brackets serve as a working platform for inspection and monitoring operations in a fish farm as shown in figure 3.2.



Figure 3.2: Double-pipe floating collar of a gravity-based fish cage (Source: Aqualine AS)

3.1.2 Net structure

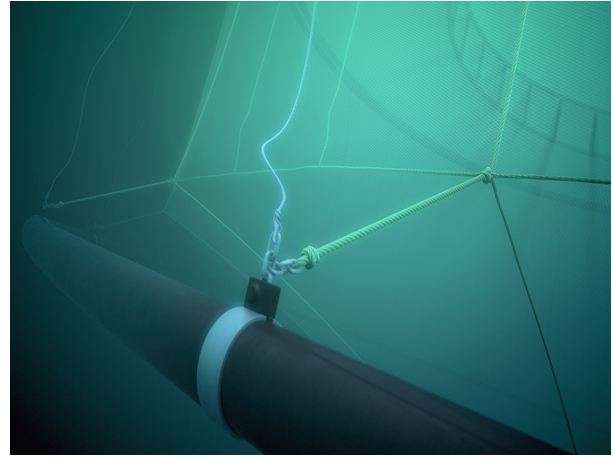
Net structure is the primary component of a fish cage as it contains the biomass. Typical cage systems consist of a cylindrical net structure with conical bottom. To ensure flexibility, it is made up of materials with very low bending stiffness. Thus, a net is subjected to high drag forces when exposed to environmental loads leading to large deformations. The volume reduction shall not go beyond a critical percentage of the original volume as it is harmful for the organism being farmed. Generally, centre point weights are added at the end of the conical bottom as seen in figure 3.1. This is done to maintain a better shape of the net structure and preserve volume under severe weather conditions [30].

Further tension is provided by the sinker tube attached to the net structure via chains as shown in figure 3.3b. The meshes can be formed either by knotting or braiding, and can be

of different shapes and sizes. Figure 3.3a shows a knotless fish net with square meshes. An optimal mesh design is very critical for the integrity of the net structure. Under dimensioning could lead to fish leakage due to net failures and over-dimensioning could lead to problems such as abrasion against floating collar or sinker tubes again increasing the risk of fish escapes.



(a) Knotless fishing net with square meshes
(Source: GuangTong Plastic Netting)



(b) Sinker tube connected to the net structure
(Source: The Aquaculture Communications Group)

Figure 3.3: Net structure and sinker tube of a gravity-based fish cage

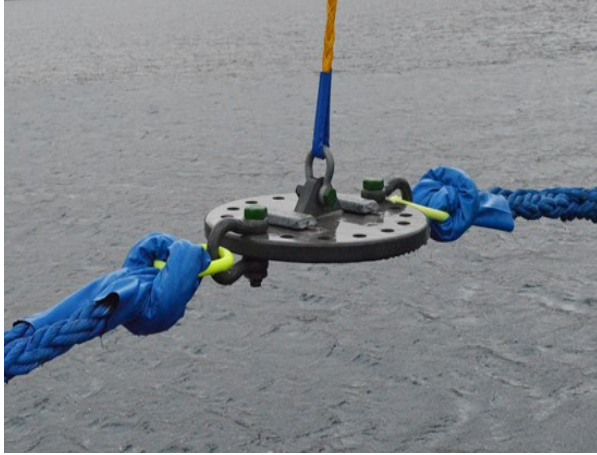
3.1.3 Sinker tube

Sinker tube is a ring like structure suspended at the bottom of the net structures and thus, also often referred as “bottom ring”. Like floating collar, it is also a hollow HDPE pipe but filled with chains or other high density materials to keep it always submerged in water [30]. As mentioned earlier, the bottom ring is connected to the net structure via chains providing sufficient tension in the same. The weight of the sinker tube adds to the self-weight of the net structure and this further ensures that the internal volume inside the net is maintained at all times especially when the system is exposed to currents and waves.

3.1.4 Buoy system

Buoys are hollow structures connected to the connection plate submerged beneath the sea surface via buoy cables as shown in figure 3.4a. Its primary function is to provide additional buoyancy to the mooring system and is attached at the corners of the mooring frame for symmetric distribution of the buoyant force across the fish farm. The buoys are said to increase the visibility of the farm as they visually outline the fish cells [30].

A typical mooring buoy used in marine aquaculture can be seen below in figure 3.4b.



(a) Connection plate with attachment points for various cables (Source: Vónin Ltd.)



(b) Mooring buoy floating in a near shore fish farm (Source: Polyform AS)

Figure 3.4: Buoy system of a fully functional fish farm

3.1.5 Mooring system

An illustration of the mooring system of a fully functional fish farm is shown in figure 3.5.

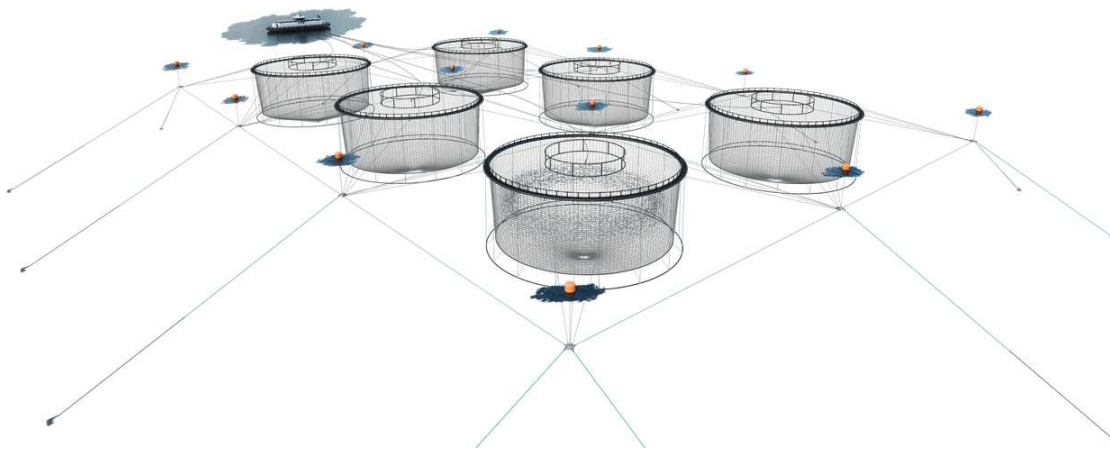


Figure 3.5: Mooring system of a fully functional fish farm (Source: AKVA Group)

A mooring frame is a network of cables arranged in a grid-like structure which is anchored to the seabed [30]. A plan view of the frame can be imagined as the cage in the centre fastened with bridles to the corners where it coincides with the frame cables running between two

consecutive corners. These vertices are equipped with a connection plate made up of steel which serves as the attachment point for these cables and the buoy cable as shown earlier in figure 3.1. This frame is often referred to as one fish “cell” and the configuration of the mooring system largely depends on the alignment of these fish cells in any fish farming unit. The frame is never visible to eyes from above a fish farm because it is positioned a few metres below the water surfaces for ease of access to the cages for operation and maintenance.

3.2 Introduction of the numerical tool

The software used for the numerical analysis is an in-house tool called “FhSim” developed by SINTEF Ocean AS. It was inceptioned in 2006 and has been under constant development since. Over the years, it has served as a common platform to simulate various marine operations in the time domain using models described as ordinary differential equations (ODE) [31]. It is basically a set of two applications, FhSim for simulation and a pre-processor definition for model visualization called “FhVis”.

3.2.1 A general overview of FhSim architecture

Figure 3.6 below provides a general overview of the organization of FhSim.

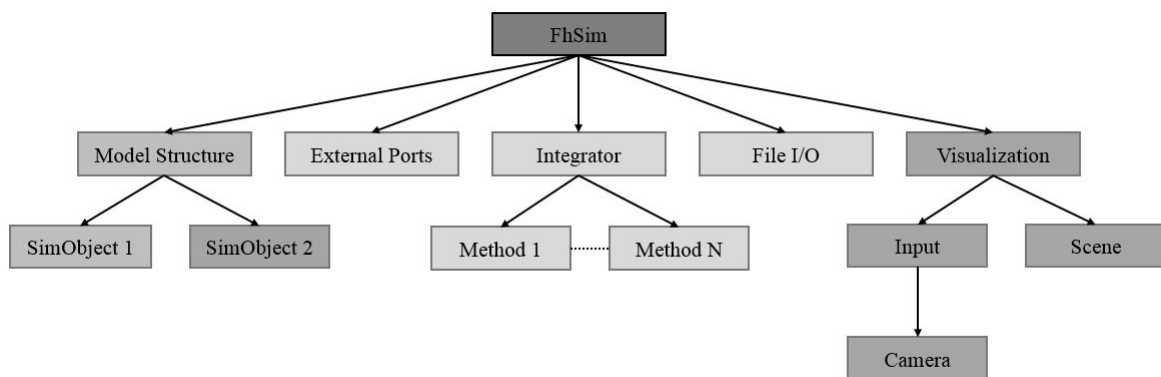


Figure 3.6: Flow-chart showing architecture of FhSim (Source: SINTEF Ocean AS)

FhSim uses object-oriented programming structure and is built into a complex structure from pre-defined sub-structures known as simulation objects or “SimObjects”. These are defined by internal properties like the geometry and external properties such as input and output ports. There also exist support functions such as integrator, output definitions for time and

file. The models are realised as a single SimObject or several inter-connected SimObjects. The advantage of having this modularity of the system architecture is the increase in the efficiency of the system in terms of simulation, visualization and flexibility. FhSim is not a graphic user interface(GUI)-based program and therefore is initialised through the terminal window of either Windows or Linux systems.

3.2.2 Fish cage model realization in FhSim

The model of a typical Norwegian flexible gravity-based fish cage is realized by a two-pipe floating collar, cylindrical net structure with a conical base, sinker tube and chains connecting the net with the sinker tube. There are several ropes representing net reinforcements, frame cables, bridles, buoy cables and a mooring frame. A centre point weight is added at the bottom of the cage net to maintain the shape. This model has been validated in the past through comparisons with experiments and has shown satisfactory results for low current velocities in particular [32].

Figure 3.7 shows the visualization of the flexible gravity-based fish cage model realized in FhVis. Several fish cage components can be seen either in the elevation view or the plan view.

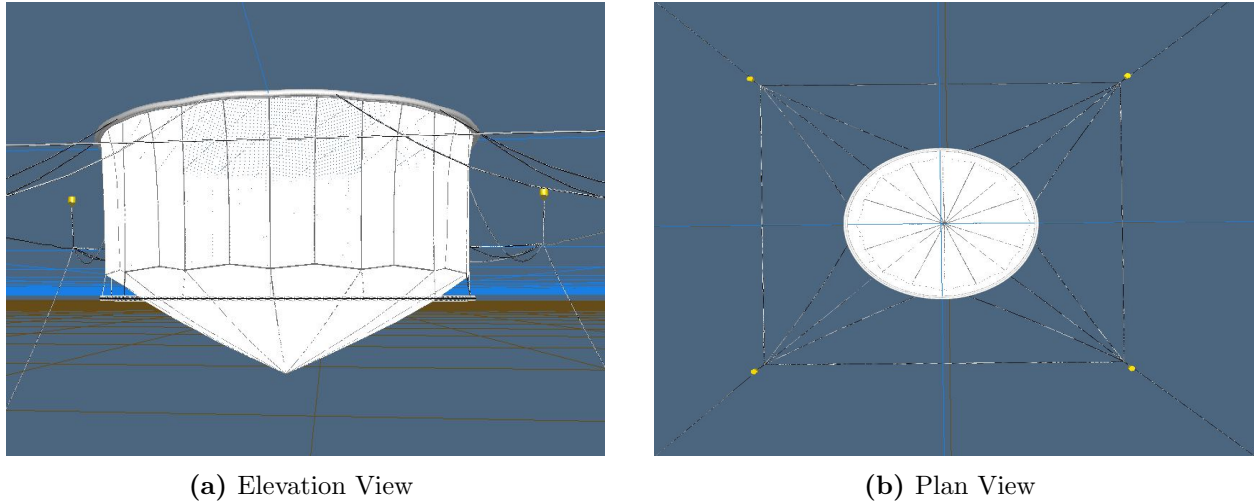


Figure 3.7: Visualization of a gravity-based fish cage model realised in FhVis

The model is generated by an input template providing information about the SimObjects, their parameters and initial states, port interconnections and integration scheme [31]. The set of differential equations defining the model are solved using numerical integration methods

such as Euler or Runge-Kutta 4-5. Newton’s second law is used to establish the equation of motion to derive an expression for the acceleration of the finite elements and the displacements are then found by integrating the acceleration twice over time [21].

Figure 3.8 shows a representation of how the variables are transferred across the model during simulations in FhSim. The position and velocity are the output ports and the force is fed back. “Mooring” is an integrated model and comprises of the mooring frame with bridles, connection plate, buoys and associated cables like buoy cables, frame cables and mooring lines. The sinker tune and chains are also an integrated model. The cage net and floating collar, however, are individual models as highlighted in the figure. The realization of the sea environment with current and waves is a shared model which other models may query for current velocities in case of currents and wave particle velocities amongst several parameters, in the case of waves.

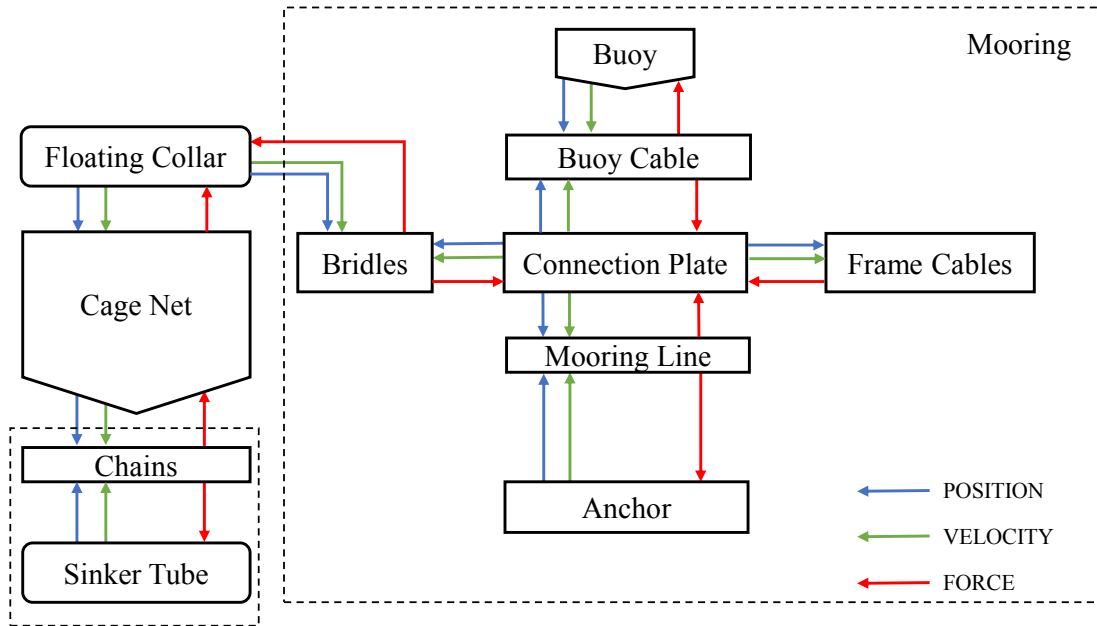


Figure 3.8: Transfer of variables across interconnected SimObjects during numerical analysis in FhSim (Source: SINTEF Ocean AS)

3.3 Numerical models implemented in FhSim

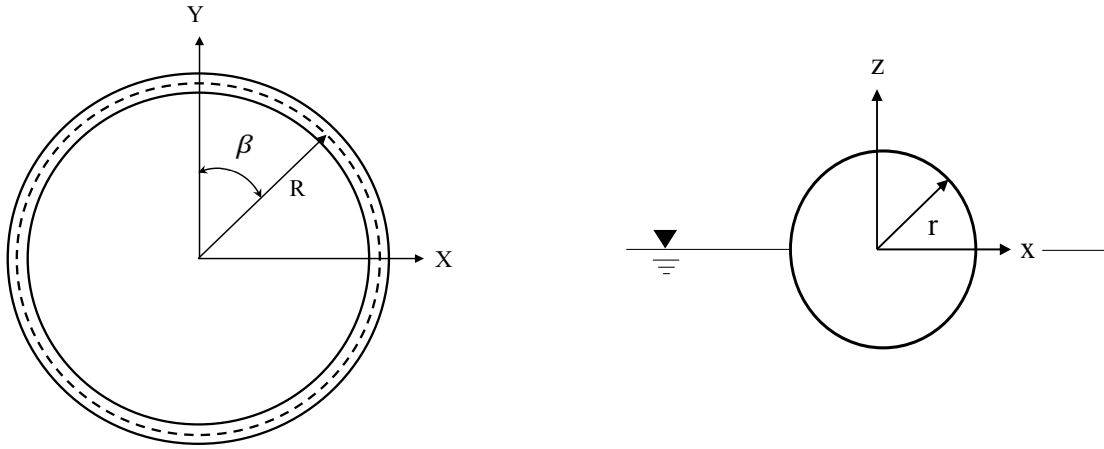
The numerical model so realized in FhSim comprises of several components as explained in the previous section and each of these components is based on a mathematical model. While

the different cables and other components with cable-like properties are modelled using bar elements, a more detailed mathematical model is used for floating collar and the net cage.

3.3.1 Structural model of the floating collar

The floating collar is modelled as two flexible circular concentric rings made up of HDPE pipes with six degrees of freedom. Hydro-elasticity is essential for the collar and theoretically, this property of the collar causes it to nearly follow the waves with long wavelengths. The wavelengths of practical interest are of the order of the diameter of the floating collar but long enough with respect to the cross-section of the pipe [33].

In 2011, Faltinsen [34] formulated the velocity potentials and added mass for circular collar of a flexible fish cage. This was used in the study by Endresen [2] in his thesis to investigate the vertical wave loads and response of the floating collar. Linear potential theory is used to find the added mass for vertical motions of the floating collar which is partially submerged in water. Local and global coordinates of a one ring model is illustrated in figure 3.9 below [2]. FhSim software used for the numerical study in this thesis is based on this theory. It basically calculates the response of the floater in response to sine waves and sums up these responses.



(a) Far field view with global coordinates

(b) Near field view of the cross-section with local coordinates system

Figure 3.9: Single torus model representing the floating collar (Reproduced from Endresen [2])

3.3.2 Response calculation of the floating collar

The Euler beam equation can be used to model the radial and vertical responses of the collar expressed by equation 3.1 below[2].

$$\begin{aligned} F_R(s, t) &= m \frac{\partial^2 v}{\partial t^2} + EI \left(\frac{\partial^4 v}{\partial s^4} + \frac{1}{R^2} \frac{\partial^2 v}{\partial s^2} \right) \\ F_Z(s, t) &= m \frac{\partial^2 z}{\partial t^2} + EI \frac{\partial^4 z}{\partial s^4} \end{aligned} \quad (3.1)$$

where

v is the radial response of the floater

z is the radial response of the floater

m is the per unit length mass of the floater

EI is the bending stiffness of the floater

F_R is the per unit length radial force on the floater

F_Z is the per unit length vertical force on the floater

The motions of the torus are represented by sinusoidal modes in the vertical and horizontal directions [35]. The motion of every floating collar element in the three directions - x, y and z is expressed by the equation 3.2. Endresen addressed only the vertical motion in his work as he compared the displacements calculated from the linear model with a non-linear model for excitation forces [2]. The excitation forces were obtained by integrating the hydrostatic and hydrodynamic pressures over the wetted surface of the floating collar and the responses were then calculated by superposition of the modes.

$$\begin{aligned} x(\beta, t) &= b_1 + v(\beta, t) \cos \beta \\ y(\beta, t) &= v(\beta, t) \sin \beta \\ z(\beta, t) &= \sum_{n=0}^{\infty} a_n(t) \cos n\beta \\ v(\beta, t) &= \sum_{n=2}^{\infty} b_n(t) \cos n\beta \end{aligned} \quad (3.2)$$

where

β is the angle in the torus' X-Y plane

\mathbf{a}_0 is the heave motion

\mathbf{a}_1 is the pitch motion

\mathbf{a}_2 is the first vertical elastic mode

\mathbf{b}_1 is the surge motion

\mathbf{b}_2 is the first horizontal elastic mode

3.3.3 Structural model of the net structure

The structural model implemented in FhSim for net structure is based on the triangular-element formulation described by Priour in 1999 [18]. In this method, the discretization of the net is achieved by triangular elements. It is assumed that the material properties and geometry are constant within each element and more importantly, the orientation of the twines remains constant within the element. Each element consists of a number of meshes in the “U” and “V” local coordinate system followed for the twines as shown in figure 3.10 below.

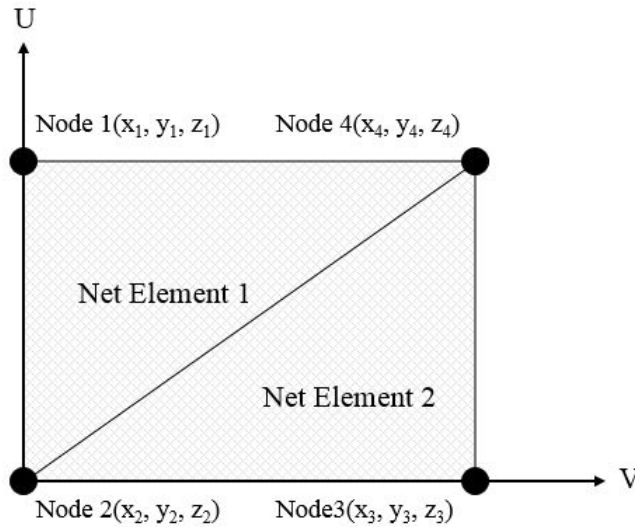


Figure 3.10: Priour’s triangular element for numerical modelling of net structures

The net has a non-uniform elastic response depending on the orientation of the loading of the twines in relation to the direction of the force. The model of the elasticity of the net accounts for this and the forces in the U-V directions are calculated from the node displacements.

The mass of the net is discretized into mass points which are nothing but the nodes at

the corners. The forces from the strain in the net are added to each node connected to the triangle. The entire dynamics, however, is calculated in the global frame. Therefore, there is a number of reference frame transformations in the implementation of the triangular elements in FhSim. The net is then simulated from Newton's second law by calculating the accelerations of the nodes when considering the force contributions from the triangular net elements. This is integration of a first order ODE, and requires only the first derivative. It is important to note that the stiffness of the triangular elements is dependent on displacement direction. The stiffness is also zero when the net is in compression and this is a non-linear effect.

Reinforcement cables in the net are accounted in the same calculation as springs between two nodes without considering the effect of the different elastic responses in different directions. These contribute forces to the two end nodes which the cables are connected to. Longer cables are made in the model by continuing the cable to the next node.

3.3.4 Hydrodynamic model of the net structure

The hydrodynamic forces acting on the triangular elements are found by applying Morison's equation [31]. The drag and friction is calculated on the cables which are basically non-linear springs between two nodes and the net panels with a quadratic drag or the Morison type force model. Orientation of the cable or of the twines in the net panel is arbitrary and the incoming velocity is decomposed into the local coordinate system running tangentially or normal to the rope or to the twines. Once the incoming velocity is decomposed in the reference system of the net element, the normal and tangential forces on a set of twines in the direction U and in the direction V are calculated. These forces are transferred to the global coordinate system and applied to the nodes. The relative motion of the nodes are taken into account by averaging the node velocities when calculating the effective incoming water flow.

3.3.5 Mooring system

Mooring lines are modelled as interconnected rigid bar elements. These elements are constrained at the ends to provide the desired structural properties such as axial and torsional stiffness and bending. The constrained forces are controlled to avoid numerical stabilities through Baumgarte stabilisation method, the parameters of which are related to the cable's physical properties [36]. The hydrodynamic forces on the mooring system are calculated based on

Morison type force model.

3.4 Model parameters

The dimensions of a typical Norwegian fish cage used for the numerical modelling in this thesis are listed below in table 3.1.

Table 3.1: Specifications of a typical Norwegian fish cage used for developing the numerical models

Component	Parameter	Value	Unit
Floating Collar	Inner collar diameter	51	m
	Outer collar diameter	51	m
	Pipe diameter	0.25	m
	Pipe wall thickness	28.40	mm
	Pipe E-modulus	0.9	GPa
	Pipe weight	81	Kg/m
	Drag coefficient	1	-
Cage Net	Vertical wall depth	15	m
	Cone-tip depth	28	m
	Twine diameter	2.5	mm
	Twine length	25	mm
	Twine density	1125	Kg/m ³
	Solidity ratio	0.19	-
	Twine E-modulus	0.1	GPa
	Tangential coefficient	0.01	-
	Drag coefficient	1.1	-
Sinker Tube	Tube diameter	51	m
	Pipe diameter	0.25	m
	Initial depth	17.50	m
	Tube weight	51	Kg/m
	Centre point weight	100	Kg
Buoy	Diameter	2	m
	Vertical wall depth	1	m
	Cone-tip depth	2	m
	Weight	1073	Kg

The net structure comprises of 321 nodes and 608 net panels in total. A single layer is formed by a set of 32 nodes that are equally distributed along the circumference of the structure. There are 10 such layers along the vertical wall depth and a single node is present at the cone-tip depth. The floating collar serves as the hang-off point for the net structure and has 32 net connections corresponding to these nodes.

There are 12 fastening points around the circumference of the floating collar for bridles. These bridles have a spread angle of 45° and are in sets of 3 connected to each of the 4 corners of the mooring frame via the connection plate. The outer two bridles in this set is 50 metres in length and the inner bridle is 46 metres in length. The bridles are 0.05 metre in diameter and the material density is 1100Kg/m^3 with an E-modulus of 1 GPa. The mooring frame is 100×100 metres in size and is located 8 metres below the watersurface. Therefore, the frame cables are 100 metres in length. The length of the buoy cable is 10 metres. The other parameters of the frame and buoy cables are identical to the bridles.

In any numerical analysis using finite element analysis (FEM), the number of elements in a component is an important parameter. The anchor and frame cables comprise of 25 elements each. The bridle and buoy cable is comprised of 4 elements each. The bottom ring has 36 elements and the connected cables for net tension have 2 elements.

3.4.1 Time-domain analysis

Table 3.2 specifies the parameters of the time-domain simulations in FhSim under environmental loading.

Table 3.2: Parameters for time-domain numerical analysis in FhSim

Model	Description	Integration Method	Time Step	Duration [s]
A	Single-cage model	Runge-Kutta 4-5	0	600
B	Multiple-cage model	Forward Euler	Fixed ^{1 2}	600

¹ $0.65\text{e-}03$ for pure currents condition

² $1.25\text{e-}03$ for combined wave-current condition

Convergence studies are important when using numerical tools. Therefore, a convergence study was conducted for model B after the preliminary study of the model A. It was found that a time step of $2.15\text{e-}03$ is marginal for the numerical stability of the net structure used in this thesis. The net calculations do not collapse totally at this time step due to damping

but exhibit a few oscillations during the steady state. This is evident from the results of single-cage model presented later in chapter 4. Therefore, the fixed time step as tabulated above was used for numerical simulations of multiple-cage model. Euler method is quite efficient in comparison to Runge-Kutta 4-5 when solving the mooring model in multiple-cage system.

3.4.2 Method of calculating volume of the net structure

The volume of the net structures in this thesis has been calculated as per Cheng's method based on the principle of vector cross product [37]. In this method, the net structure is considered to be made up of "m" pies with "n" vertices stacked together. An arbitrary point O(0,0,0) is considered as origin and "n" vectors equal to the number of vertices are defined. The area of each layer A_i can be computed using equation 3.3 where $P_{n+1} = P$.

$$A_i = \sum_{j=1}^n S_{\Delta OP_j P_{j+1}} = \frac{1}{2} \left| \sum_{j=1}^n (x_j y_{j+1} - x_{j+1} y_j) \right| \quad (3.3)$$

The volume of each layer is calculated based on the Heronian formula for the frustum of a skewed prism given by equation 3.4.

$$V = \frac{h}{3} \left(B_1 + \sqrt{B_1 B_2} + B_2 \right) \quad (3.4)$$

where

B_1 is the area of one base

B_2 is the area of the other base

h is the perpendicular distance between the two bases

Therefore, an approximate volume of the net structure is given as the summation of the volumes of "m" pies and is expressed by equation 3.5.

$$V_{net} = \sum_{i=1}^m \frac{\Delta h_i}{3} \left(S_i + \sqrt{S_i S_{i+1}} + S_{i+1} \right) \quad (3.5)$$

The volume-remaining coefficient, C_v referred throughout the discussion of results in this thesis is defined as the ratio of transient volume to the original volume of the net structure given by equation 3.6.

$$C_v = \frac{V_T}{V_0} \quad (3.6)$$

where

V_T is the net structure volume at $T=t$

V_0 is the net structure volume at $T=0$

4 Analysis of a single-cage system

In order to understand the effect of accidental failures on the hydrodynamic response of multiple-cage system under currents and waves, it is essential to first study the responses of a single-cage system.

4.1 Model set-up

Figure 4.1 shows the visualization of the single-cage system with one fish cell in FhVis. The frame cables, bridles and the anchors have been labelled for easier referencing throughout this section. The positive X and Y axes are represented by the red and green arrows respectively, emerging out of the cage. The +Z axis, represented in blue, corresponds to the sea depth and is facing into the paper.

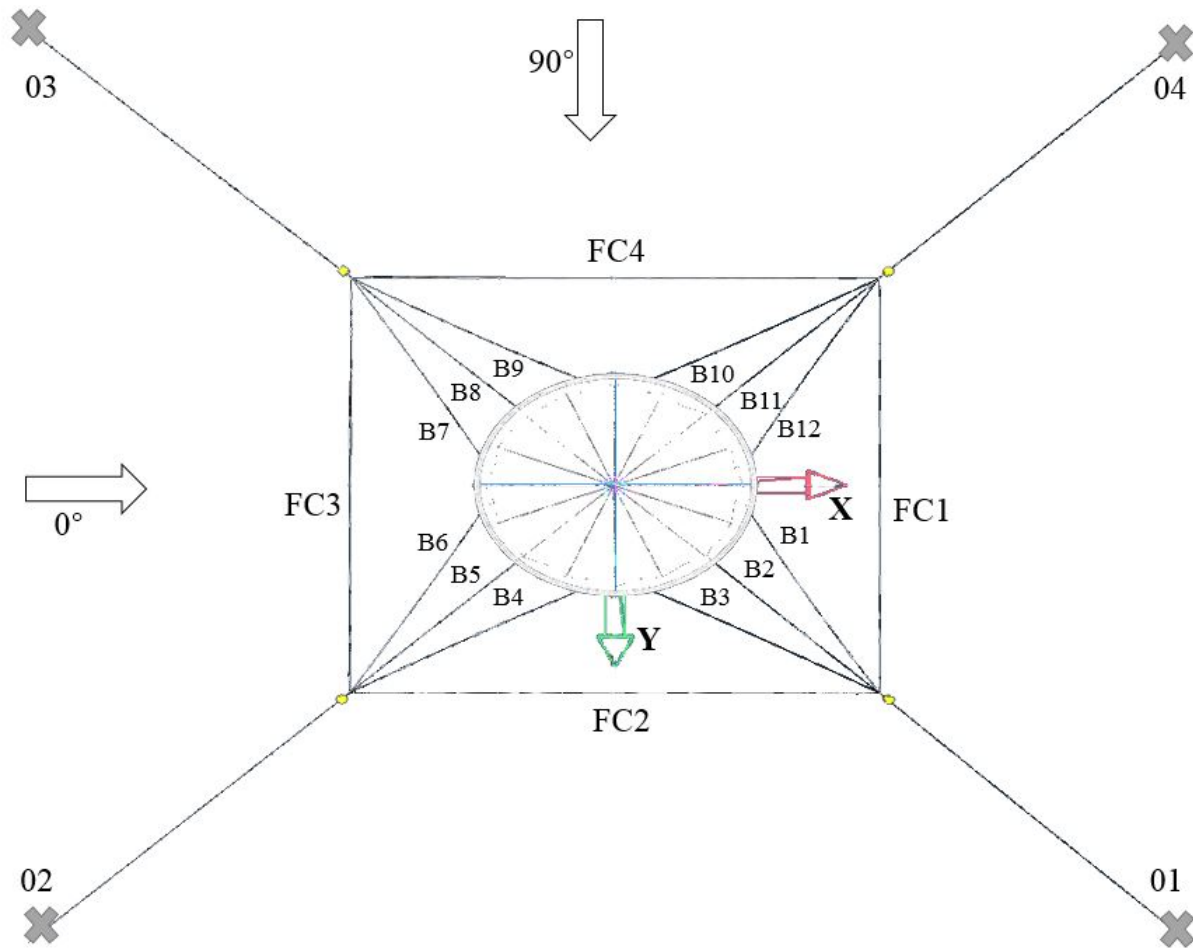


Figure 4.1: Plan view of the single-case system with a single fish cell as realized in FhVis

4.2 Simulation set-up

The loading and the environmental conditions for single-cage system are defined in this section.

4.2.1 Loading conditions

To study the responses of the completely intact model under accidental failures in this single-cage system, it was imperative to first discern the critical cables.

Several factors affect the current velocity in near sea waters and fjords. There is variability in the current velocities from 0.20 m/s to 1 m/s [38]. To account for this entire range, the model was subjected to 4 different current velocities ranging from 0.25 m/s to 1 m/s with intermediate increments as shown in the table 4.1. The current was assumed to be steady and uniform over the entire depth, and the heading direction is with respect to X-axis. The time run for each simulation was 600 seconds for the system to reach equilibrium.

Table 4.1: Environmental parameters for the single-cage model under pure currents condition

Case	Current	
	Velocity [m/s]	Direction
C0.25	0.25	0°
C0.50	0.50	0°
C0.75	0.75	0°
C1.00	1.00	0°

Figure 4.2 shows the responses of the single-cage system when the currents are flowing 0° to the intact model. It can be seen from the time-series of the volume-remaining coefficient in figure 4.2a that the model reaches equilibrium at around 500 seconds. Clearly, there is a significant change in the net volume from 80% at 0.25 m/s to nearly 40% at 0.50 m/s. The net deformations are critical for fish welfare and in such low volumes, it might not be feasible for the fish to flourish healthily and without stress. Therefore, a current velocity of 0.50 m/s is considered to be critical and is used for simulations under combined wave-current condition.

In order to determine the critically loaded cables of the model - mooring lines, frame cables and bridles, the mean tension forces were plotted for different cables in the mooring frame for the current velocity of 0.50 m/s. It can be seen from figure 4.2b that the axial mooring

lines 2 and 3 are in the direction of the flow of the current. Thus, experience highest tension forces than the other two mooring lines to the right of the Y axis of the cage. Also, the six bridles to the left of the Y-axis are in tension and the remaining six bridles located to the right of the Y-axis are slack for the similar reasons. This is captured in figure 4.2c where bridles B5, B6 and B4 experience high tension forces in increasing order. Frame cables FC2 and FC3 experience more tension forces than FC1 and FC4, and interestingly, none of them are exactly equal in magnitude as seen in figure 4.2d.

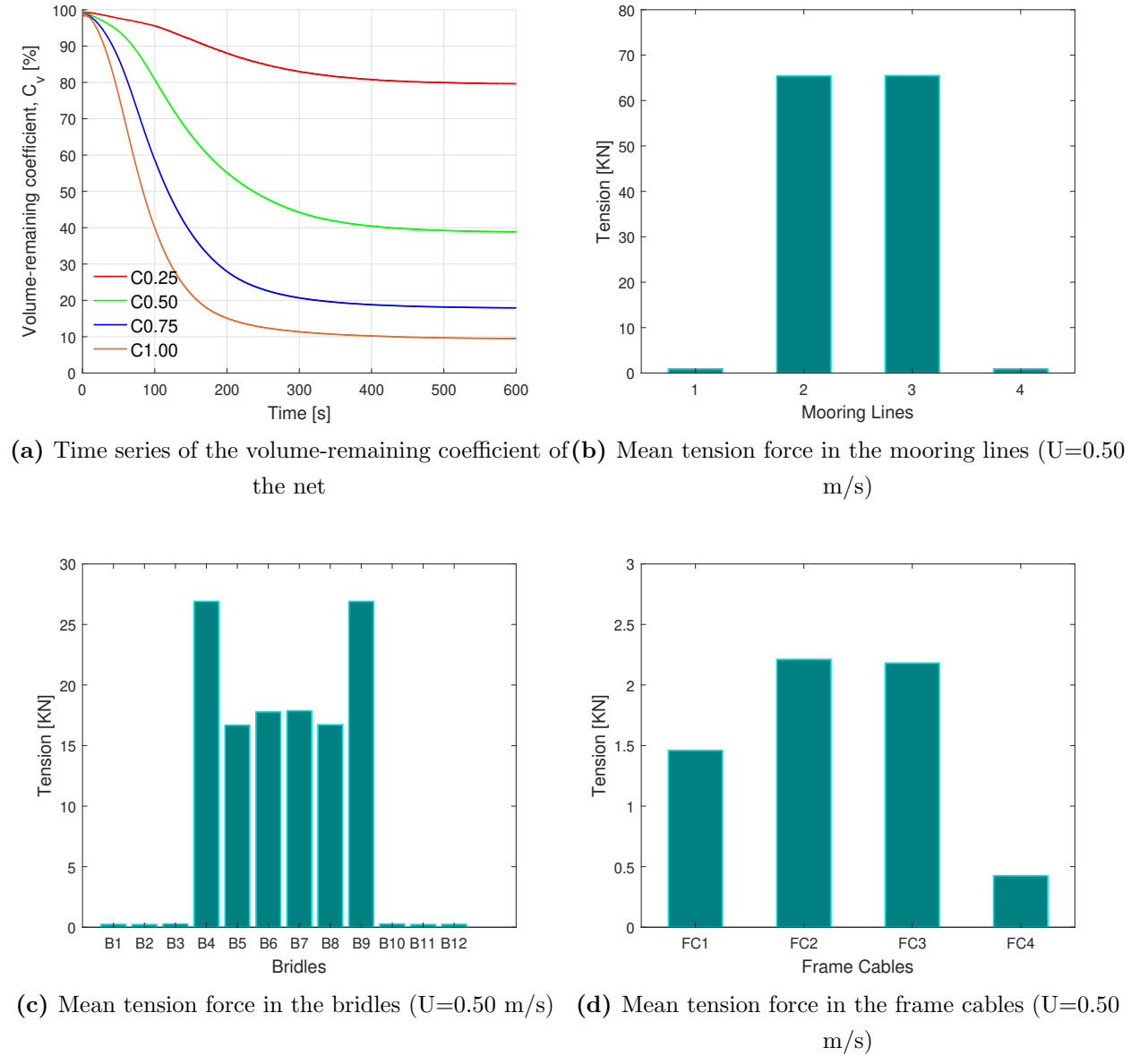


Figure 4.2: Response of the single-cage system when the currents are flowing 0° to the model

It is very essential for the bridles and frame cables to stay intact for the stability of the fish farm. An accidental failure in any of these critical cables can adversely affect the global loads in the mooring frame. These could be the result of several factors such as operational errors, vessel cage interactions or the environmental loading itself. Some cables could experience forces higher than they are designed to withstand. This, in turn, might start a chain of catastrophic events in the fish farm leading to an overall structural failure if the mooring lines are not designed to bear these additional loads. Therefore, in addition to the environmental loads, it is imperative to analyse the responses of the fish cages under accidental failures. The different loading conditions can thus be defined below in table 4.2.

Table 4.2: Loading conditions for the single-cage model

Case	Description
LC1	Intact model
LC2	Failure in frame cable FC2
LC3	Failure in bridle B4
LC4	Failure in bridle B5
LC5	Failure in bridle B6

4.2.2 Environmental loading

When the fish is farmed at sea, the currents and waves are present simultaneously. Therefore, it becomes important to study the effect of waves on the response of the cages already exposed to current loads. The current loading is static as it is constant in nature and the wave forces are dynamic in nature as they contribute to a time-varying load on the system. For the analysis under the combined wave-current condition, the waves and currents are assumed to be approaching the cage from the same direction i.e. with a 0° heading.

The environmental parameters for the combined wave-current condition are shown below in the table 4.3. The time run for each simulation was 600 seconds for the system to again reach equilibrium. As mentioned in chapter 3, the different models query the shared sea environment model in FhSim. For waves, the input template seeks two important parameters - the wave number and wave frequency. Wave number is a function of wavelength. Thus, three different wavelengths corresponding to 1D, 1.5D and 2D are defined for the simulation runs, where D is the diameter of the fish cage. The waves are regular and are based on the linear wave theory.

Table 4.3: Environmental parameters for the single-cage model under combined wave-current condition

Case	Current		Wave				
	Velocity [m/s]	Direction [Degrees]	Height [m]	Length [m]	Period [s]	Steepness [-]	Direction [Degrees]
C0.50H2WL50	0.50	0°	2	50	6	0.04	0°
C0.50H2WL75	0.50	0°	2	75	6	0.03	0°
C0.50H2WL100	0.50	0°	2	100	6	0.02	0°

4.3 Results and discussions

The results and discussions for the single-cage model are divided into two sections - the intact model which defines the first loading condition LC1, and the sensitivity study on different loading conditions with accidental failures and environmental conditions.

4.3.1 Responses of a single-cage model under intact condition

Figure 4.3 shows the time-series response of the single cage model for different current velocities with a 0° heading.

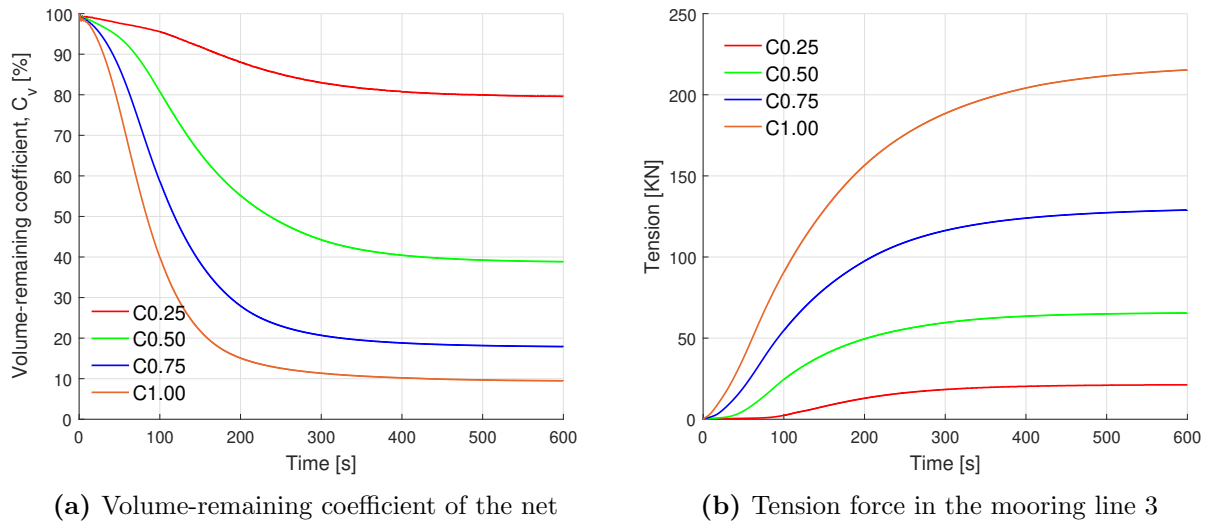


Figure 4.3: Time-series response of the single-cage system when the currents are flowing with a 0° heading

Once again, it can be seen that there is significant drop in volume for current flowing with velocities higher than 0.25m/s as seen in figure 4.3a. However, the tension forces in mooring line 3 are not proportional to the volume reduction as seen in figure 4.3b.

Figure 4.4 shows the effect of different current velocities with a 0° heading on the tension forces in the critical cables that define the loading conditions.

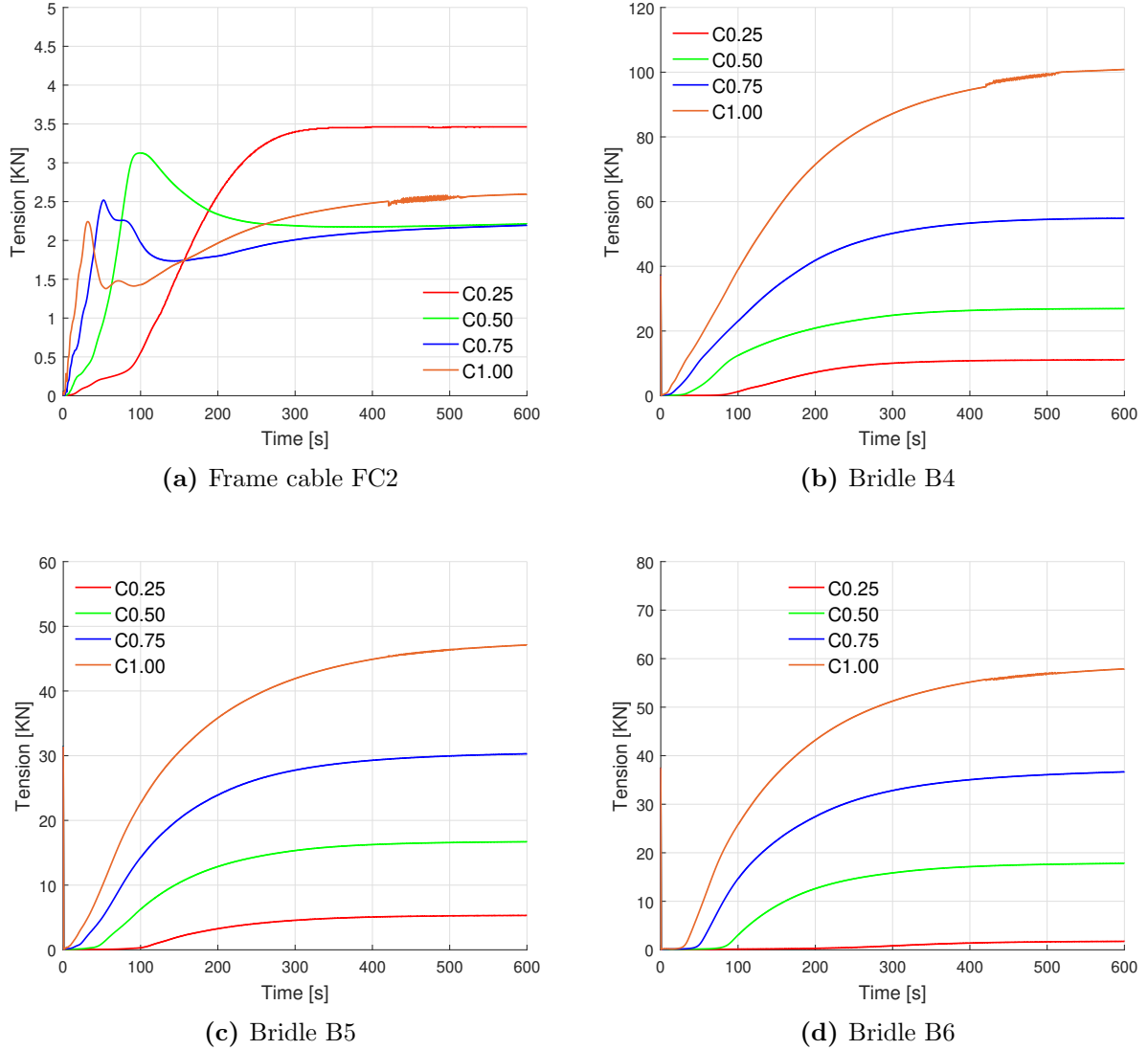


Figure 4.4: Time-series of the tension forces in the critical cables of the single-cage system when the currents are flowing with a 0° heading

For all current velocities except 0.25 m/s, all the frame cables experience a sudden initial

rise in the tension forces in the first 100 seconds of the simulation as clearly seen in figure 4.4a. Interestingly, the tension force decreases in magnitude with the increasing current velocity. There is a drop for a few more seconds and then, it increases again with an increase in time until the system reach equilibrium. For 0.50 m/s current velocity, the peak drops smoothly before reaching equilibrium unlike the higher velocities which exhibit double peaks. However, the system reaches equilibrium after attaining the maxima for the velocity of 0.25 m/s. Some inherent oscillations can be observed in the plot for the highest current velocity of 1 m/s.

For the bridles B4, B5 and B6, the tension forces increase with an increase in the current velocity. The highest loads are experienced by the bridle B4 as seen in figure 4.4b. It is followed by bridles B6 and B4 as shown in figures 4.4d and 4.4c respectively. It can be confirmed from the plots that these bridles also exhibit some inherent oscillations around the same time as the frame cable FC2. They are prominent in bridle B4 than the other two bridles although all three of them are connected to the frame cable FC2 at the connection plate. These oscillations are transferred from the net structure to the mooring frame via the floating collar.

There should not be any inherent oscillations when the model is exposed to pure currents. A convergence study regarding the integration method and aize of the time step for the numerical analysis is required before developing the model B with multiple-cage system. It is very important to perform these studies while using numerical tools. For the current velocity of 0.50 m/s, the tension forces in all the three bridles is under 30 KN and it would be interesting to see the effect of addition of waves on the steady state achieved under pure current condition for the initial 600 seconds.

Figure 4.5 shows the effect of regular waves on volume-remaining coefficient of the net. Addition of waves in the next 600 seconds leads to a further reduction in the mean C_v and it exhibits periodic fluctuation. For a particular wave height, the mean value and the amplitude of C_v about that mean value increases with an increase in the wavelength.

According to the Airy wave theory, the maximum wave particle velocity is inversely proportional to the wavelength. Thus, it decreases with an increase in the wave length. It is also directly proportional to the wave amplitude and so the wave height. When the wavelength is equivalent to the diameter of the fish cage which is 50 metres and the wave height is 2 metres, the maximum wave particle velocity at the free surface is approximately 1.11 m/s.

This implies that the wave particle velocity at the free surface is more than twice the value of the current velocity. If the cage net volume is reduced to 39% of the original volume in the first 600 seconds under pure currents, the effect of wave load on a further reduction in the net volume can be strikingly significant. The cage volume is further reduced by 15%, leaving the cultivation volume at around 14% of the original volume under this particular wave. This is almost a 64% drop from pure currents condition.

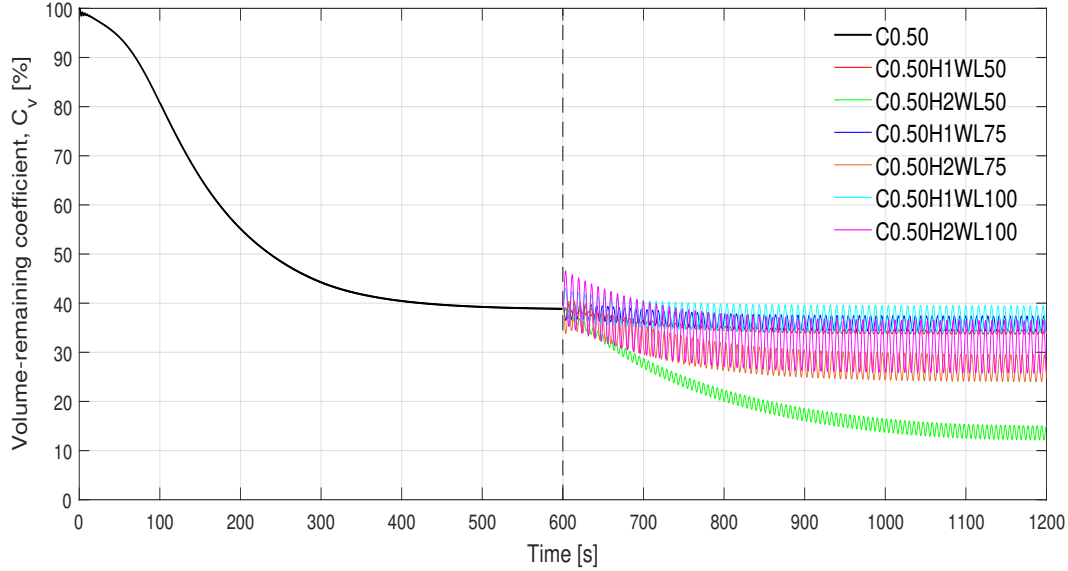


Figure 4.5: Effect of regular waves on the volume-remaining coefficient of the net of the single-cage model subjected to 600 seconds of prior loading under pure currents

Figure 4.6 shows the effect of waves on tension forces in mooring line 3 of the cage. Addition of waves in the next 600 seconds leads to an increase in the mean tension and it does exhibit periodic fluctuation. However, the amplitude is quite stable as compared to the volume-remaining coefficient discussed earlier. It can be seen that the mean value of tension forces increases with a decrease in the wavelength.

The wave steepness mentioned in table 4.3 is defined as the ratio of wave height to the wavelength. The period is proportional to the wavelength. Thus, a shorter wave period will have a higher wave steepness. When the regular waves hit the cage, the drag forces acting on the net are transmitted to the mooring lines via the floating collar and the bridles. Clearly, the tension force in the mooring line increases with an increase in the wave steepness. By the time the model is subjected to the case C0.50H2WL50 with a 0.04 steepness, the tension forces in the mooring line under study are 110KN at the steady state. This is nearly a 70%

increase as compared to the pure currents condition. This is a significant rise and must be accounted for while designing the mooring lines to withstand such severe environmental conditions.

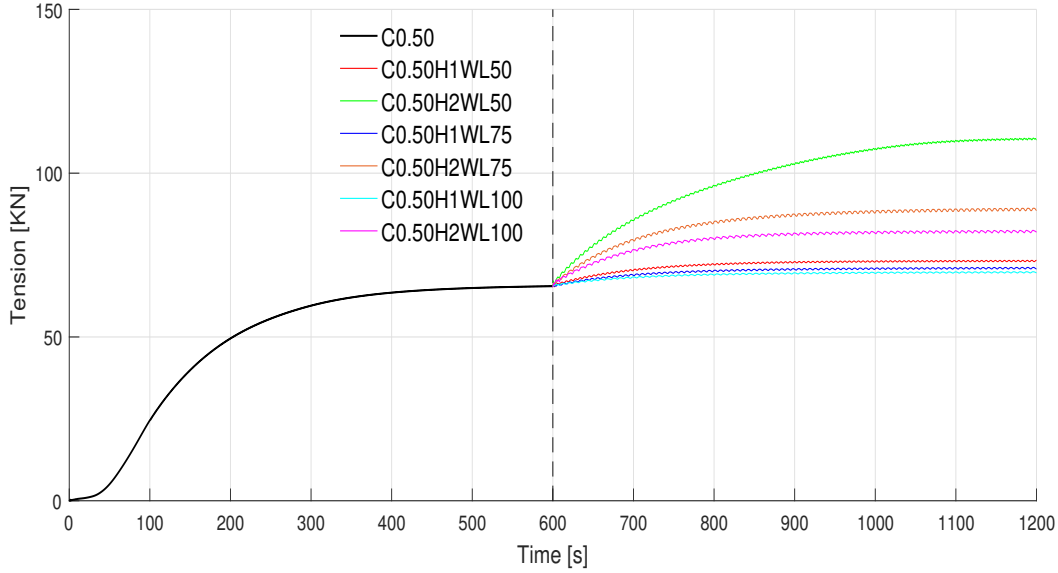


Figure 4.6: Effect of regular waves on the tension force in the mooring line 3 of the single-cage model subjected to 600 seconds of prior current loading

Figure 4.7 shows the effect of waves on the tension forces in the frame cable FC2 of the mooring frame of the cage. Addition of waves in the next 600 seconds only affects the mean tension slightly, although it exhibits periodic fluctuation with high amplitudes.

It can not be clearly seen in the plot, however, the amplitude decreases with a change in the wavelength from 50 metres to 75 metres. At 100 metres wavelength, it is the same as 75 metres which indicates that the fluctuations could be significant when the wavelength is in whole multiples of the cage diameter and does not vary much for the intermediate values.

It can be noticed that the lower extreme of the amplitude is close to 0. The cable is under tension at one moment and then either slacks or compresses in the other. It is discussed earlier for figure 4.4a that there are several inherent oscillations during analysis under pure currents. This is certainly an area of improvement in the net model before developing the second model with multiple fish cages.

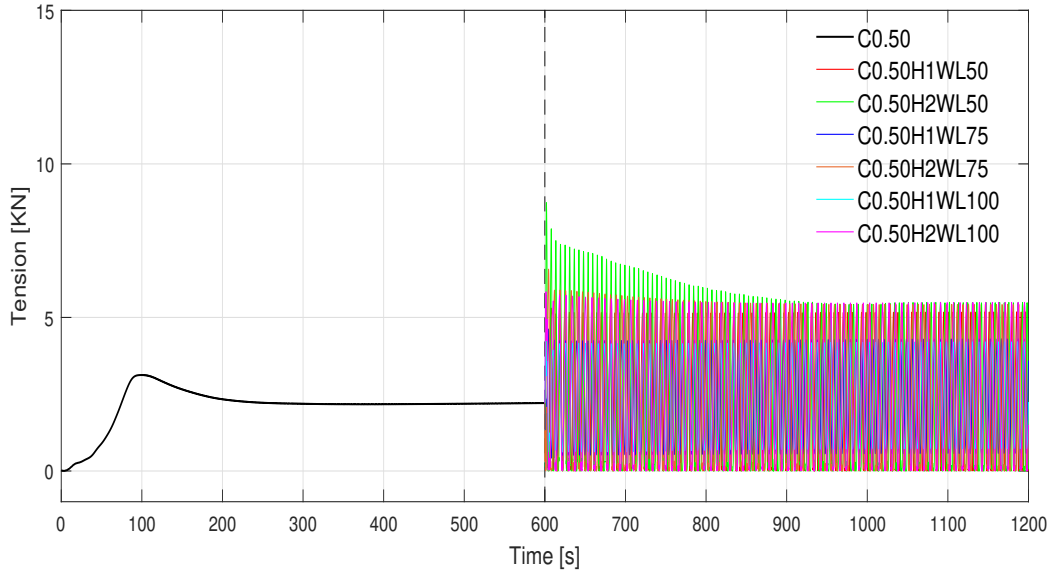


Figure 4.7: Effect of regular waves on the tension force in the frame cable FC2 of the single-cage model subjected to 600 seconds of prior current loading

The next three figures 4.8, 4.9 and 4.10 show the effect of waves on the tension forces in the bridles B4, B5 and B6 of the cage. Addition of waves in the next 600 seconds leads to an increase in the mean tension and it exhibits periodic fluctuation about that mean value.

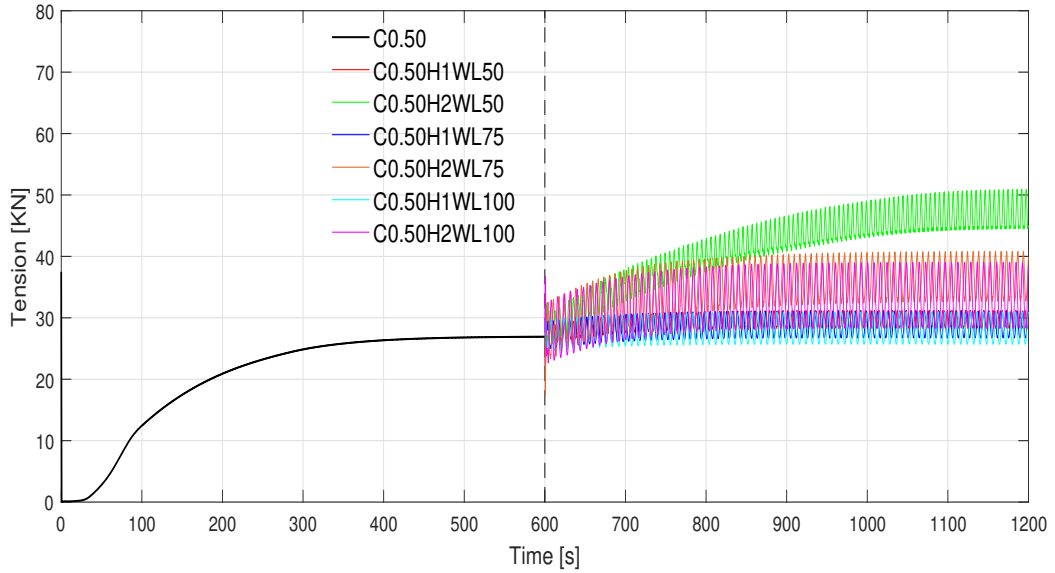


Figure 4.8: Effect of regular waves on the tension force in the bridle B4 of the single-cage model subjected to 600 seconds of prior current loading

For all the bridles, it can be seen that the mean value of tension force decreases with an increase in wavelength, more significantly for the higher wave height of 2 metres. There is only a slight change between the mean tension forces of the bridles for the 1 metre wave height. The drag forces acting on the net are transferred to the mooring lines via these cables and irrespective of the magnitude, they must respond in a similar pattern to a particular environmental loading, in theory.

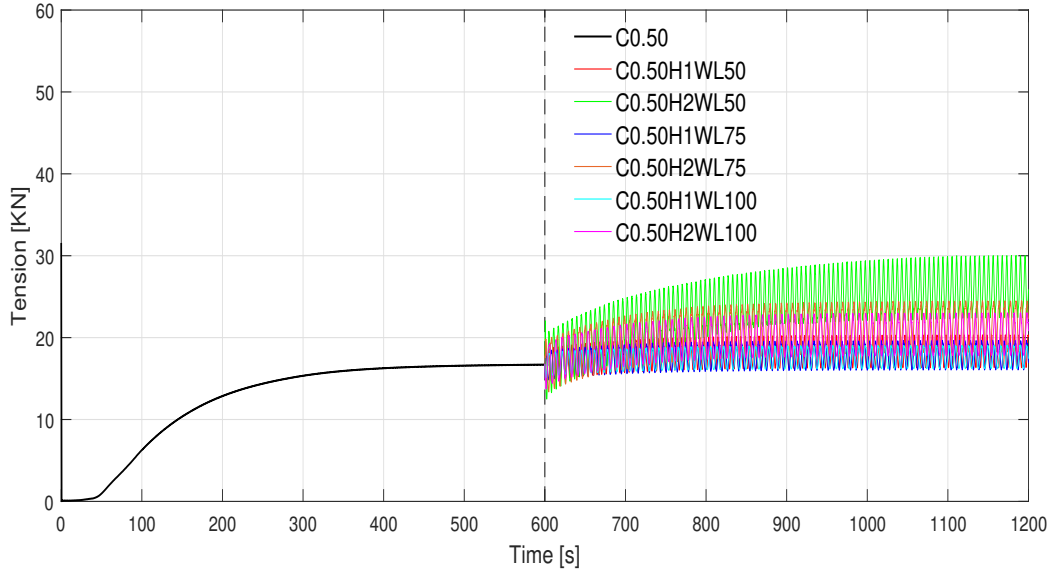


Figure 4.9: Effect of regular wave on the tension force in the bridle B5 of the single-cage model subjected to 600 seconds of prior current loading

By the time the model is subjected to the steepest wave loading at the steady state, the mean tension forces in the three bridles B4, B5 and B6 are 47 kN, 26 kN and 32 kN respectively which is nearly a 75%, 53% and 78% increase as compared to analysis under pure currents. Interestingly, the variation of amplitude of the tension forces varies from bridle to bridle. While for B4, the amplitude of the mean tension force increases with an increase in the wavelength, it approximately remains the same with an increase in wavelength for B5. For B6, the response is opposite and there is a decrease in the mean tension force amplitude with an increase in the wavelength. The circular floating collar is based on the potential theory and follows the wave motion. Therefore, the most probable reason for the variation amongst the bridles is the respective location of their fastening points on the floater.

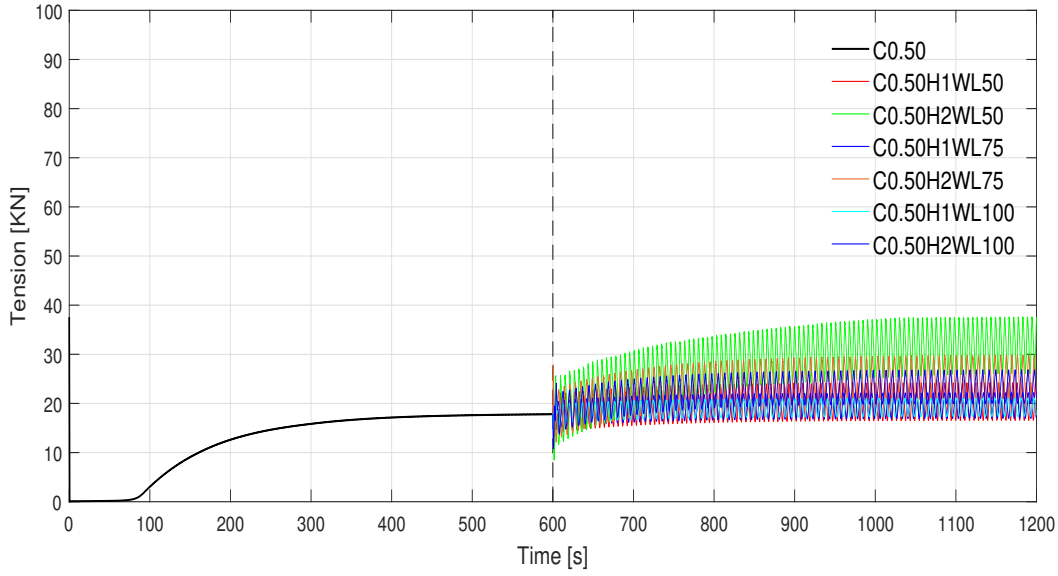


Figure 4.10: Effect of regular waves on the tension force in the bridle B6 of the single cage model subjected to 600 seconds of prior current loading

Table 4.4 below lists the mean values of the volume-remaining coefficient and the tension forces in the cage net and the critical cables. These have been referenced throughout the presentation of results and their discussions earlier in this section.

Table 4.4: Mean values of volume-remaining coefficient and tension forces for net and critical cables respectively of the intact model of single-cage system subjected to different environmental loads

Case	Volume-remaining Coefficient [%]	Tension Forces [kN]				
		ML3	FC2	B4	B4	B6
C0.50	39	65	2	27	17	18
C0.50H1WL50	34	73	3	30	18	20
C0.50H2WL50	14	110	2	47	26	32
C0.50H1WL75	36	71	2	29	18	20
C0.50H2WL75	27	89	2	36	22	25
C0.50H2WL100	37	70	2	28	18	19
C0.50H2WL100	31	82	3	33	20	23

It can be clearly seen from the table that for a particular wave height, the volume-remaining

coefficient decreases with a decrease in the wavelength and is extremely low when the wave length is the same as the diameter of the fish cage. The corresponding effect of this reduction in net volume due to higher drag can be seen in the mean tension force of the mooring line ML3. Frame cable FC2 experiences loads under 3KN and exhibit small changes for the range of environmental parameters in the simulation matrix. For bridles, B4 experiences the highest loads followed by B6 and B5.

4.3.2 Responses of a single-cage model under different loading conditions

Sensitivity analysis is important when using numerical tools. These studies are performed to investigate how certain independent variables impact a dependent variable. To see the effect of accidental failures on the volume-remaining co-efficient of the net and the tension forces in mooring line 3, the different loading conditions as tabulated in the table 5.2 were simulated for the same environmental parameters.

For pure current condition, figure 4.11 shows the effect of accidental failures in different cables on the net volume and the tension forces in mooring line 3 under pure current loading.

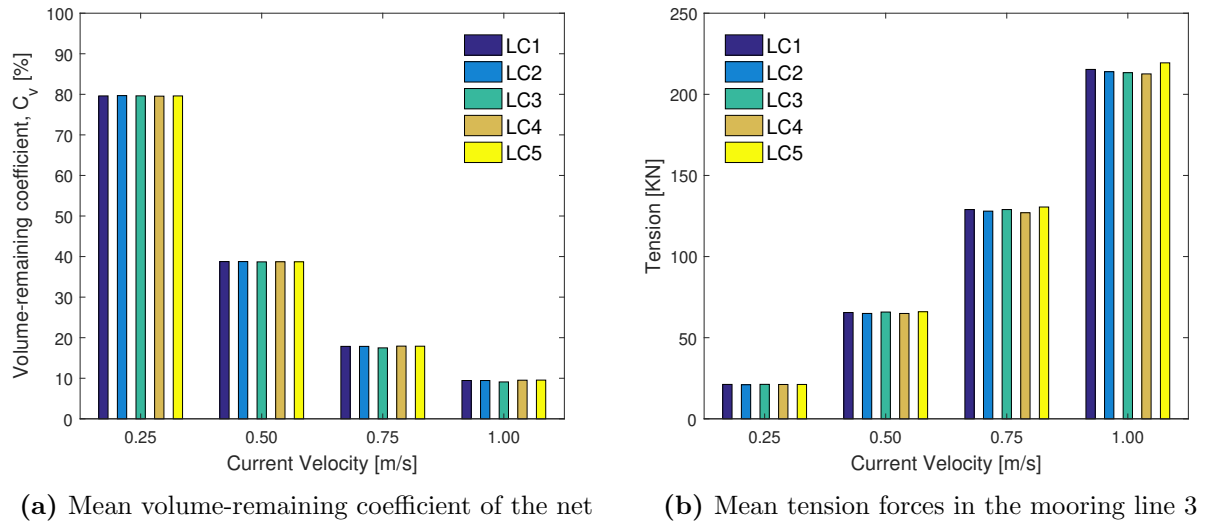


Figure 4.11: Effect of accidental failures in cables defined by the loading conditions on the responses of the single-cage model (pure current condition)

It can be seen that the mean volume of the net is not significantly affected by the rupture in the respective cables. However, there are noticeable differences in the tension forces for the different loading conditions. The changes are more significant for higher current velocities

and can be clearly distinguished for 1 m/s. The mean tension force is relatively lower for LC4 with failure in bridle B5 and higher for LC5 with failure in bridle B6 as compared to the intact model in LC1.

The loads are transferred between the structural elements and on to the anchors in the sea bed. It is seen above that there are no significant changes in the mean tension forces in the mooring line 3. The bridles, frame cables and the mooring lines interact at the connection plate located at the corners of the mooring frame. Therefore, it might be possible that upon failure in a particular critical cable, the additional loads are transferred on to the neighbouring cables instead of the mooring lines. To further analyse this, the mean tension forces in the critical cables under different loading conditions were plotted.

Figure 4.12 shows the variation of mean tension forces in the critical cables FC2, B4, B5 and B6 under different loading conditions. To reiterate, the model is intact in loading condition LC1, the frame cable is broken in LC2, and the bridles B4, B5 and B6 are broken in LC3, LC4 and LC5 respectively.

It can be seen from figure 4.12a, the tension forces in the frame cable FC2 are highest at a current velocity of 0.25 m/s. It decreases for 0.50 m/s, remains the same for 0.75 m/s and then increases for 1 m/s. As expected, it is zero for LC2 where FC2 itself is broken. The tension forces drop significantly low for LC3 where B4 is broken. This is explained by the figures 4.12c and 4.12d where B5 and B6 share the additional loads when B4 is broken. Similarly, an increase can be seen in the mean tension force of FC2 for LC4 where bridle B5 is broken. The additional loads are shared by B4 and B6 as seen in figures 4.12b and 4.12d.

However, the highest tensions experienced by the frame cable FC2 are for LC5 where bridle B6 is broken. It rises significantly for the current velocities 0.50 m/s and 0.75 m/s. For the current velocity 0.50 m/s, the magnitude of the mean tension force under LC5 is nearly 400% higher as compared to LC1 where the model is intact. Thus, an accidental failure in bridle B6 could lead to a failure in the frame cable FC2 if the latter is not designed to withstand at least 10 KN under such extreme conditions.

When the frame cable FC2 is broken i.e. in LC2, bridle B4 does not experience any significant changes in the mean tension force as compared to the intact model. This is also true for bridle B6 mean tension forces but for higher current velocities than 0.25 m/s. Naturally, B4 and B6 has zero values for LC3 and LC5 respectively where they are broken. B4 and B6 experience highest tension forces under LC4 because of the failure in bridle B5 which is the

immediate neighbour for both the bridles. Therefore, bridle B5 is critical for the design of B4 and B6.

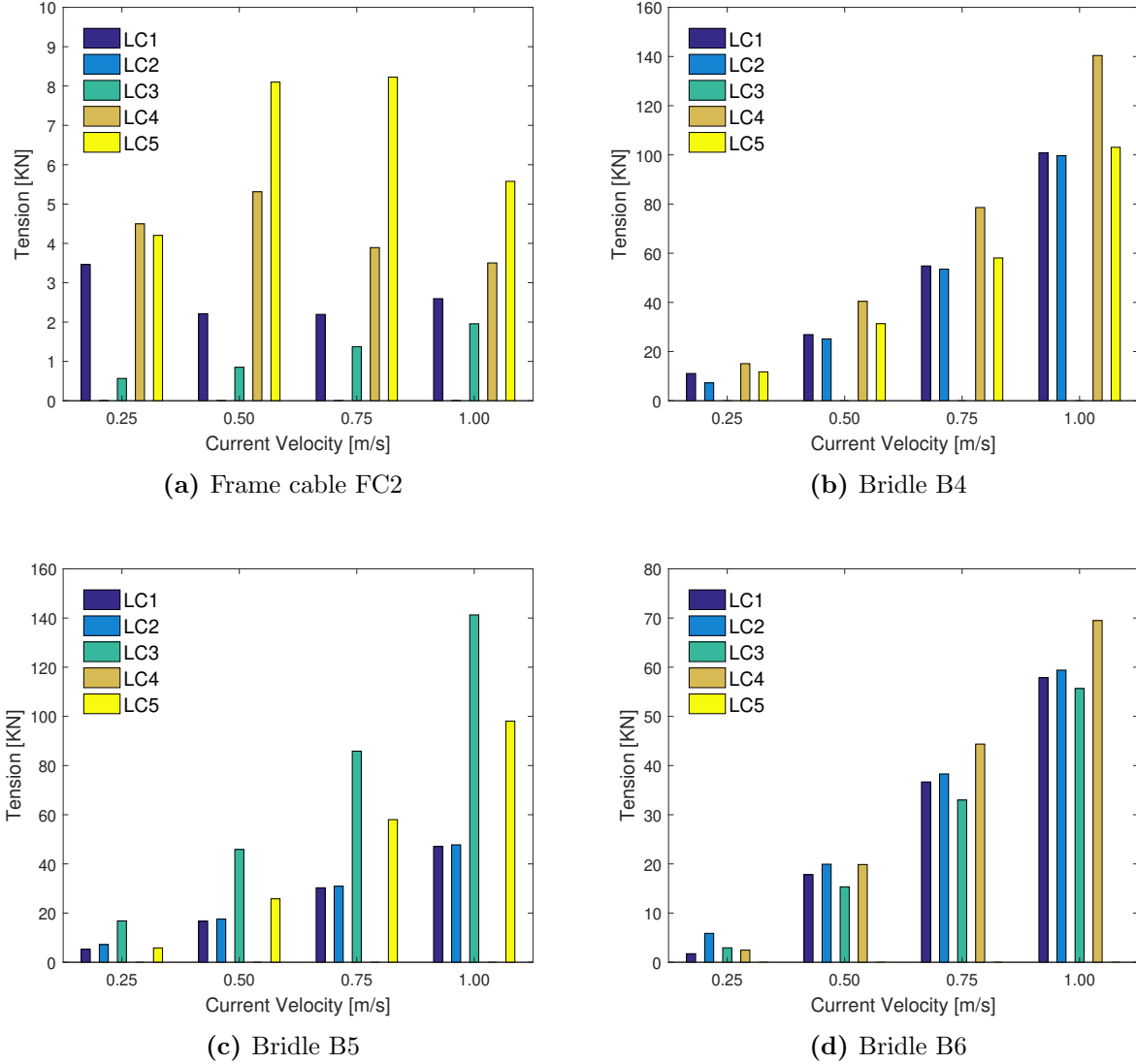


Figure 4.12: Effect of accidental failures in cables defined by the loading conditions on the mean tension forces in the critical cables of the single-cage model (pure current condition)

It is also evident that the magnitude of tension forces in B6 is lowest amongst the set of these 3 bridles, nearly half as compared to B4 and B5. The horizontal distance of B6 fastening point on the floating collar is longest as compared to the other two bridles. The drag forces acting on the net are transferred to the top collar which translates in the direction of the flow of the current. This motion is restricted by the bridles to the left of the +Y-direction

of the cage. The end point of a bridle attached to the floater can only translate along the circumference of the imaginary circle with the centre point as the connection plate. When the floater translates in +X direction, the B4 bridle experiences the maximum tension force because the trajectory of the fastening point does not coincide much with the trajectory of the bridle.

Bridle B5 exhibits similar variations with B4 and B6 in terms of increasing mean tension forces with an increase in the current velocity. It experiences the highest forces under LC3 where B4 is broken and comparatively lower forces under LC5 where bridle B6 is broken because the frame cable FC2 experiences these additional loads instead.

Moving on to the dynamic analysis, figure 4.13 shows the effect of accidental failures in different cables on the net volume and the tension forces in mooring line 3 under combined waves-current loading. The bar height represents the mean values for the steady states and the error bars represent the dynamic fluctuation from that mean value.

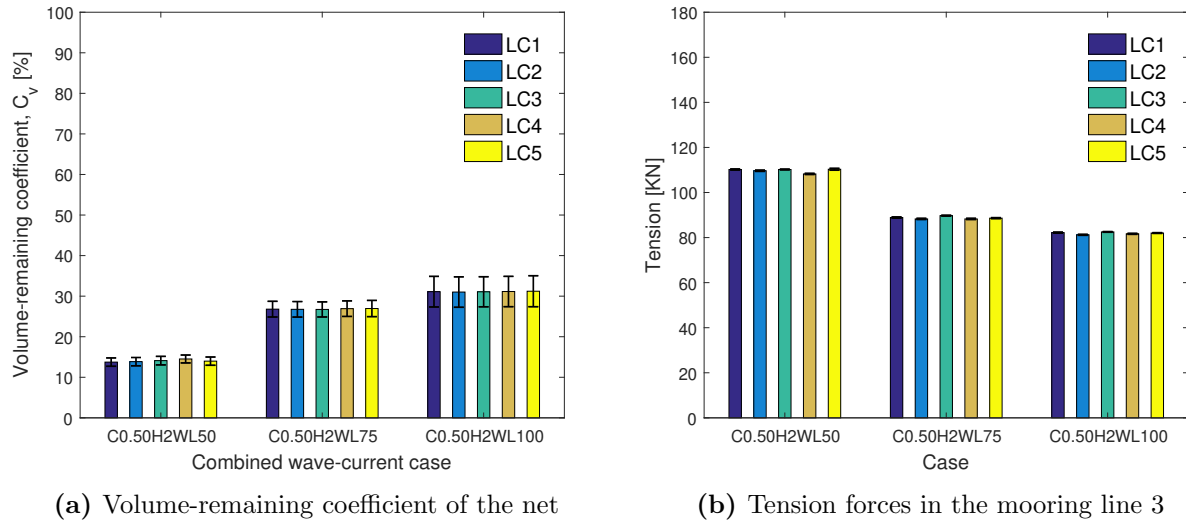


Figure 4.13: Effect of accidental failures in cables defined by the loading conditions on the responses of the single-cage model (combined wave-current condition)

It can be seen in the figure 4.13a that the volume-remaining coefficient for the intact model increases with an increase in the wavelength. So, the net experiences highest deformations for the steepest regular wave case C0.50H2WL50. The partially submerged floating collar follows the wave motion and the nodes of net structure below the water surface follow the circular motion of the wave particles. As stated earlier, the wave particle velocity is the

highest for this particular case. It reduces to 4% of its free-surface value at about 25 metres which is within the range of the depth of the net. Therefore, the wave loads accentuate the net deformation already caused by pure current loading. It can also be seen that the different loading conditions do not significantly affect the C_v for the same environmental parameters. The standard deviation increases with an increase in the wavelength. Therefore, the higher wavelength will give a higher amplitude of the fluctuation.

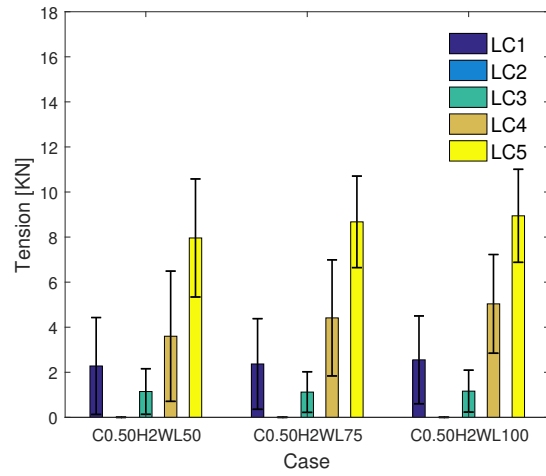
The mean tension forces in mooring line 3 increase in-line with the net deformation as seen in figure 4.13b. Higher drag force means higher the net deformation, lower volume-remaining coefficient and higher mooring line loads. The amplitude of fluctuation is negligible as seen by the error bars in the plot. This is because the tension forces transferred to the mooring lines are quite stable over the range of wave loads the model is subjected to. As seen earlier, the bridles experience larger amplitudes than the mooring line 3 because they are directly fastened to the floating collar.

Figure 4.14 shows the effect of accidental failures in different cables on the tension forces in the critical cables of the single-cage model under combined waves-current loading. It can be seen in figure 4.14a that the mean value of tension forces in the frame cable FC2 increase with an increase in the wavelength. The increase is not significant for LC1 where the model is intact and for LC3 when bridle B4 breaks, however, it is considerable for LC4 and LC5 where bridle B5 and B6 is broken respectively. The amplitude, on the other hand, decreases with an increase in the wavelength.

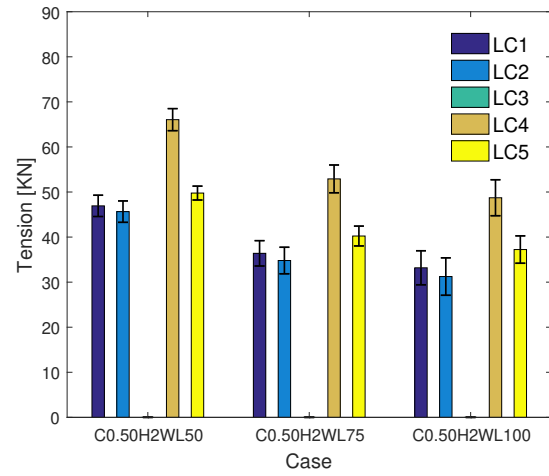
For bridle B4 in figure 4.14b, the mean tension force decreases and the amplitude increases with an increase in the wavelength. Interestingly, the loads experienced by this bridle in the absence of any accidental failures are slightly higher than the mean tension forces under LC2 where frame cable FC2 is broken. Instead, there is an increase in the loads experienced by the immediate neighbouring cable B5 as seen in figure 4.14c.

For bridle B5 and B6, the mean tension force decreases but the amplitude of fluctuation decreases unlike B4. Interestingly, the loads experienced by this bridle for LC3 where bridle B4 is broken are lower than the mean tension forces for LC1 when the model is intact. There is a significant increase in the mean tension force in B5 for LC3 instead because it is the immediate neighbouring bridle to B4. Clearly, B5 should be able to withstand these additional loads. As seen in figure 4.14, the amplitude of fluctuation about the mean tension force for bridle B6 is the highest for the steepest wave case for loading condition LC4 where

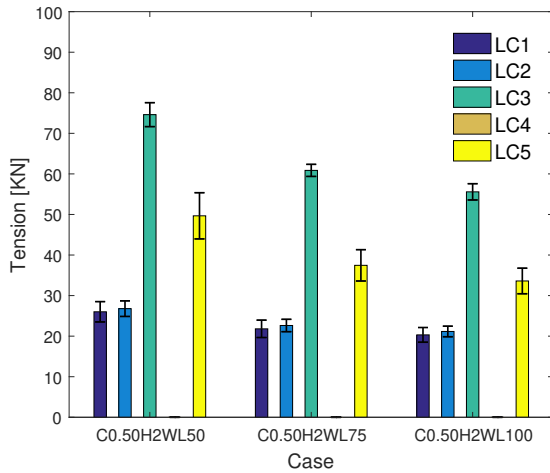
bridle B5 fails.



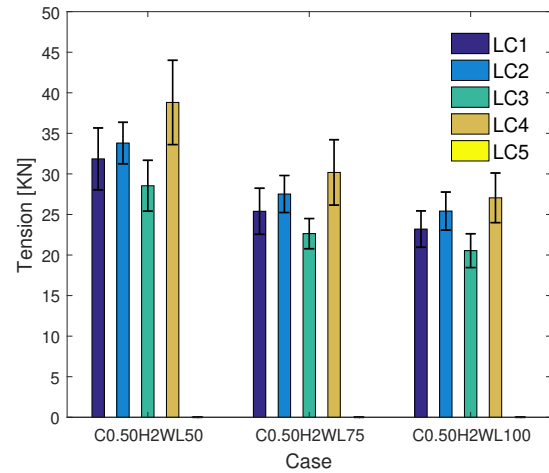
(a) Frame cable FC2



(b) Bridle B4



(c) Bridle B5



(d) Bridle B6

Figure 4.14: Effect of accidental failures in cables defined by the loading conditions on the mean tension forces in the critical cables of the single-cage model (combined wave-current condition)

5 Analysis of a multiple-cage system

After the preliminary study on a single-cage system as presented in chapter 4, a numerical model of a fully functional fish farm with 1x3 cell configuration was developed. A configuration like this is beneficial in several ways. If installed parallel to the currents flowing alongshore, the main axial mooring line is forced to remain straight during the installation of the farm [39]. It further enhances the shielding effect from each cage to the successive cages. Although the shielded cages experience lesser deformations than the first cage in the direction of the flow of the currents, the shielding reduced the flow of fresh water and oxygen to the fishes in these cages.

5.1 Model set-up

Figure 5.1 shows the plan view of the multiple-cage system as visualised in FhVis. The cables and the anchor points have been labelled for easier referencing throughout this chapter. The +X and +Y axes are represented by the red and green arrows respectively, emerging out of cell 1. The +Z axis is represented by a blue arrow and is facing into the paper.

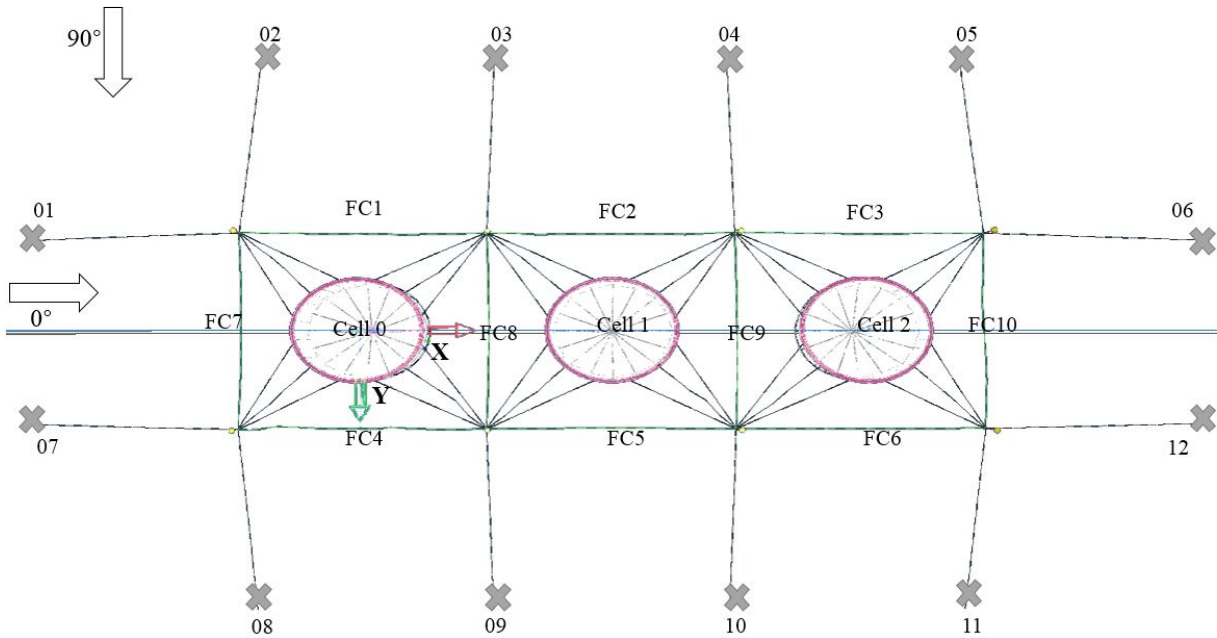


Figure 5.1: Plan view of the multiple-cage system in a 1x3 cell configuration as realised in FhVis

5.2 Simulation set-up

The loading and environmental conditions for multiple-cage system are defined in this section.

5.2.1 Loading conditions

A metocean measurement programme of waves and currents was initiated in early 2011 at five different locations in the northern North sea. This was a collective initiative of the researchers at Equinor ASA, the Norwegian university of science and technology in Trondheim and the university of Stavanger. The current was measured every 10 minutes and the project was completed in the second half of 2015. The summary statistics of the current measurements show that the mean current velocity, at around 80 metres depth at a location off Norwegian coast, is 0.18 m/s with a maximum of 0.96 m/s [40].

To study the behaviour of the completely intact multiple-cage model in this range, it was subjected to 5 different current velocities ranging from 0.20 m/s to 1 m/s with intermediate increments as shown in the table 5.1. The current could usually come in perpendicular or in some kind of inclination to the +X axis of the fish farm. It becomes imperative to examine more combinations of oblique. currents. Therefore, two current headings were considered - 0° (parallel to +X axis) and 90° (perpendicular to +X axis). The current was assumed to be steady and uniform over the entire depth, and the heading direction is with respect to X-axis. The time run for each simulation was 600 seconds for the system to reach equilibrium.

Table 5.1: Environmental parameters for the multiple-cage model under pure currents condition

Case	Current	
	Velocity [m/s]	Direction
C0.20	0.20	$0^\circ/90^\circ$
C0.40	0.40	$0^\circ/90^\circ$
C0.60	0.60	$0^\circ/90^\circ$
C0.80	0.80	$0^\circ/90^\circ$
C1.00	1.00	$0^\circ/90^\circ$

Figure 5.2 shows the time-series of the volume-remaining coefficient of the net structure of cell 1 of the multiple-cage system under current headings 0° and 90° . It can be seen that the plots for both the headings are in equilibrium beyond half-time of the simulation run i.e. 300 seconds.

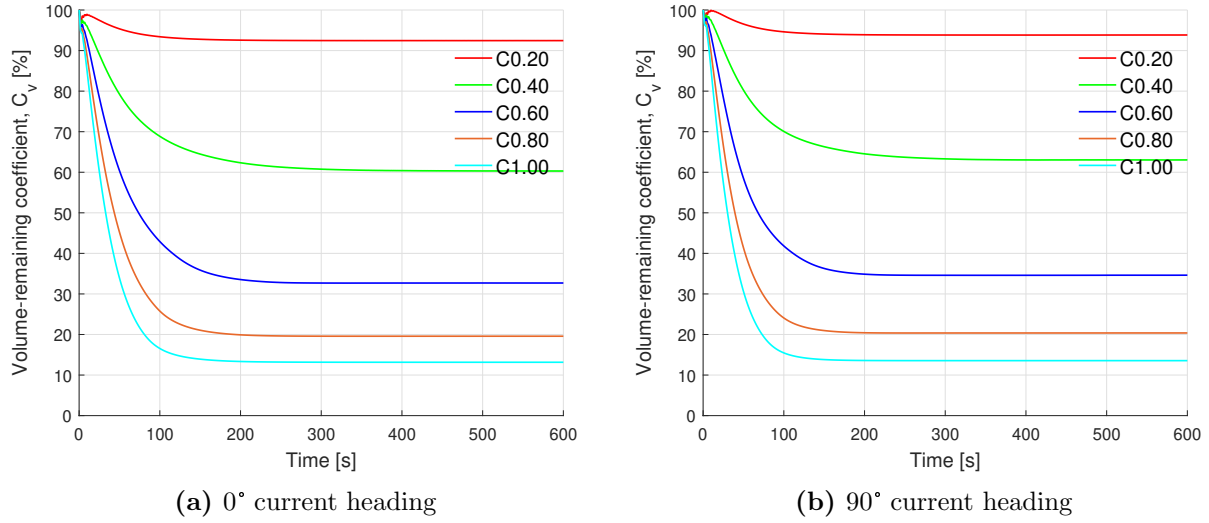


Figure 5.2: Time series of the volume-remaining coefficient of the net structure of cell 1 of the multiple- cage system under pure currents condition

It can be clearly noticed from figure 5.2a that for 0° current heading, the current velocities higher than 0.20 m/s lead to substantially large net deformations. The net volume is reduced to 60% of the original volume and a further drop beyond this value does not seem to provide sufficient living space for the fish. Therefore, a current velocity of 0.40 m/s is considered to be critical and is used for simulations under combined wave-current condition.

For 90° current heading as shown in figure 5.2b, the results are alike for the higher current velocities then 0.60 m/s. For instance, for 0.40 m/s, the C_v is 63% which is 3% higher as compared to C_v when the currents are flowing with 0° heading. This intact model defines the first loading condition of the simulation matrix and is referred to as LC1 hereafter.

In order to determine the critically loaded mooring lines of the system for current velocity of 0.40 m/s, the mean tension forces were plotted as shown in figure 5.3. For 0° currents, the highest tensions are experienced by the axial mooring lines 1 and 7 as evident from figure 5.3a. Thus, it is important to study the effect of the accidental failures in the other cables on the response of either of these two mooring lines, for instance mooring line 1. Due to model symmetry about X-axis of the model, the magnitude of the mean tension force in the mooring lines on either side of this axis is similar.

Figure 5.3b shows that the highest mean tension forces are experienced by mooring lines 3 and 4 for currents with a 90° heading to the model. The effect of accidental failures in the

other cables on the response of either of these two mooring lines, for instance mooring line 3 is investigated. The model is symmetrical about +Y axis of cell 2, the magnitude of mooring line 3 is similar to mooring line 4, line 1 is similar to line 6 and line 2 is similar to line 5.

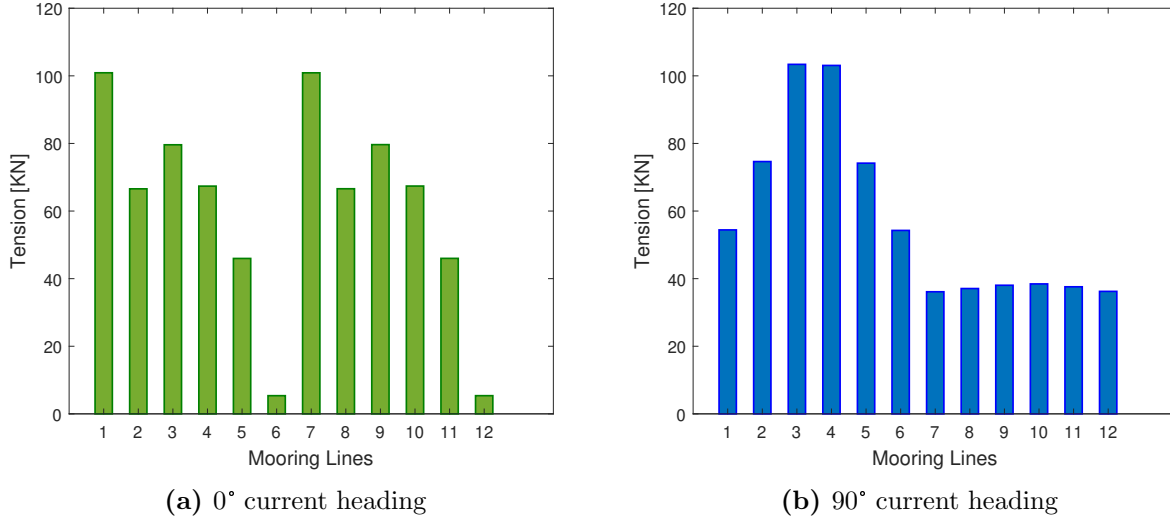


Figure 5.3: Mean tension forces in mooring lines of the multiple-cage system ($U=0.40$ m/s)

It is very essential for the mooring frame to stay intact in order to maintain equilibrium of forces in the system. Therefore, in order to determine the critically loaded frame cables, the mean tension forces in all the cables of the mooring frame were plotted as shown in figure 5.4. It is clearly evident from figure 5.4a that the frame cables FC1 and FC4 experience high tensions followed by FC2 and FC5 when the model is subjected to 0° current heading. Interestingly, the frame cable FC10 has the highest tension in the mooring frame for this case. The most probable reason is the insufficient pre-tension in anchor 6 of the system to maintain a firm shape of the mooring frame of cell 3. Frame cables FC3 and FC6 experience negligible tension forces and upon visualization in FhVis, there is an evident sag in these cables. It can also be seen from figure 5.3a that the there is comparatively lower tensions in the mooring lines 5 and 11. The connecting plates are displaced away due to the flowing currents which contributes to further tension in FC10.

On the other hand, for the 90° current heading, the highest tension forces are experienced by the frame cable FC5 followed by FC7 and FC10, which are close enough to FC4 and FC6. However, the magnitude of tension forces for cross-currents as shown in figure 5.4b is not as high as current heading 0°. It is inferred that, irrespective of the magnitude, the highest

tensions are experienced by the same frame cable number for both 0° and 90° currents. In this thesis, the effect of accidental failures in frame cables FC4, FC5 and FC10 on mooring lines 1 and 3 will be studied for 0° and 90° case respectively.

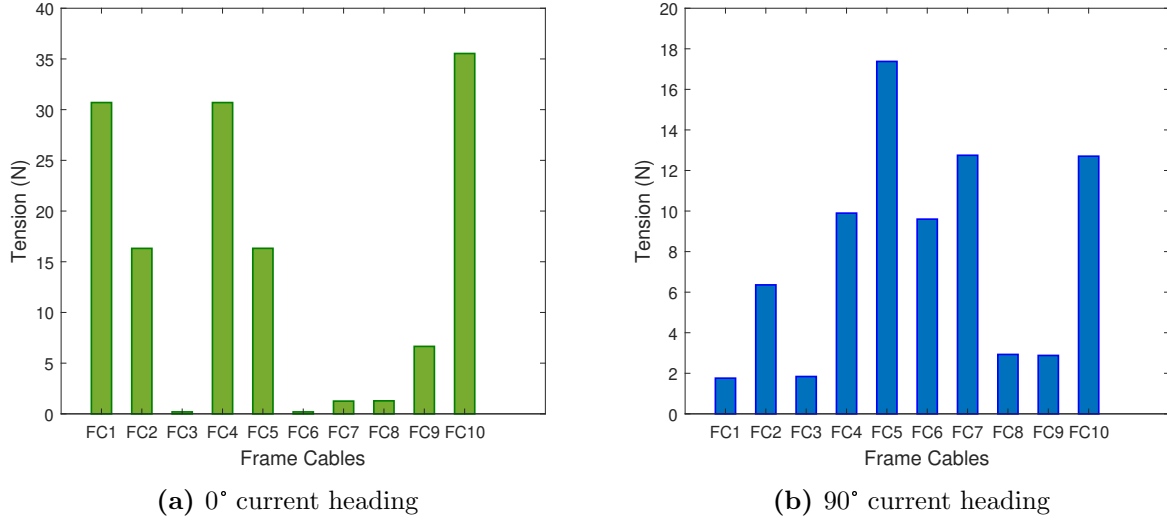


Figure 5.4: Mean tension forces in frame cables of the multiple-cage system ($U=0.40$ m/s)

For each of the critical frame cable of the mooring frame, a loading condition is defined. These are presented in table 5.2 below. The total time run of each simulation is 600 seconds and for LC2, LC3 and LC4, a failure at 0th second has been considered for the respective frame cables. This ceases the computation of the reaction forces at the closest boundary element to the point of break in the frame cable. The break point for each loading condition is at a distance of 20 metres into the corresponding cell.

Table 5.2: Loading conditions for the multiple-cage model

Case	Description
LC1	Intact model
LC2	Failure in frame cable FC4
LC3	Failure in frame cable FC5
LC4	Failure in frame cable FC10

5.2.2 Environmental loading

Wave loading is critical for the floating collar and since the forces are transferred back and forth between the different elements, it becomes necessary to investigate the effect of waves on the entire system. To simplify the numerical analysis, regular waves have been considered to be added to the pure currents for the combined wave-current condition. The regular waves are characterised in terms of wave height and a wave period. The wave period is dependent on the wave frequency which in turn is a function of the wave number and gravitational acceleration by dispersion relation. Wave number is dependent on the wavelength of the wave. Therefore, three wavelengths corresponding to 1D, 2D and 3D are defined for the simulation runs, where D is the diameter of the fish cage. The environmental matrix for the combined wave-current condition is defined below in table 5.3.

For the analysis under the combined wave-current condition, the current velocity is 0.40 m/s. Also, the waves and currents are assumed to be approaching the cage from the same direction. The model is first subjected to the current for 600 seconds before the regular waves are added and the simulation is run for another 600 seconds. Therefore, the total time run for these simulations is 1200 seconds.

Table 5.3: Environmental parameters for the multiple-cage model under pure currents condition

Case	Current		Wave				
	Velocity [m/s]	Direction [Degrees]	Height [m]	Length [m]	Period [s]	Steepness [-]	Direction [Degrees]
C0.40H1L50	0.40	0°/90°	1	50	6	0.02	0°/90°
C0.40H2L50	0.40	0°/90°	2	50	6	0.04	0°/90°
C0.40H1L100	0.40	0°/90°	1	100	8	0.01	0°/90°
C0.40H2L100	0.40	0°/90°	2	100	8	0.02	0°/90°
C0.40H1L150	0.40	0°/90°	1	150	10	0.01	0°/90°
C0.40H2L150	0.40	0°/90°	2	150	10	0.01	0°/90°

5.3 Results and discussions

The results and discussions for the multiple-cage model are divided into two sections - the intact model which defines the first loading condition LC1, and the sensitivity study on different loading conditions with accidental failures and environmental conditions. For this model, an additional sensitivity study on net solidities is presented.

5.3.1 Responses of a multiple-cage model under intact condition

5.3.1.1 Pure currents condition

Figure 5.5 shows the time-series response of the multiple-cage model for different current velocities with a 0° heading. As mentioned earlier while defining the loading conditions, there is significant drop in net volume for currents flowing with velocities higher than 0.20m/s as seen in 5.5a. The increase in tension forces in mooring line 1 increases with an increase in the current velocity as shown in 5.5b. The higher the current velocity, the higher is the drag on the net structure. This drag force is transferred to the mooring line via the floating collar and the mooring frame.

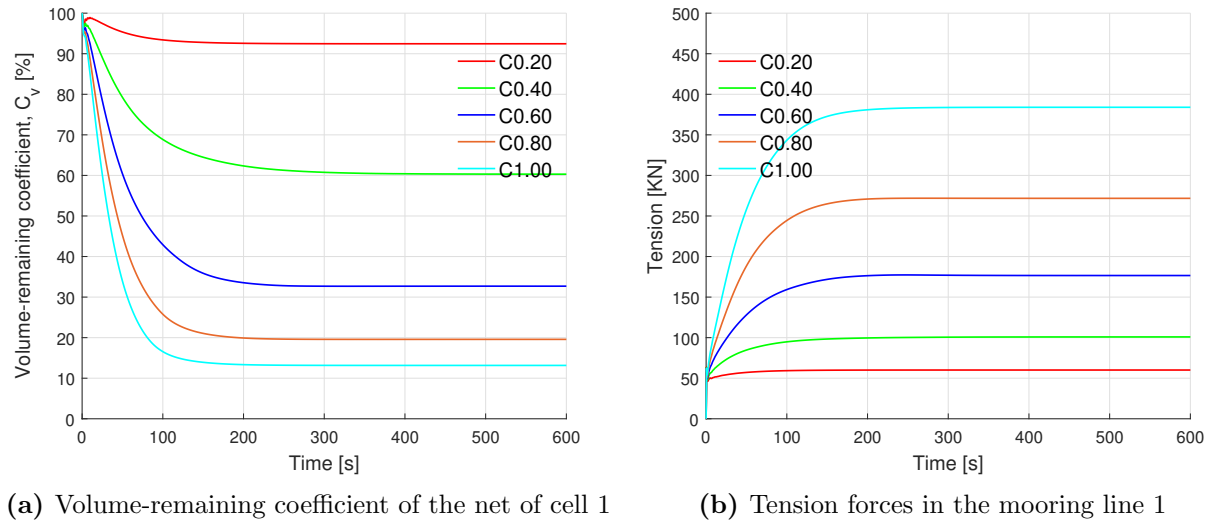


Figure 5.5: Time-series response of the multiple-cage system when the currents are flowing with a 0° heading

The response of this system for a 90° can be seen in figure 5.6. As mentioned earlier, the volume-remaining coefficient for the two headings are quite similar in magnitudes except for lower current velocities than 0.60 m/s as shown in figure 5.6a. The corresponding rise in the tension forces in mooring line 3 is plotted in figure 5.6b. In proportion to the drag experience by the net structure, the loads increase as the current velocity increases. The magnitude of the tension forces experienced by mooring line 3 for 90° heading is not as high as mooring line 1 loads for the 0° heading.

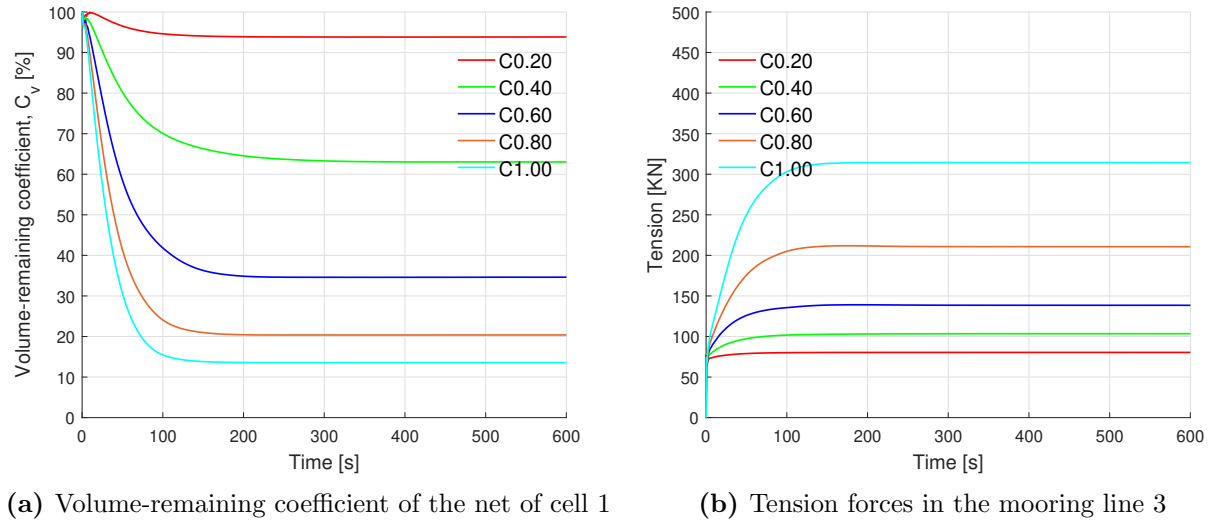


Figure 5.6: Time-series response of the multiple-cage system when the currents are flowing with a 90° heading

The geometry of the multiple-cage model is plotted in figure 5.7 for currents flowing with 0° heading towards it. The floating collar and the bottom ring are represented by the red and the blue colors respectively. The black dots represent the nodes of the net structures. The buoys and connection plates are represented by the cyan and magenta color markers.

The significant tension observed in FC10 can be explained by these geometry plots. The connection plates connected to this frame cable move apart at $T=600s$ as seen in figure 5.7b. The set of buoys connecting FC7 remain located in the initial position due to tension in the mooring lines 1 and 7. The other set of buoys connected to frame cables FC8 and FC9 move in the direction of the current flow. Their connection plates are not displaced in proportion to the buoys. They are also connected to the other plates. Thus, their motions are rather restricted. Figure 5.7c gives a clear illustration of the 10 different layers of the net structure with 32 nodes in each layer and a single node at 28 metres depth where the centre point weight is hung off.

When the system reaches equilibrium in under pure currents, large net deformations can be seen in figure 5.7d. The node layers are compressed against each other and the bottom ring moves up by a few metres and can be seen at the same depth where the mooring frame is submerged in water. That is clearly a very significant reduction in the cage net volume and corresponds to the volume-remaining coefficient of 60%.

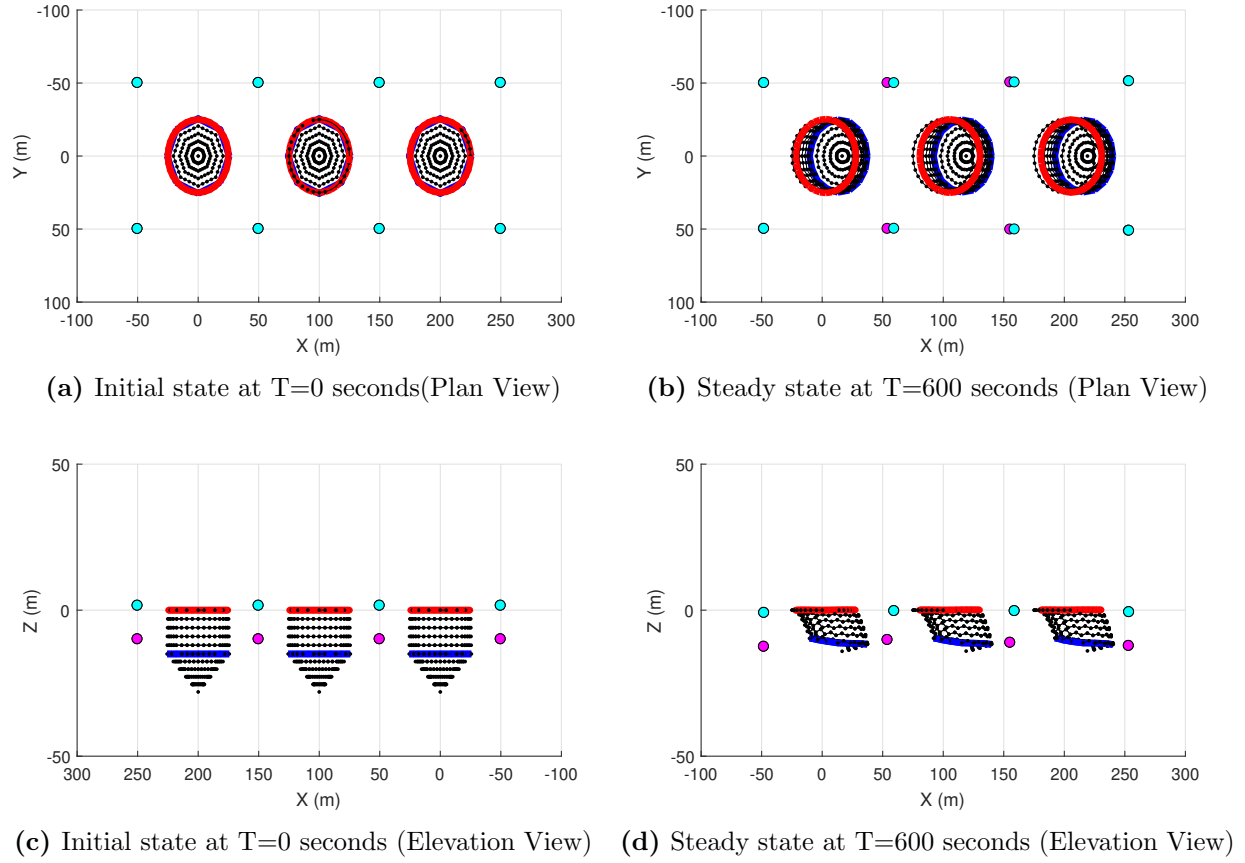


Figure 5.7: Geometry of the multiple-cage model at different time intervals when the current is flowing with a 0° heading ($U=0.40$ m/s)

Similar geometry plots of the multiple-cage model were plotted for currents flowing with 90° towards it, as shown in figure 5.8. It can be seen that the set of buoys on the frame cables FC8 and FC9 move in the direction of the current flow in figure 5.8b. This visualization explains the mean tension forces plotted in the figure 5.3b where the connected mooring lines 3 and 4 to the left of +X axis can be seen to experience the highest tension forces.

Figures 5.8c and 5.8d show how the nodes of the three different net structures superimpose each other in Y-Z plane at the initial and steady state respectively. This shows that the shielding effect is not implemented between the two net structures of this model with 1x3 configuration in FhSim. The wake effect is implemented locally within the net structure only. At steady state, there are large deformations in the nets, however, slightly lesser than the 0° heading. The bottom ring can be seen lower than the submergence depth of the mooring frame and this explains the 3% difference in the volume-remaining coefficient of the

two headings in discussion.

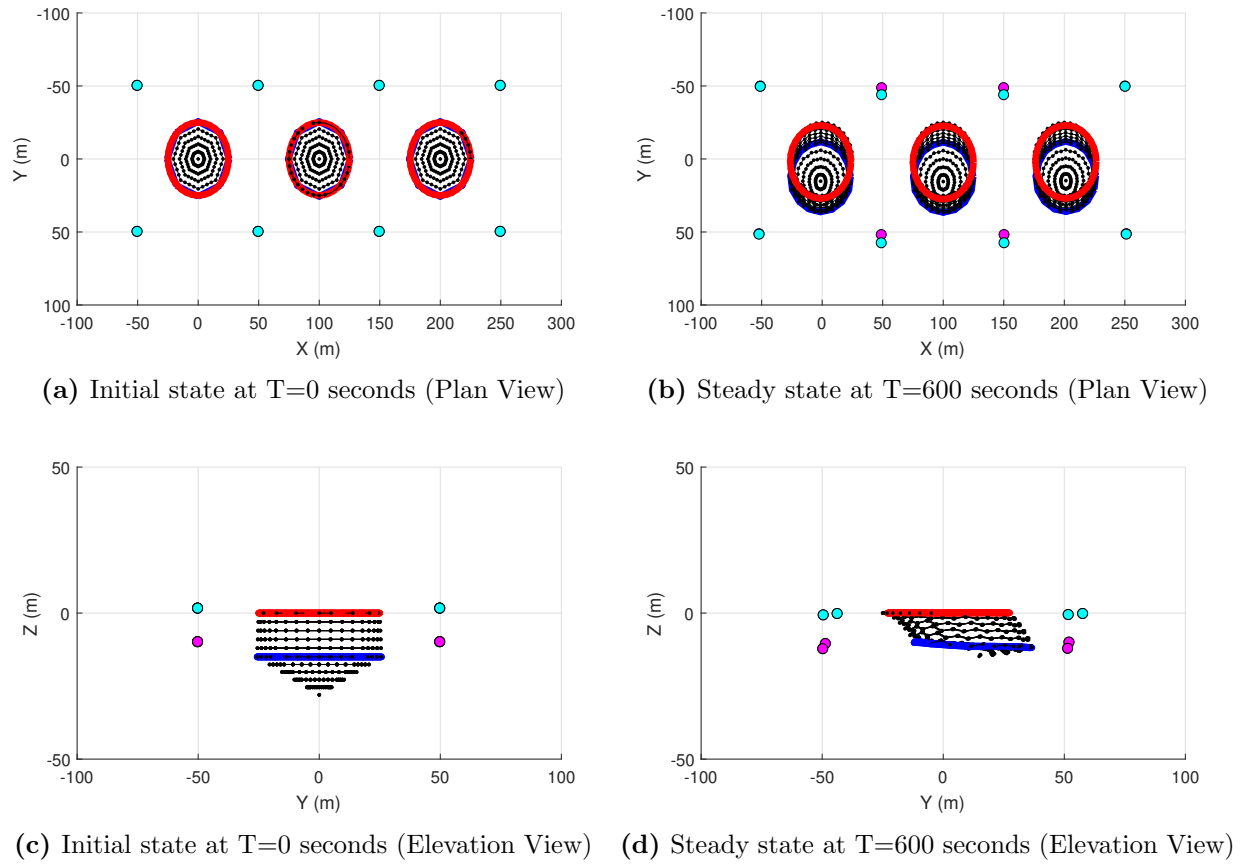
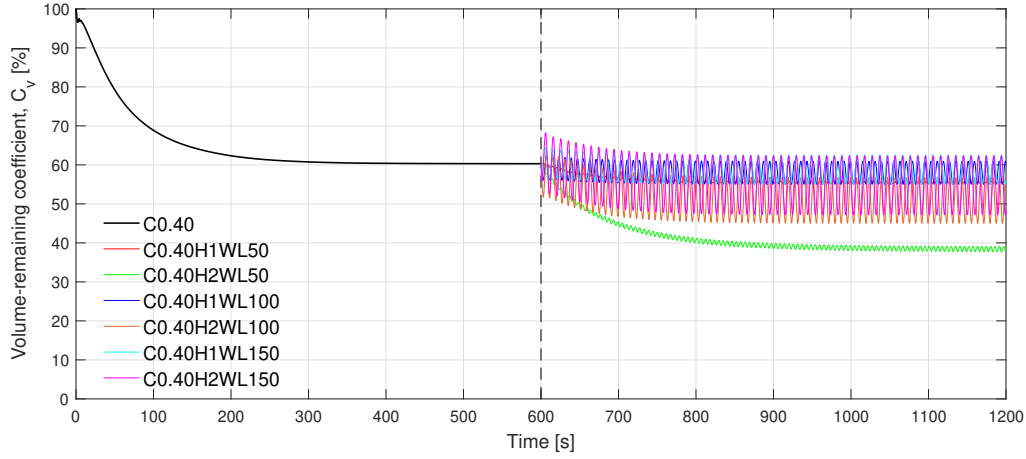


Figure 5.8: Geometry of the multiple-cage model at different time intervals when the current is flowing with a 90° heading ($U=0.40$ m/s)

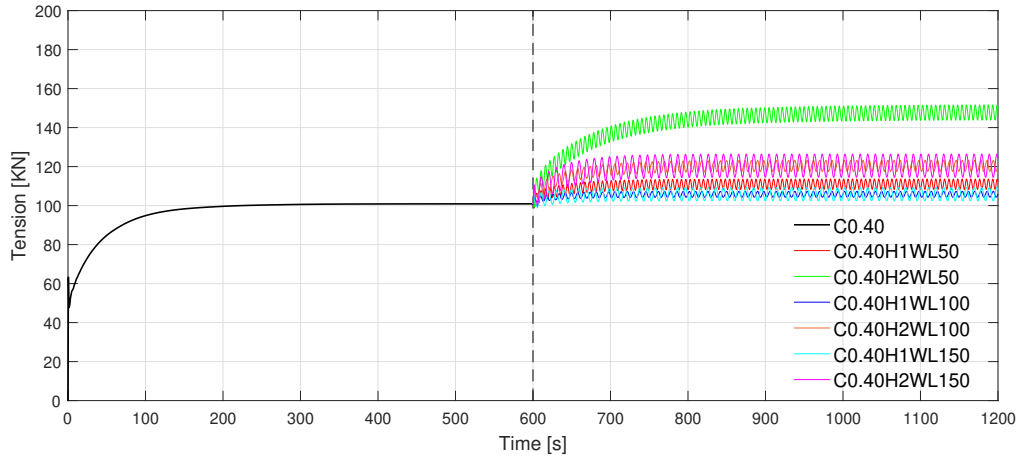
5.3.1.2 Combined wave-current condition

Figure 5.9 shows the effect of regular waves on the response of the multiple-cage system for 0° current heading. It can be seen from figure 5.9a that the mean value and the amplitude of the remaining net volume increases with an increase in the wavelength from 50 metres to 100 metres. However, for a wavelength of 150 metres, C_v is lower than the value at 100 metres wavelength. When the wavelength is equivalent to the diameter of the fish cage and the wave height is 2 metres, the maximum wave particle velocity at the free surface is 1.11 m/s which is nearly three times the current velocity 0.40 m/s. The net volume is reduced to 60% of the original volume in the first 600 seconds of simulation and is further dropped to 38% for this particular combined wave-current case C0.40H2WL50. The drop is about 36%

of the analysis under pure currents only. For the other cases, the mean C_v is closer to the value at C0.40 case.



(a) Volume-remaining coefficient of the net structure of cell 1

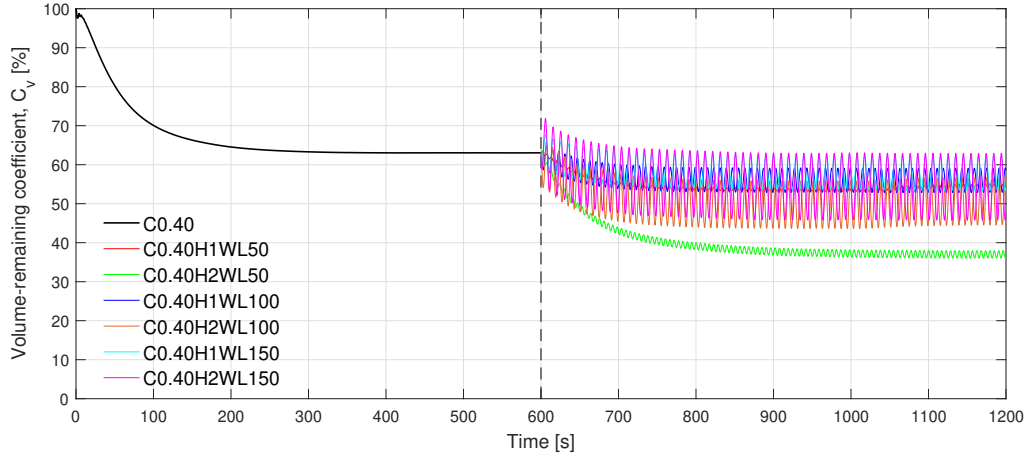


(b) Tension forces in mooring line 1

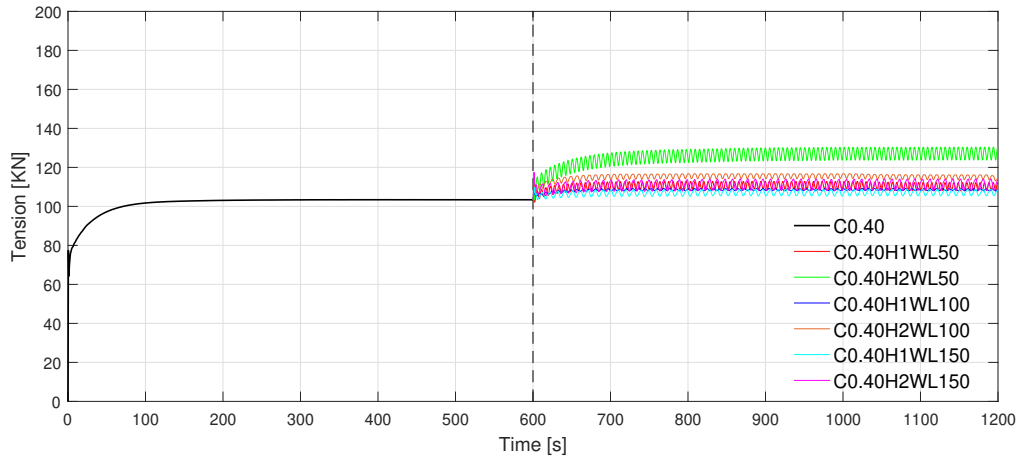
Figure 5.9: Effect of regular waves on the response of the multiple-cage model subjected to 600 seconds of prior current loading (0° current-wave heading)

The corresponding effect on the mean tension forces in mooring line 1 is shown in figure 5.9b. Addition of regular waves in the next 600 seconds leads to an increase in the mean value. The increase is significant for the 50 metres wavelength with a 2 metre wave height corresponding to the higher drag experienced by the net structure. The amplitude, however, does not fluctuate as strongly when compared to the volume-remaining coefficient discussed earlier.

Figure 5.10 shows the effect of regular waves on the response of the multiple-cage system for 90° current heading. The general response for this case is very similar to the 0° current heading. The mean value of the volume-remaining coefficient increases and the amplitude of fluctuation increases with an increase in the wavelength as seen in figure 5.10a. The reduction for the steepest wave case C0.40H2WL50 is higher by 2% as compared to the 0° heading.



(a) Volume-remaining coefficient of the net structure of cell 1



(b) Tension forces in mooring line 3

Figure 5.10: Effect of regular waves on the response of the multiple-cage model subjected to 600 seconds of prior current loading (90° current-wave heading)

The effect on the mean tension force in mooring line 3 can be seen in figure 5.10b. There is an increase in the loads on addition of the regular waves for the next 600 seconds. Naturally, the

amplitude also increases with an increase in the wavelength and wave height. As mentioned earlier, the waves contribute to a lower C_v for 90° heading than the 0° heading. This is opposite to the observations for pure currents condition. However, this corresponding effect is not reflected on to the mooring line 3 loads on the same scale as mooring line 3 loads which are higher.

Figure 5.11 shows the geometry plots of the multiple-cage model for the critical combined wave-current condition with 0° heading. The floating collar and the bottom ring are represented by the red and the blue colors respectively. The black dots represent the nodes of the net structures. The buoys and connection plates are represented by the cyan and magenta color markers.

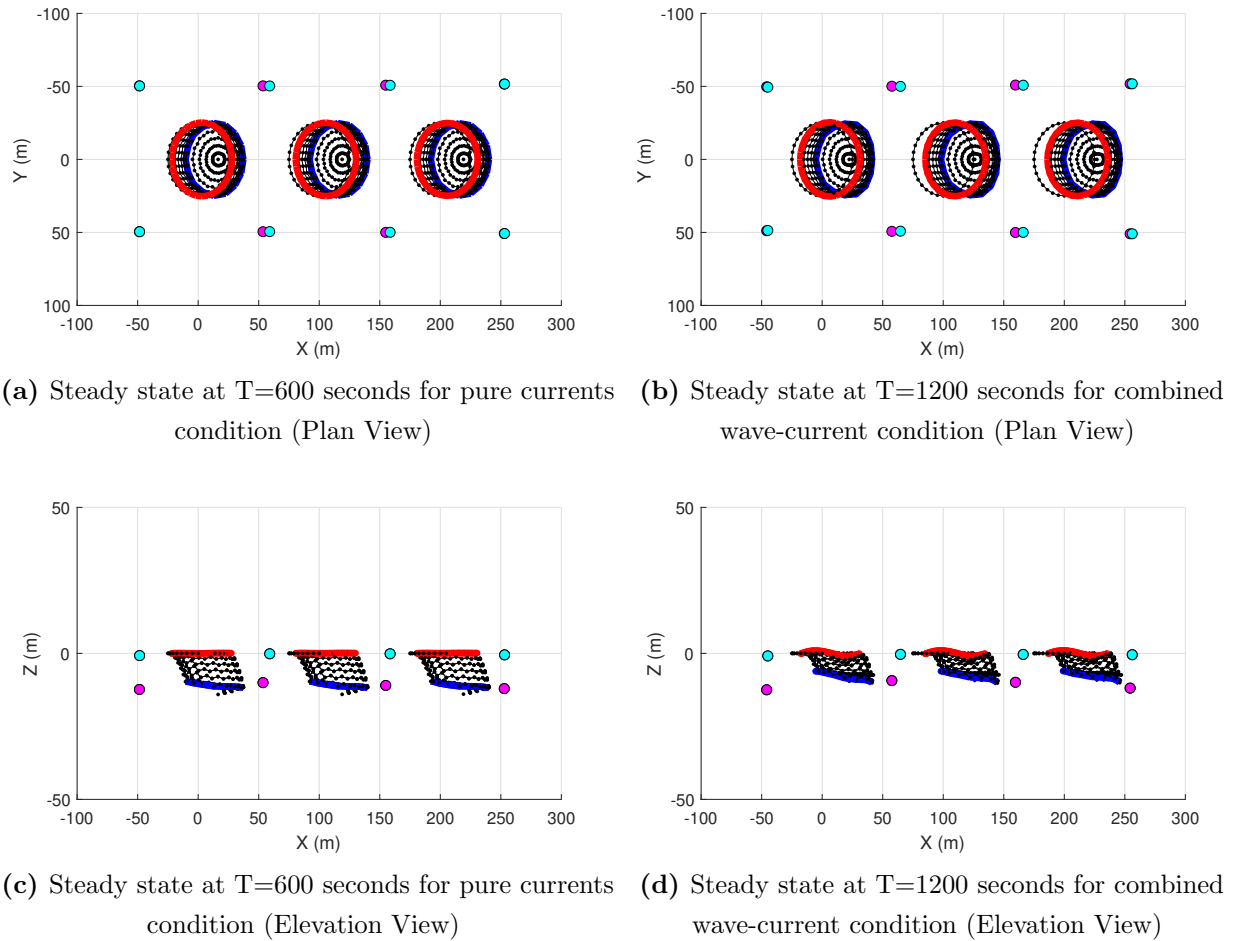


Figure 5.11: Effect of regular waves on the steady state geometry of the multiple-cage model for 0° current heading (Case C0.40H2WL50)

The effect of the addition of regular waves to the model in steady state for pure currents can be seen in figure 5.11b. The net cages are displaced even further than the position in figure 5.11a. The increase is lowest for cell 1 as the motion is restricted by the mooring lines 1 and 7, and highest for cell 3. The floating collar model implemented in FhSim follows the potential theory and this can be clearly visualised from figure 5.11d. The floater is seen to follow the sine profile of the regular waves. The volume is further reduced on addition of the waves as the node layers can be seen further compressed against each other. The bottom ring moves further up and tilts by a higher angle.

Similar geometry plots of the multiple-cage system for 90° heading are shown below in figure 5.12.

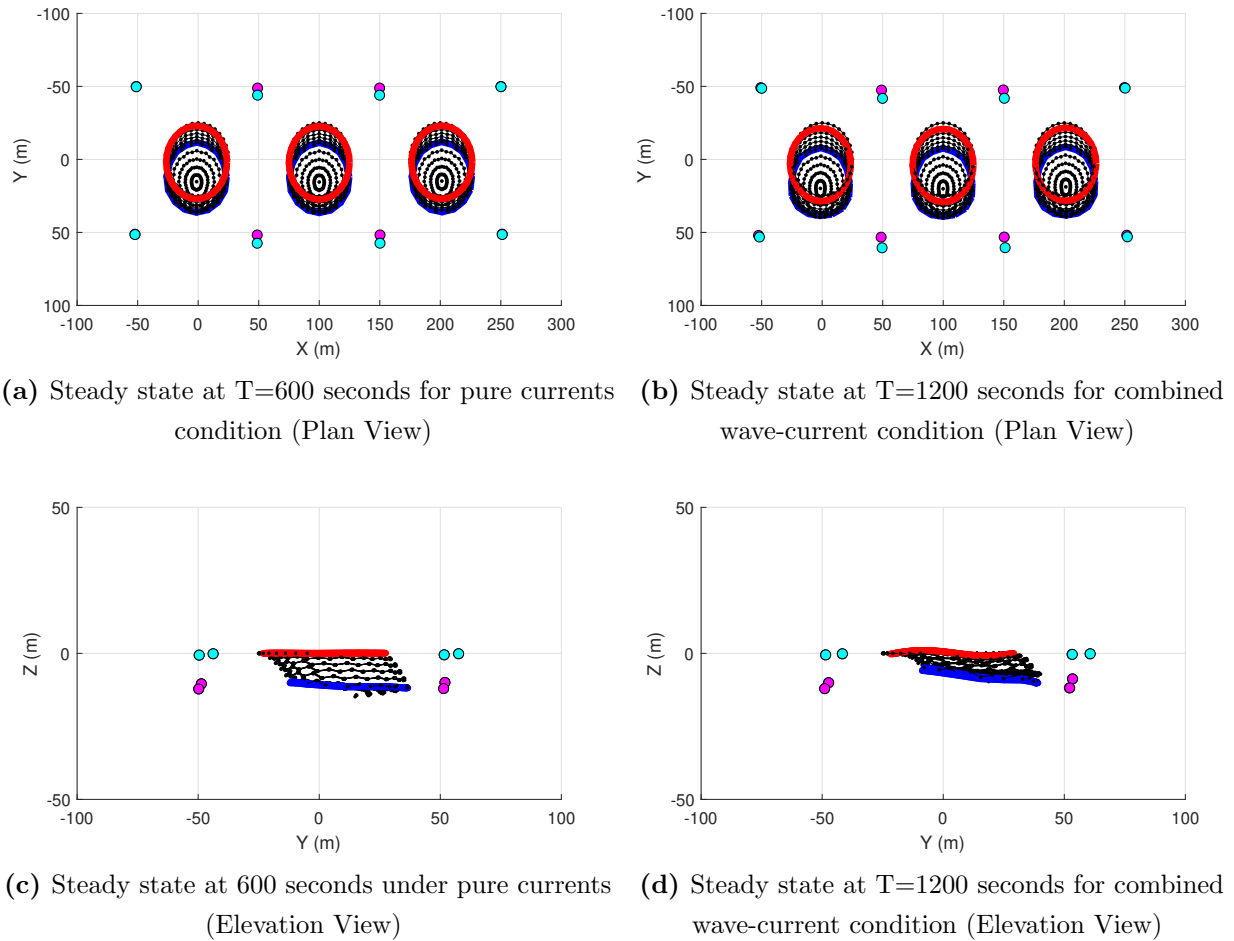


Figure 5.12: Effect of regular waves on the steady state geometry of the multiple-cage model for 90° current heading (Case C0.40H2WL50)

The effect of addition of regular waves on the displacement of the net structures is not significant as seen in the plan view in figure 5.12b. However, a substantial reduction in the net volume can be seen in the elevation view in figure 5.12d as compared to figure 5.12c. This visualization complements the time-series plots discussed earlier where a 90° wave heading added to a 90° current heading reduces the cultivation volume inside the fish cage to 36% of the original volume.

Tables 5.4 and 5.5 lists the mean values of the volume-remaining coefficient and the tension forces in the mooring lines and critical cables for 0° and 90° combined wave-current headings respectively. These have been referenced throughout the presentation of results and their discussions earlier in this section.

Table 5.4: Mean values of volume-remaining coefficient of the net structure of cell 1, and tension forces in the mooring line 1 and critical cables of multiple-cage system subjected to different environmental loads (0° heading)

Case	Volume-remaining Coefficient [%]	Tension Forces [KN]			
		ML1	FC4	FC5	FC10
C0.40	60	101	31	16	36
C0.40H1WL50	55	112	36	19	40
C0.40H2WL50	38	149	51	28	42
C0.40H1LW100	60	106	33	18	38
C0.40H2WL100	56	121	42	22	41
C0.40H1WL150	56	108	33	15	36
C0.40H2WL150	48	124	42	19	40

It can be seen from the table above, that for a particular wave height, C_v increases with the change in wavelength from 50 metres to 100 metres, however, decreases again for 150 metres wavelength. The corresponding effect is reflected by the mean tension forces for these combined wave-current cases. When the wave height is 2 metres and wavelength is 50 metres, the net volume is reduced to 38% of the original volume and there is a significant increase in the mean tension force. Amongst the three frame cables listed, FC10 experiences the highest loads under pure currents condition. However, the highest loads are experienced by FC4 instead for regular waves with a wave height of 2 metres. In fact, for the case C0.40H2WL50, the mean tension force reaches 51KN, a 65% increase from C0.40.

Table 5.5: Mean values of volume-remaining coefficient of the net structure of cell 1, and tension forces in the mooring line 3 and critical cables of multiple-cage system subjected to different environmental loads (90° heading)

Case	Volume-remaining Coefficient [%]	Tension Forces [KN]			
		ML3	FC4	FC5	FC10
C0.40	63	103	10	17	13
C0.40H1WL50	55	112	11	20	13
C0.40H2WL50	36	130	12	19	12
C0.40H1LW100	59	109	12	19	12
C0.40H2WL100	56	114	13	21	12
C0.40H2WL150	54	109	11	18	13
C0.40H2WL150	48	114	11	19	12

As seen in the values listed in the table above, the effect of regular waves on C_v for C0.40 is slightly more severe than the 0° combined wave-current heading. The corresponding effect can be seen on the mean tension forces in the mooring line 3, although not as significant as the loads experienced by mooring line 1 for the other heading in discussion. The frame cables for this case do not experience severe changes with change in the environmental parameters. The average mean tension forces in FC10 remains near 12 KN for the different combined wave-current cases and a similar response can be seen for the other two frame cables.

5.3.2 Responses of a multiple-cage model under different loading conditions

For pure currents condition, figure 5.13 shows the effect of the accidental failure in frame cables on the net volume of cell 1 for the 2 different headings.

Beginning with 0° heading, the mean volume-remaining coefficient is not affected by the accidental failure in the three critical frame cables defining the loading conditions LC2, LC3 and LC5. C_v represented by the bar heights can be seen nearly equal in magnitude as seen in figure 5.13a. A similar response is observed in figure 5.13b for the 90° heading. It is evident from the plots, the effect on the volume-remaining coefficient is more severe for when the waves and currents both are flowing 90° to the multiple-cage model. However, for both the current headings, the loading conditions do not significantly affect the magnitude of the coefficient. The drop in remaining volume decreases with an increase in the current velocity.

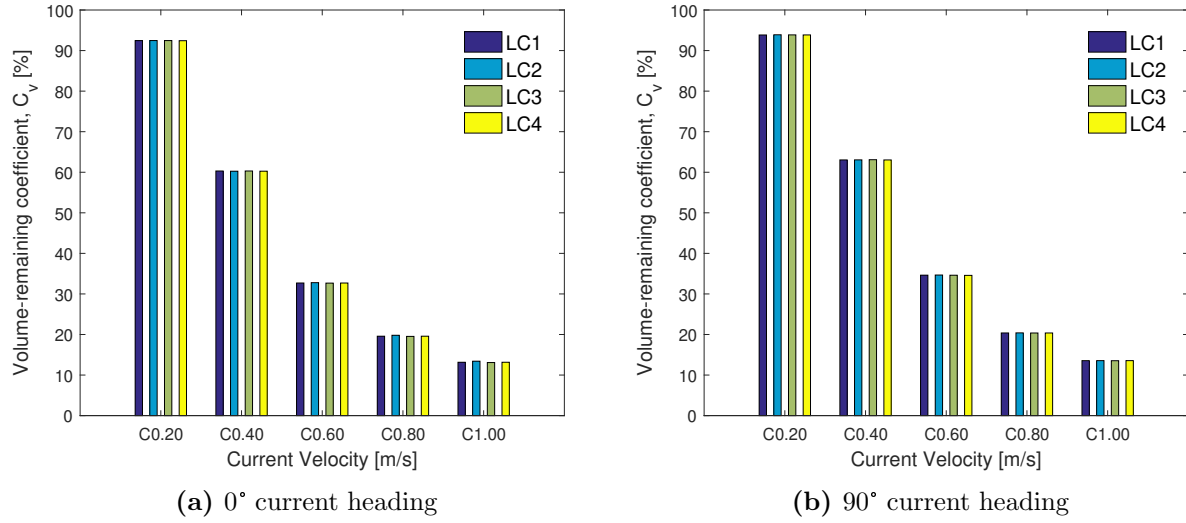


Figure 5.13: Effect of accidental failures in cables defined by the loading conditions on the volume- remaining coefficient of the net structure of cell 1 under pure currents condition

Figure 5.14 below shows the effect of the accidental failure in frame cables on the critical mooring lines for the 2 different current headings under discussion.

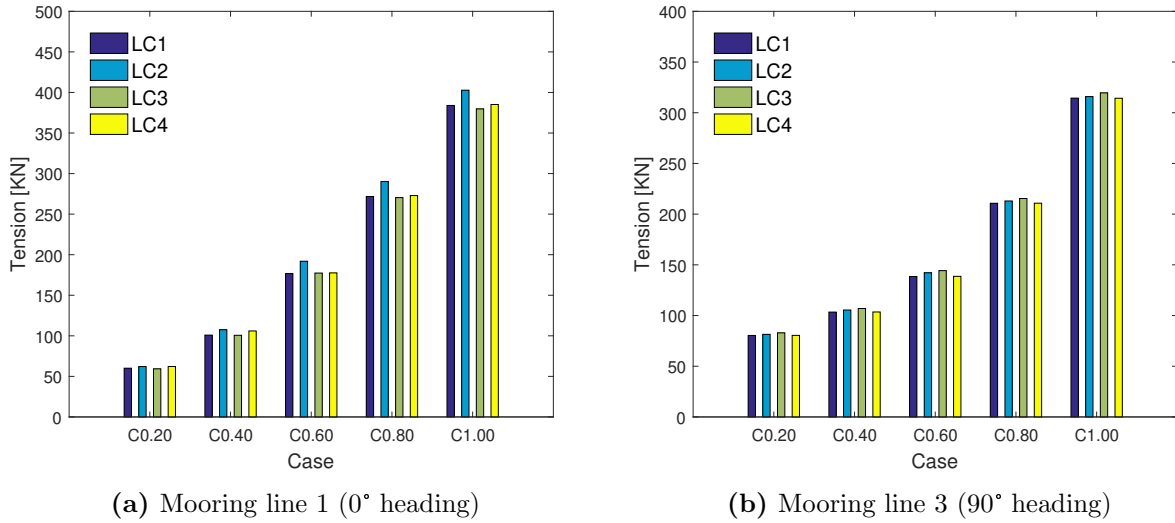


Figure 5.14: Effect of accidental failures in cables defined by the loading conditions on the critical mooring lines of the multiple-cage model under pure currents condition

For currents flowing 0° to the model, the mean tensions force in the mooring line 1 changes for the different loading conditions. This change is more evident as the current velocity

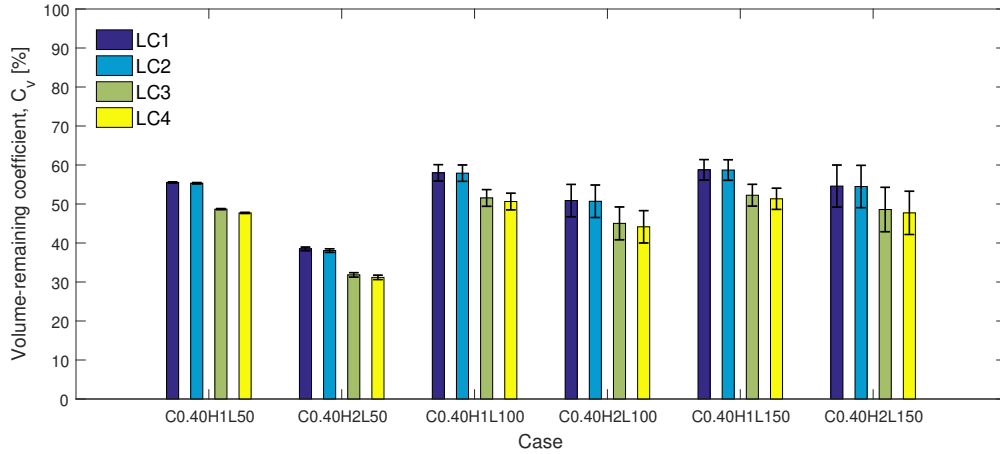
increases as seen in figure 5.14b. The mooring line load is consistently highest for loading condition LC2 where FC4 is broken for the entire range of current velocities. When intact, this frame cable transfers the loads to mooring line 7 via the connection plate. In case of accidental failure, the forces in the frame cables FC5 and FC6 are transferred on to the mooring line 1 through FC8 and FC9.

For 90° current heading, there is not a significant effect of the loading conditions on the tension forces in mooring line 3 as seen in figure 5.14b. For a particular case, the highest mean tension forces are experienced for loading condition LC3 where FC5 is broken followed by LC2 where FC4 is broken. The accidental failure in FC10 does not lead to any additional loads on the mooring line 3. The response is alike for the entire range of current velocities.

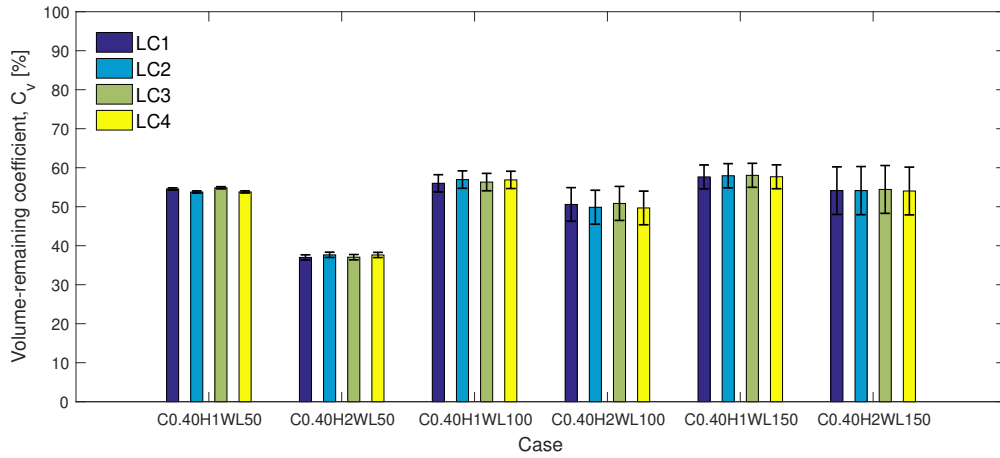
Figure 5.15 shows the effect of the accidental failures in frame cables on the net volume of cell 1 for the 2 different headings of combined wave-current condition. The bar height represents the mean values for the last 100 seconds of the simulation when the system is in equilibrium and the error bars represent the dynamic fluctuation from the mean value.

It can be seen from the figure 5.15a for 0° heading that for a particular wave height, the mean value of the volume-remaining coefficient decreases with a decrease in the wavelength. The net volume is the lowest when the model is subjected to waves with height 2 metres and length equivalent to the diameter of the cage. The amplitude of fluctuation is not significant in this case. The amplitude increases with an increase in the wavelength for a particular wave height. The failure in frame cable FC4 in LC2 does not lead to a significant change in the net volume maintained for case C0.40. C_v reduces for the other two loading conditions LC3 and LC4 where frame cable FC5 and FC10 are broken. This is a change from the pure currents condition when the loading conditions did not affect the volume-remaining coefficient for a particular case.

For the wave-currents flowing with a 90° heading, the mean value of the volume-remaining coefficient decreases with an decrease in the wavelength. Like 0° heading, the net volume is the lowest for the case C0.40H2WL50. The amplitude of the fluctuation increases significantly with an increase in the wavelength. There is clearly not a significant effect of the accidental failures in the frame cables on the volume for this current heading as evident from figure 5.15b.



(a) 0° current heading



(b) 90° current heading

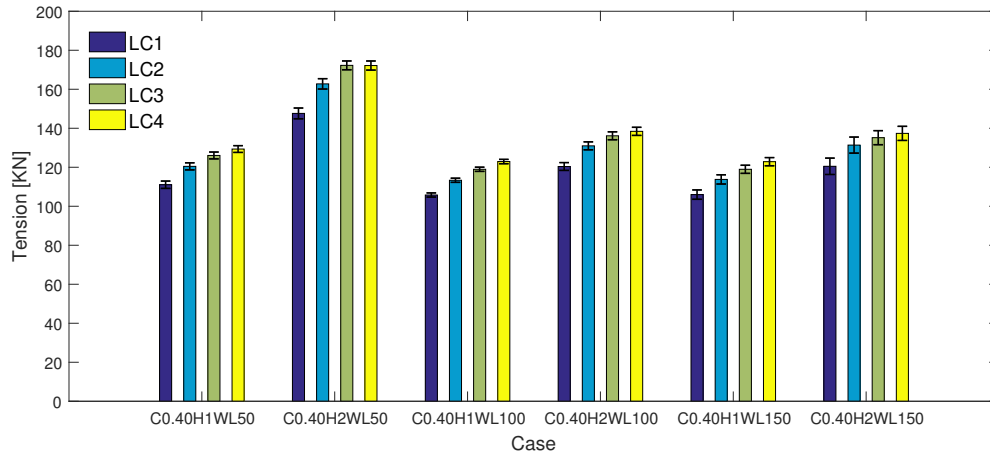
Figure 5.15: Effect of loading conditions on volume-remaining coefficients of the net structure of cell 1 under combined wave-current condition

Figure 5.16 shows the effect of the accidental failures in frame cables on the critical mooring lines for the 2 different headings of combined wave-current condition.

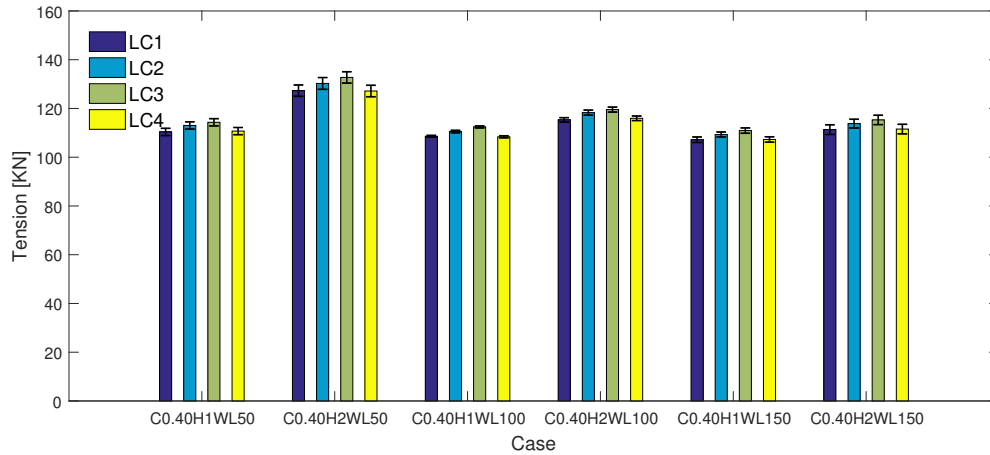
For the the currents flowing 0° to the model, the mean value of the mooring line 1 tension decreases with an increase in the wavelength as seen in the figure 5.16a. This corresponds to the change in volume-remaining coefficients since the higher drag forces acting on the net structure lead to higher loads transferred to the mooring lines. For a particular case, the highest loads are experienced for LC4 where FC10 is broken. This has changed from the pure currents condition when failure in FC4 was responsible for the highest tension forces.

Clearly, mooring line 1 must be designed to withstand the additional loads due to possible accidental failures in frame cable FC4 and FC10. For a particular wave height, the amplitude increases when the wavelength changes from 50 metres to 150 metres..

On the other hand, failure in frame cables does not contribute to a significant additional load on the mooring line 3 for 90° current heading as seen in figure 5.16b. The mean value of the tension forces is still the highest for the wavelength of 50 metres. The amplitude of fluctuation is not high and increases with an increase in the wavelengths. The loads in the mooring line 3 increase for LC2 and LC3 in order but decrease for LC4.



(a) Mooring line 1 (0° heading)



(b) Mooring line 3 (90° heading)

Figure 5.16: Effect of accidental failures in cables defined by the loading conditions on the critical mooring lines of the multiple-cage model under combined wave-current condition

5.3.3 Sensitivity study on net solidities

The Norwegian technical standard NS9415 mandates the requirement of considering the additional loads due to biofouling for design and dimensioning of the fish farming unit [9]. It should be accounted for, by increasing the twine diameter by 50%, in the load calculations. The net structure used in the both the models in this thesis has a solidity ratio of 0.19. Therefore, it is important to calculate loads on the cages with net solidities up to at least 0.29. Therefore, a sensitivity studies on these 2 extreme solidity ratios is performed with an intermediate value of 0.24 for better comparison. The loading conditions and the environmental matrix for pure current condition do not change, however, the environmental matrix for the combined wave-current condition has been shortened for this study and is tabulated below.

Table 5.6: Environmental parameters for the sensitivity study on net solidity of the multiple-cage system under combined wave-current condition

Solidity Ratio	Current Velocity [m/s]	Wave		
0.19	0.40	H=2m, WL=50m	H=2m, WL=100m	H=2m, WL=150m
0.24	0.40	H=2m, WL=50m	H=2m, WL=100m	H=2m, WL=150m
0.29	0.40	H=2m, WL=50m	H=2m, WL=100m	H=2m, WL=150m

Figure 5.17 shows the effect of net solidity on the volume-remaining coefficient of the net structure of cell 1 for different loading conditions under pure currents with a 0° heading. An increase in solidity ratio increases the drag force on the net as more water flows around the structure than through it. This additional drag leads to an increase in the net deformation. Thus, the volume-remaining coefficient reduces further as the solidity ratio increases. The percentage change in C_v due to the increasing solidity ratios increases with the increase in velocity from 0.20 m/s to 0.40 m/s, where it reaches the maximum. It again decreases with a further increase in the current velocity. For the extreme values in the range of the current velocities under discussion, the change volume-remaining coefficient for the net solidities is the lowest.

As seen earlier, there was no significant change in the volume-remaining coefficient for the different loading conditions across the current velocities. For this very reason, it can be seen that all the sub plots for these four loading conditions are quite similar to each other.

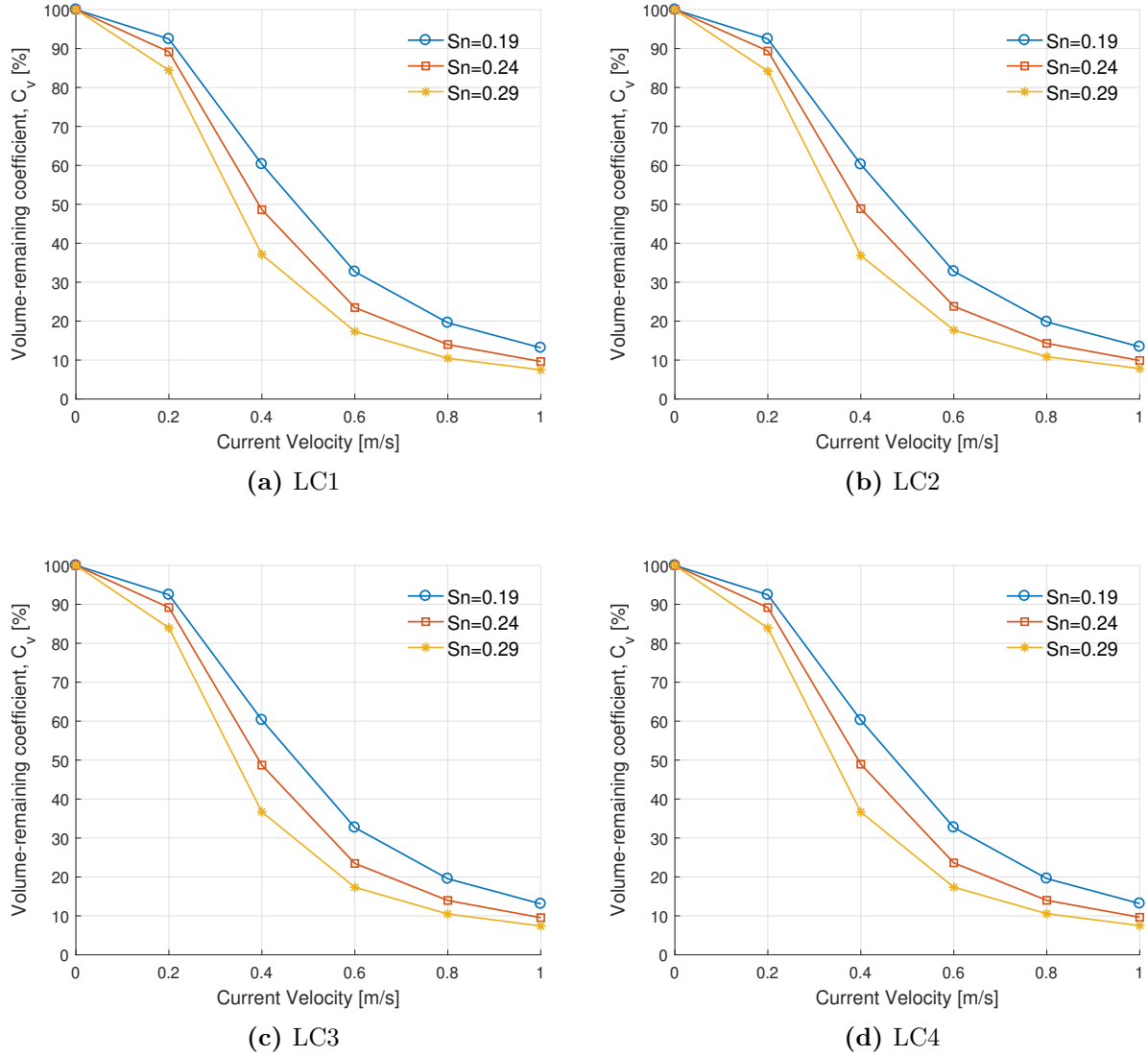


Figure 5.17: Effect of net solidities on the volume-remaining coefficient of the net structure of cell 1 of the multiple-cage model under pure currents condition (0° heading)

For the currents flowing 90° , the effect of the solidity ratios on the volume-remaining coefficient of the net structure is similar to the 0° current heading as seen in figure 5.18. As discussed earlier for the netting with solidity ratio 0.19, the magnitude of the volume-remaining coefficient is slightly higher for the 90° heading. A similar response can be seen in the plots for the other 2 solidity ratios, 0.24 and 0.29, as well.

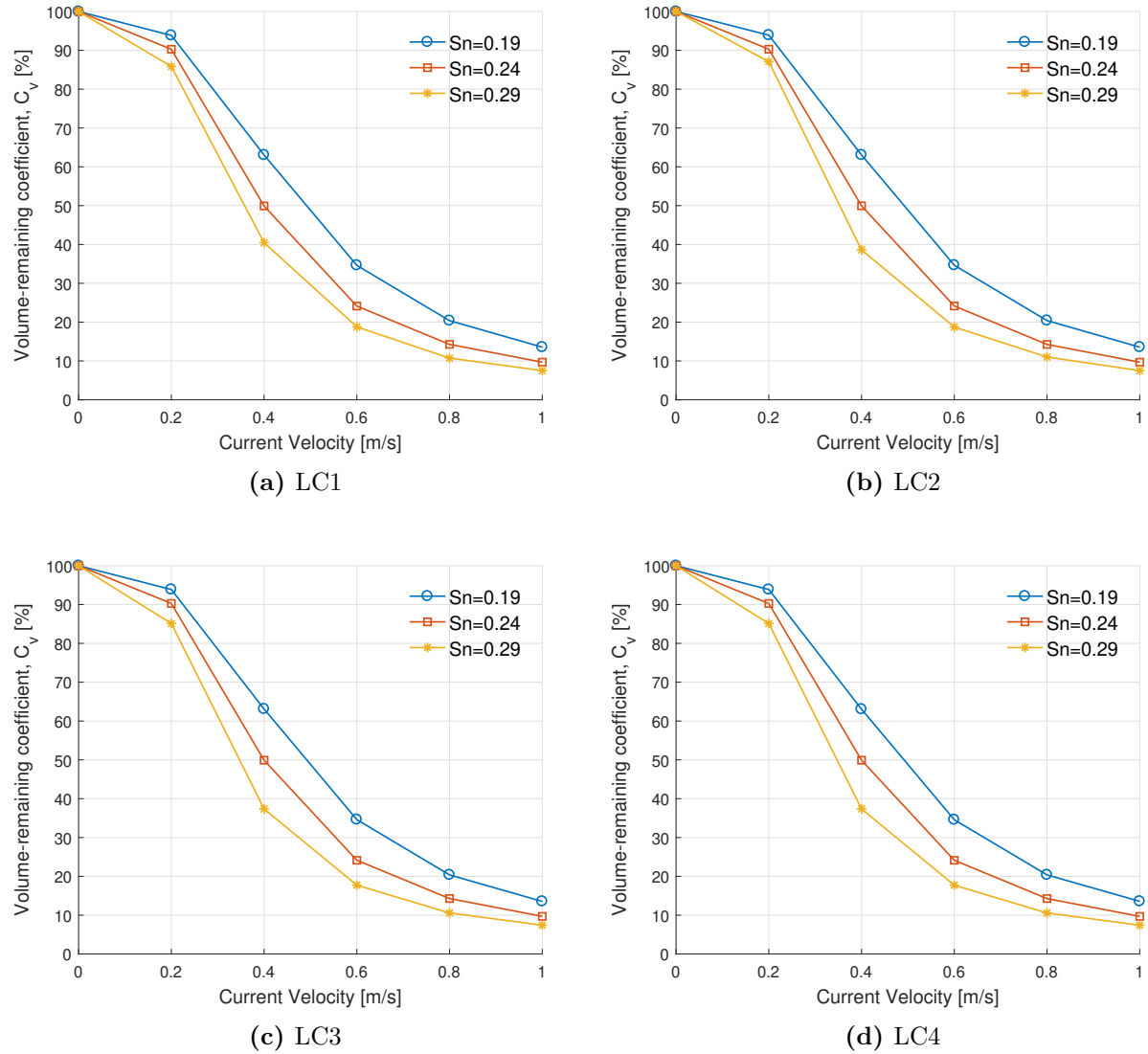


Figure 5.18: Effect of net solidities on the volume-remaining coefficient of the net structure of cell 1 of the multiple-cage model under pure currents condition (90° heading)

Figure 5.19 shows the effect of net solidity on the mean tension forces in mooring line 1 of the multiple-cage system for different loading conditions under pure currents with a 0° heading. The mean tension forces increases with an increase in the current velocity as seen in figure 5.19a. The percentage change in increase in the magnitude also increase with the increase in the current velocities. For 0.20 m/s, the mooring line 1 experiences nearly similar loads for the three different solidity ratios. Also, the percentage increase in the magnitude of the mean tension force is higher for the change in net solidity from 0.24 to 0.29 than the change

in 0.19 to 0.24. As discussed earlier for the netting with solidity ratio 0.19, the loads are slightly higher under LC2 than the other loading conditions. A similar response can be seen in the plots for the other 2 solidity ratios as well.

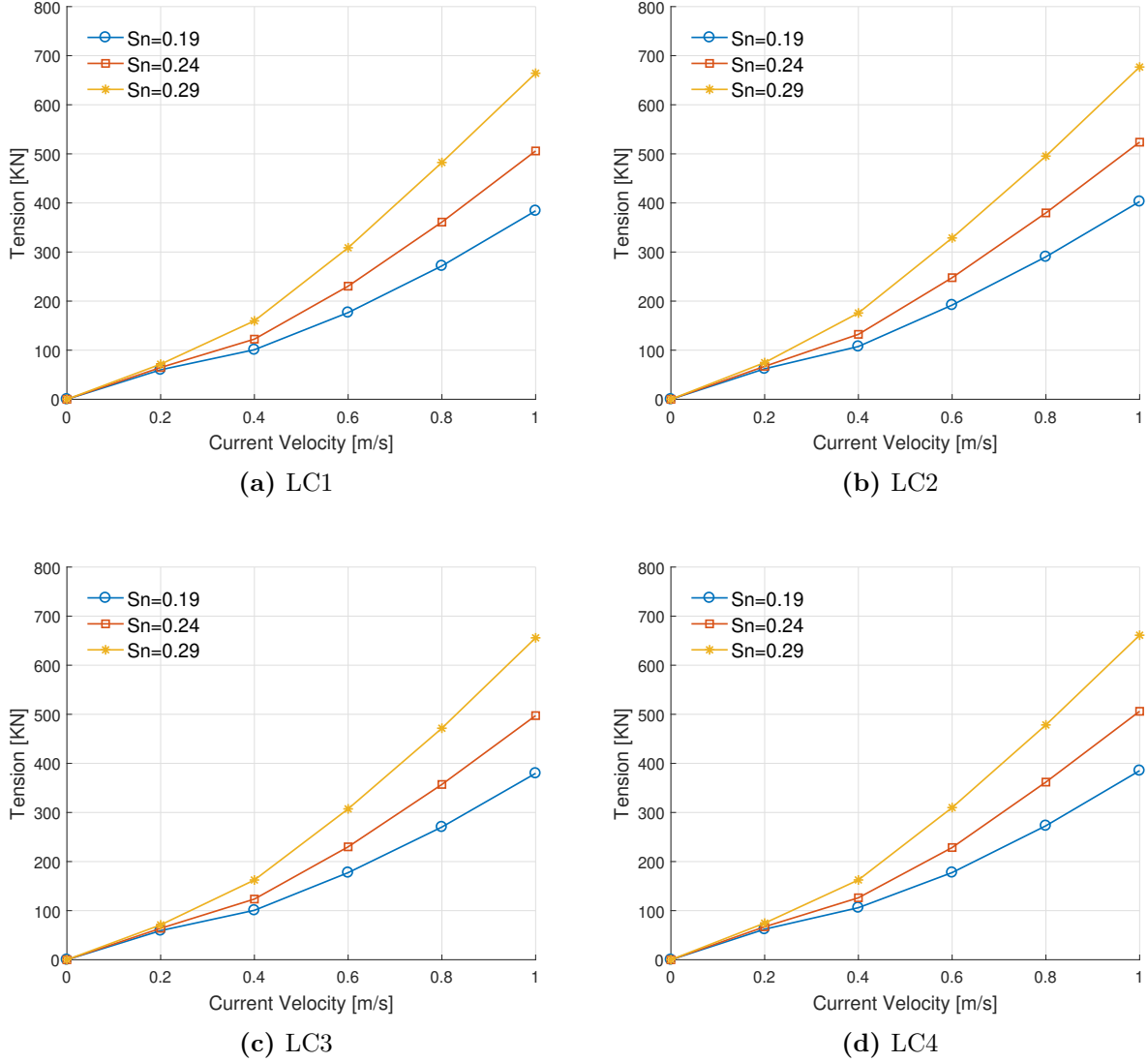


Figure 5.19: Effect of net solidities on the mean tension forces in mooring line 1 of the multiple-cage model under pure currents condition (0° heading)

For the pure currents flowing 90° , the effect of net solidity on the mean tension force in mooring line 3 of the multiple-cage system for different loading conditions under pure currents can be seen in figure 5.20. The percentage increase in the magnitude increases with the increase in the current velocities as seen for 0° heading as well. The change is more prominent

after 0.40 m/s current velocity. For 0.20 m/s, the mooring line 3 also experiences nearly similar loads for the three different solidity ratios. This is also true for 0.40 m/s where the change is not a significant one. Similar responses can be seen in the sub plots for LC2 and LC4. In LC3 where FC5 is broken, the increase in mean tension forces for the net solidity 0.29 is significant unlike the other three loading conditions.

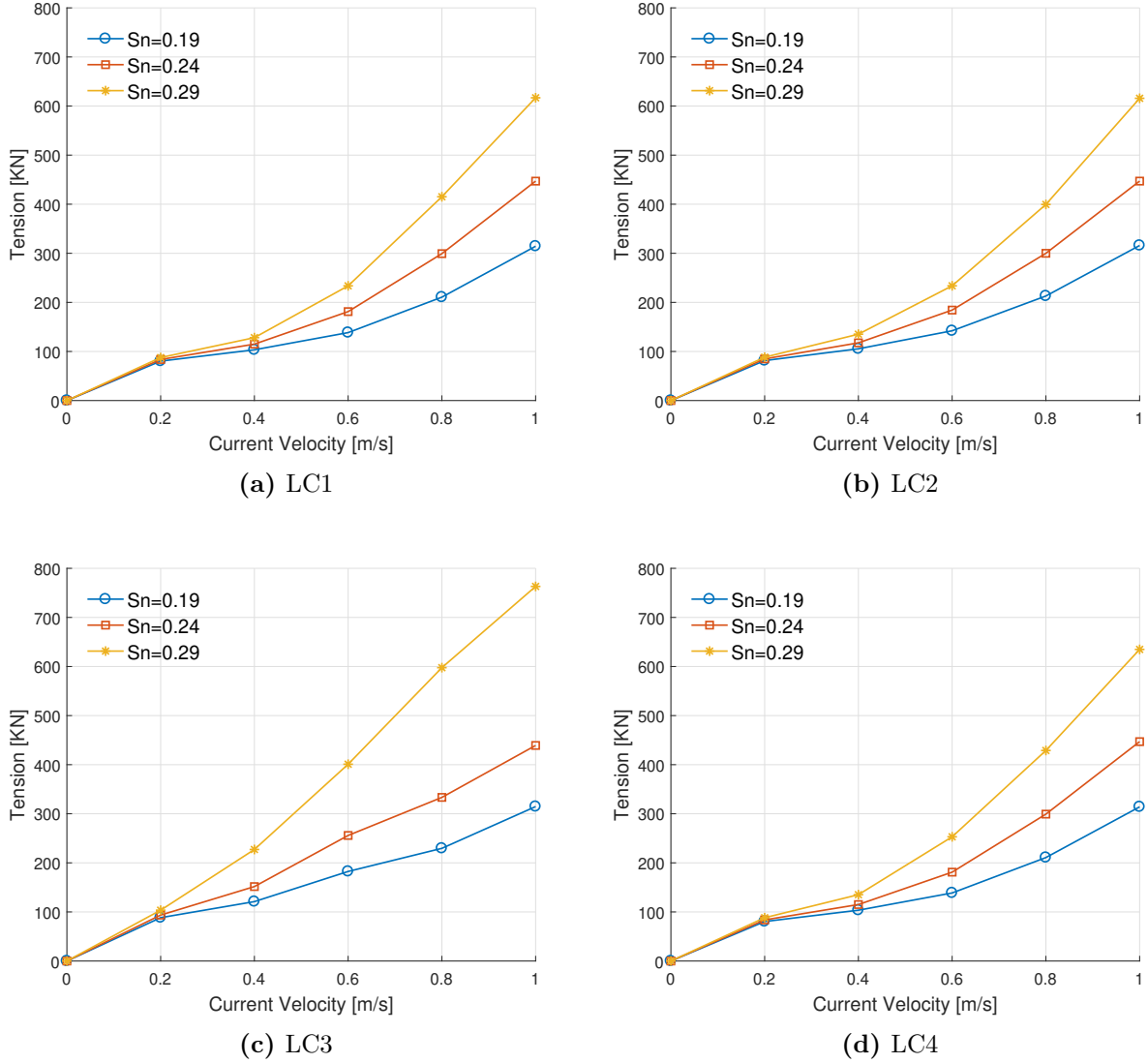


Figure 5.20: Effect of net solidities on the mean tension forces in mooring line 3 of the multiple-cage model under pure currents condition (90° heading)

For combined wave-current condition, the effect of loading conditions on the volume-remaining coefficient of the net structure of cell 1 with different solidities can be seen in figure 5.21.

For a particular loading condition, the net volume decreases with an increase in the solidity ratio. For $Sn=0.29$, the reduction is significantly low and the volume of the net is dropped to 10% of the original volume for the wave with highest steepness ratio. Interestingly, the effects are more pronounced for the 3D wavelength than the 2D wavelength, where D is the diameter of the cage.

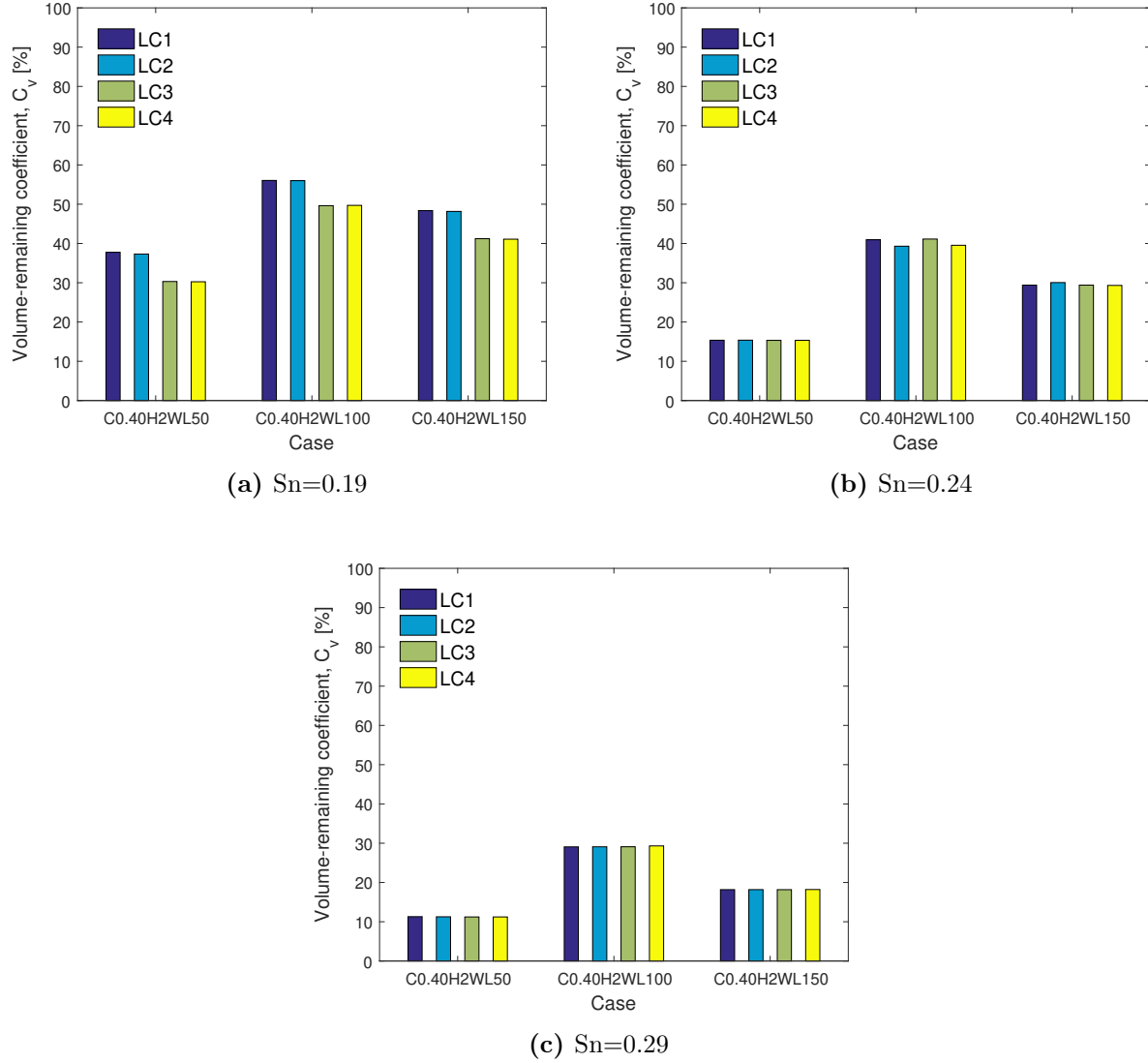


Figure 5.21: Effect of loading conditions on the volume-remaining coefficient of the net structure of cell 1 with different solidities under combined wave-current condition (0° heading)

For 90° combined wave-current heading, figure 5.22 shows the effect of the loading conditions on the volume-remaining coefficient of the net structure of cell 1 with different solidities. The

response is stable over the different loading conditions for all three net solidities as compared to the 0° loading.

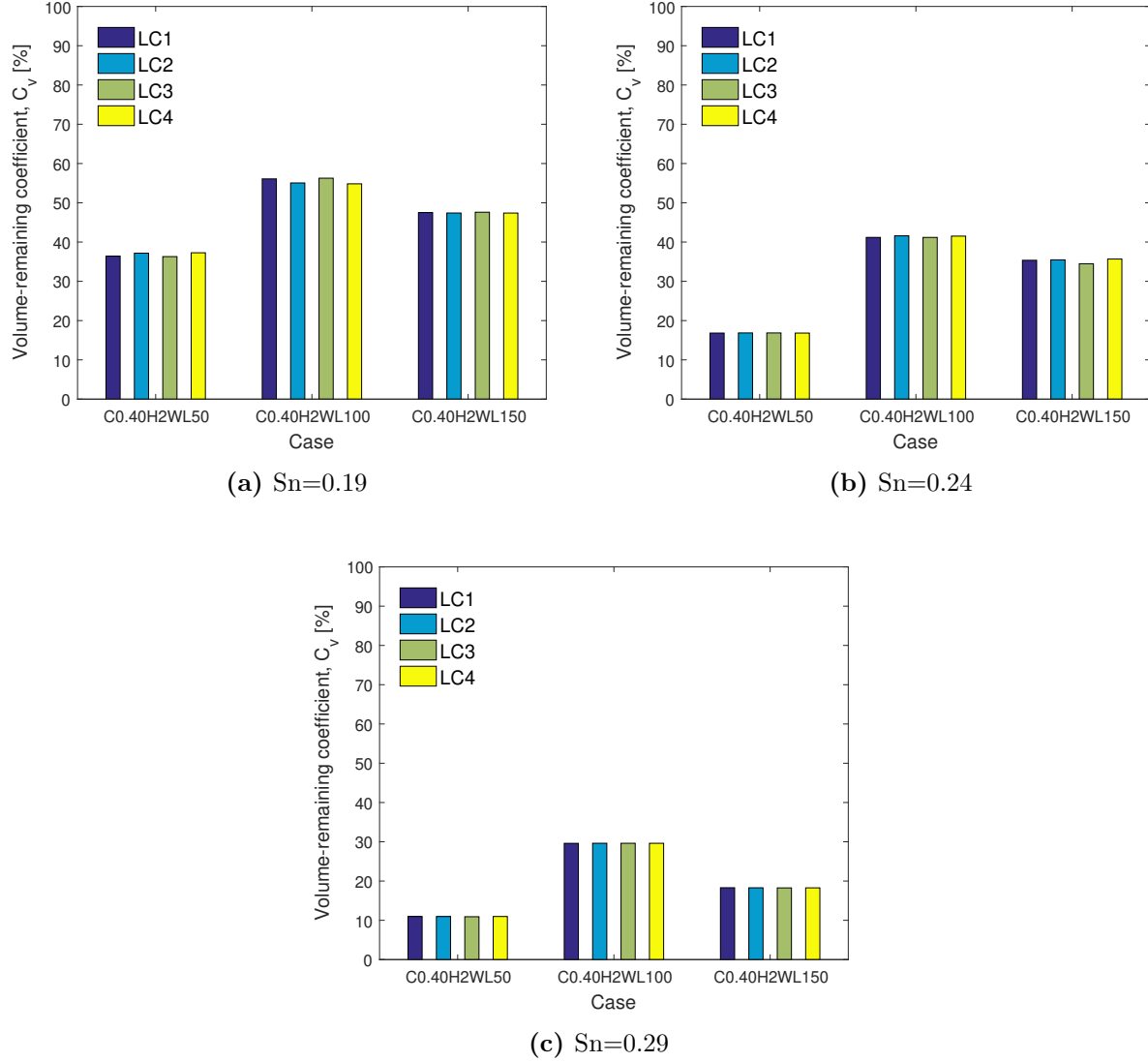


Figure 5.22: Effect of loading conditions on the volume-remaining coefficient of the net structure of cell 1 with different solidities under combined wave-current condition (90° heading)

For a 0° combined wave-current heading, the effect of loading conditions on the mean tension forces in mooring line 1 of the multiple-cage system can be seen in figure 5.23. It is evident that the loads increase with an increase in the solidity ratio for a particular case. As discussed earlier for the net with solidity ratio 0.19 and seen in figure 5.23a, the mooring line 1 experiences maximum loads for LC4 where the frame cable FC10 is broken. The pattern

changes for the other two solidity ratios where the highest mean tension forces in the mooring line are still experienced for LC2 with FC4 broken as seen in figures 5.23b and 5.23c, like the pure currents condition.

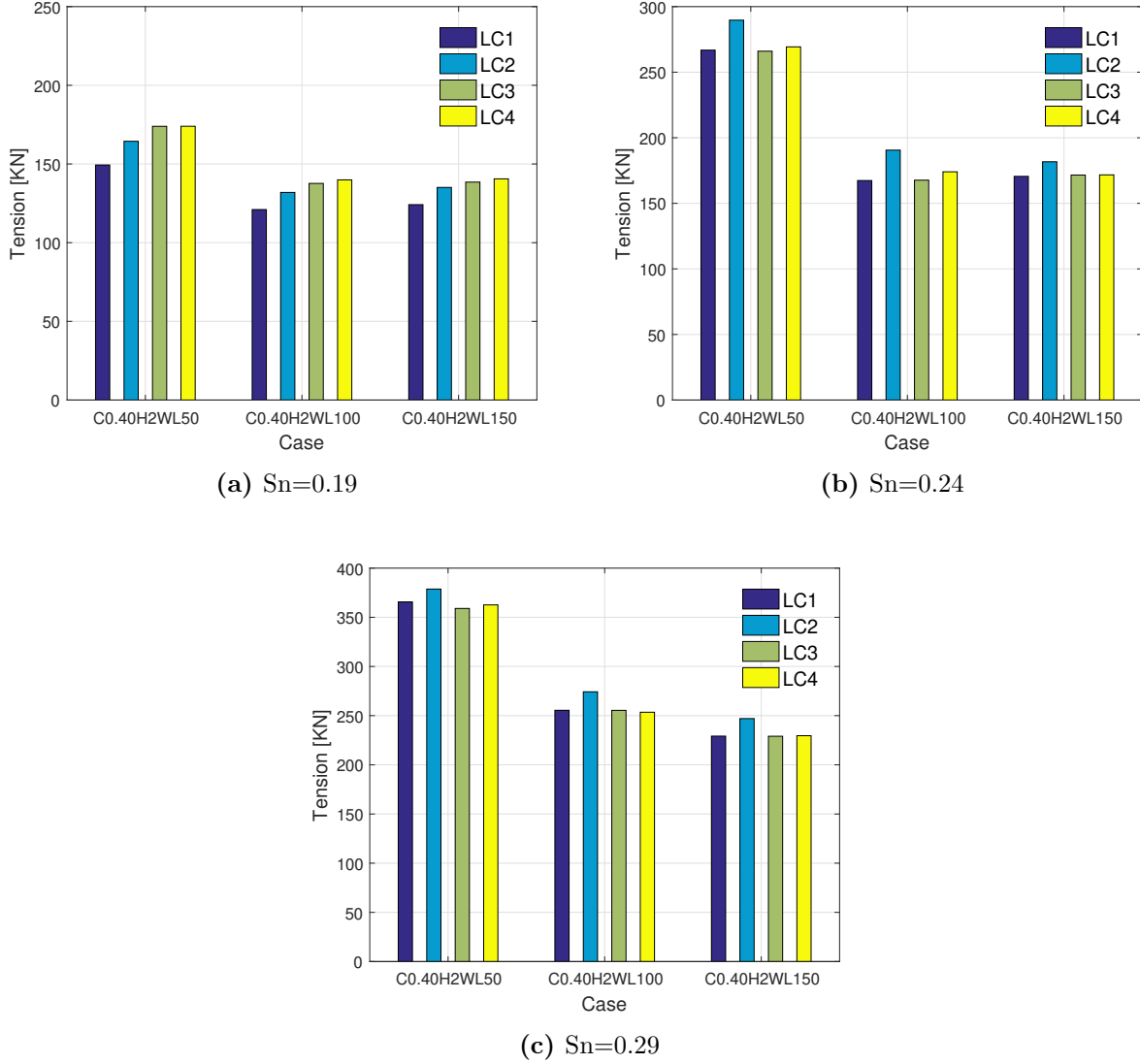
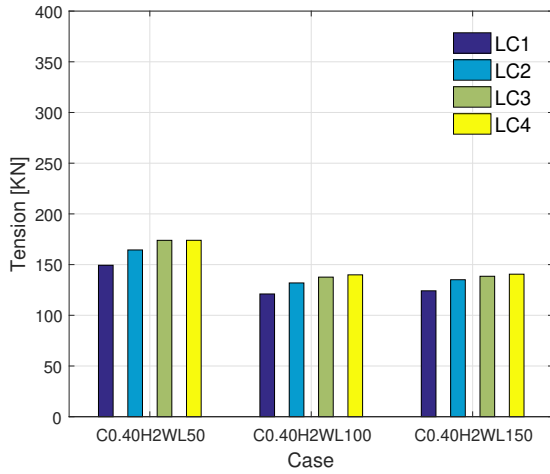


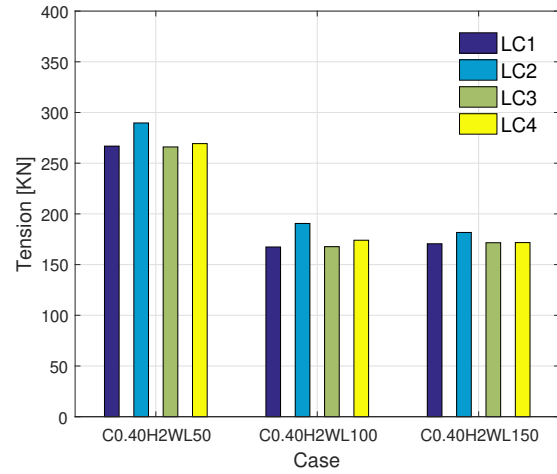
Figure 5.23: Effect of loading conditions on the mean tension forces in mooring line 1 of the multiple-cage system under combined wave-current condition (0° heading)

For 90° combined wave-current heading, figure 5.24 shows the effect of the loading conditions on the mooring 3 of the multiple-cage model. The response is stable over the loading conditions for all three net solidities as compared to the 0° heading. As discussed earlier for the net with solidity ratio 0.19 and as seen in figure 5.24a, the magnitude of the loads

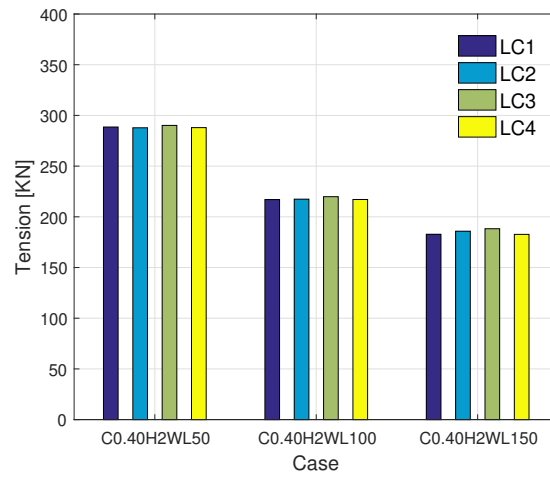
is lower than the 0° heading. For a particular case, it increases with an increase in the net solidity as seen in the figures 5.24b and 5.24c.



(a) $S_n=0.19$



(b) $S_n=0.24$



(c) $S_n=0.29$

Figure 5.24: Effect of loading conditions on the mean tension forces in mooring line 3 of the multiple-cage system under combined wave-current condition (90° heading)

6 Conclusions and future work

6.1 Conclusions

This thesis addresses the planned scope of work to investigate the effect of accidental failures in the mooring system of conventional frame-moored gravity-based fish cages, in detail. The response of the two models, a single-cage system and a multiple-cage system developed in the numerical tool FhSim, is analysed under the different loading conditions and environmental parameters. The presented calculations show the importance of dimensioning mooring frames and bridles for accidental limit states.

For both the models, 2 axial mooring lines in the direction of the water flow experience highest tension forces for the 0° current heading. Amongst the bridles attached to the floating collar, the cables in the forward half of the net structure in the direction of the water flow experience the highest tension forces. Naturally, the other mooring lines and bridles in the aft half of the net structure are slack. For pure currents, the volume-remaining coefficient C_v decreases with an increase in the current velocity. Addition of regular waves to the system when it is in a steady state under pure currents leads to a further decrease in the volume. The reduction is significant for the wave with the highest steepness and a wavelength of 50 metres, equivalent to the diameter of the fish cage used in the models. The effect of the corresponding increase in the drag forces are reflected in the mooring lines of these models. At the water surface, the wave particle velocity is highest for a wave with the above parameters. It is also significantly higher than the velocity of the currents flowing subsurface. Therefore, the influence of waves is more pronounced in the mooring forces than in the volume-reducing coefficient.

For a single-cage model, the net volume is reduced to 39% at a current velocity of 0.50 m/s. On the addition of the wave with a 2 metres wave height and 50 metres wavelength, the cultivation volume is dropped by another 15%. This high reduction in the net volume is critical for the fish welfare. For both pure currents and combined wave-current condition, the accidental failures in the critical cables do not significantly affect the mean volume-remaining coefficient of the net and the tension forces in the critically loaded mooring line. The additional loads are transferred to the other cables in the mooring frame instead. Therefore, the design of these bridles to withstand additional loads post accidental failures is crucial.

For the multiple-cage system, the net volume is reduced to 60% and 63% at a current velocity

of 0.40 m/s for a 0° and 90° current headings respectively. Therefore, the response of this model is slightly more pronounced when the currents and waves are flowing perpendicular to the +X axis of the model. For pure currents with 0° heading, the accidental failures in the critical cables do not significantly affect the mean volume-remaining coefficient of the net. However, the mooring line under study experiences additional loads on failure of the critical frame cable in the mooring frame of the first cell in the direction of currents. The response is similar for the 90° current heading. With the addition of the wave with steepness equivalent to 0.04, the mean tension forces and the amplitude of fluctuation in the magnitude of these forces in the critically loaded mooring lines increase with an increase in the wavelength. At a particular current velocity, the mean volume-remaining coefficient decreases and the mean tension force in the mooring line under study increases, with an increase in the net solidity.

It was observed that the nodes in the net structures of the three fish cages in the multiple-cage system overlap with each other in the Y-Z elevation views in the geometry plots. This was also evident when the changes in the volume-remaining coefficient of all three net structures in 1x3 configuration was found to be similar. The numerical tools, which do not have shielding effect between the cages, over predict the mooring forces since the incoming water flow is undisturbed for all cages. In other words, 100% of the water velocity is experienced by the cages irrespective of their location. Therefore, the models investigated in this thesis have deviations with their true response in the sea.

6.2 Future work

At present, FhSim has a shielding model based on Blevins wake effect, which takes into account the local shielding in each element within a net structure. As concluded earlier, the mooring forces are over predicted for multiple-cage system in FhSim. Therefore, it is imperative for the numerical tools to implement the shielding effect globally to avoid over prediction of drag for multiple cages in line with the water flow. This drawback in the wake effects implemented in the model is an opportunity for future improvements.

This thesis focuses on the accidental failures in the mooring frame on the volume-remaining coefficient of the net and tension forces in the mooring lines. In future, it would be interesting to study the motion responses of the conventional gravity-based fish cages under accidental failures in mooring system. The cage components such as buoys and floating collars will have a particular response to a failure in one of the cables of mooring frame. The natural periods of the system may change affecting the responses of the system. The change in the

motion response can be identified and used for fault detection in the system. This could be advantageous for the fish farm owners as the affected cables can be identified and repaired in time.

Numerical analysis is a powerful tool to understand the distribution of forces in complex flexible structures such as fish farms. Convergence and sensitivity studies are important when using numerical tools, especially for design and dimensioning of the mooring frame of a fish farm. The models may exhibit inherent oscillations. Therefore, it is imperative to select the appropriate time step for the integration methods during calculations. Smaller time steps increase the computational time, and is therefore, time-consuming.

For validation of the results, a comparison study is quite beneficial. It is thus, suggested that similar models can be developed in another numerical tool in future. The investigated responses can then be used to compare the tension forces calculated in the mooring lines for this thesis. This could give a percentage over prediction in the drag and mooring forces.

References

- [1] I. H. Grue, “Loads on the gravity-net-cage from waves and currents,” Master’s thesis, Norwegian University of Science and Technology, 2014.
- [2] P. C. Endresen, “Vertical wave loads and response of a floating fish farm with circular collar,” Master’s thesis, Norwegian University of Science and Technology, 2011.
- [3] “Energy transition outlook 2018,” DNV GL, 2018, Annual Report.
- [4] “Nutrition growth: the Norwegian way,” Norwegian Seafood Council, 2017, Annual Report.
- [5] “The state of world fisheries and aquaculture,” Food and Agriculture Organization of the United Nations, 2018, Annual Report.
- [6] E. Moe, “The Norwegian Aquaculture Analysis 2018,” Ernst & Young AS, 2018, Technical Report.
- [7] F. Cardia and A. Lovatelli, “Aquaculture operations in floating HDPE cages,” Food and Agriculture Organization of the United Nations, 2015, Technical Report.
- [8] Directorate of Fisheries, Norway. (2019) Total number of sites in sea water 2006-2018. [Online]. Available: <https://www.fiskeridir.no/English/Aquaculture/Statistics/Total>
- [9] “NS9415: Flytende oppdrettsanlegg Krav til utforming, dimensjonering, utførelse, installasjon og drift,” Norsk Standard, 2003.
- [10] “DNVGL-RU-OU-0503: Offshore fish farming units and installation,” DNV GL, 2017.
- [11] S. Wendelaar Bonga, “The stress response in fish,” *Physiological reviews*, vol. 77, pp. 591–625, 1997.
- [12] “Cage framing equipment,” Badinotti Group, 2018, Technical Report.
- [13] H. Aqua. (2016) Closed-containment technology - The Egg. [Online]. Available: <http://www.haugeaqua.com/Technology>
- [14] N. AS. (2016) Vessel shaped fish farm - Havfarm. [Online]. Available: <https://www.nordlaks.no/havfarm>
- [15] J. Decew, I. Tsukrov, A. Risso, M. R. Swift, and B. Celikkol, “Modeling of dynamic

- behavior of a single-point moored submersible fish cage under currents,” *Aquacultural Engineering*, vol. 43, pp. 38–45, 2010.
- [16] J. V. Aarsness, H. Rudi, and G. Løland, *12. Current forces on cage, net deflection*. Thomas Telford Publishing, 1990, pp. 137–152.
- [17] G. Løland, “Current forces on, and water flow through and around, floating fish farms,” *Aquaculture International*, vol. 1, pp. 72–89, 1993.
- [18] D. Priour, “Calculation of net shapes by the finite element method with triangular elements,” *Communications in Numerical Methods in Engineering*, vol. 15, pp. 755 – 763, 1999.
- [19] I. Tsukrov, O. Eroshkin, D. Fredriksson, M. R. Swift, and B. Celikkol, “Finite element modeling of net panel using a consistent net element,” *Ocean Engineering*, vol. 30, pp. 251–270, 2003.
- [20] T. Kristiansen and O. Faltinsen, “Modelling of current loads on aquaculture net cages,” *Journal of Fluids and Structures*, vol. 34, pp. 218–235, 2012.
- [21] H. Moe-Føre, P. C. Endresen, K. G. Aarsæther, J. Jensen, M. Føre, D. Kristiansen, A. Fredheim, P. Lader, and K. J. Reite, “Structural Analysis of Aquaculture Nets: Comparison and Validation of Different Numerical Modeling Approaches,” *Journal of Offshore Mechanics and Arctic Engineering*, vol. 137, p. 041201, 2015.
- [22] P. Lader and B. Enerhaug, “Experimental investigation of forces and geometry of a net cage in uniform flow,” *IEEE Journal of Oceanic Engineering*, vol. 30, pp. 79 – 84, 2005.
- [23] P. Lader, A. Jensen, J. Sveen, A. Fredheim, B. Enerhaug, and D. Fredriksson, “Experimental investigation of wave forces on net structures,” *Applied Ocean Research*, vol. 29, pp. 112–127, 2007.
- [24] A. Techtet, “Morrison’s equation,” Massachusetts Institute of Technology, Cambridge, MA, USA, 2004, Online Course.
- [25] P. C. Endresen, M. Føre, A. Fredheim, D. Kristiansen, and B. Enerhaug, “Numerical modeling of wake effect on aquaculture nets,” vol. 3, 2013.
- [26] R. Blevins, *Applied Fluid Dynamics Handbook*. Kreiger Publishing Company, 2003.

- [27] P. Lader and A. Fredheim, “Dynamic properties of a flexible net sheet in waves and current—a numerical approach,” *Aquacultural Engineering*, vol. 35, pp. 228–238, 2006.
- [28] B. Sumer and A. Kozakiewicz, “Visualization of flow around cylinder in irregular waves,” *International Journal of Offshore and Polar Engineering*, vol. 5, pp. 270–272, 1995.
- [29] S. Chakrabarti, *Hydrodynamics of offshore structures*. Computational Mechanics Publications, Southampton, 1987.
- [30] D. Kristiansen, F. Martin, K. G. Aarsæther, and A. Fredheim, “Numsim - numerical simulation of complex systems involving interaction between elements with large and varying stiffness properties,” SINTEF Ocean AS, 2015, Technical Report.
- [31] K. J. Reite, M. Føre, K. G. Aarsæther, J. Jensen, P. Rundtop, L. Kyllingstad, P. C. Endresen, D. Kristiansen, V. Johansen, and A. Fredheim, “Fhsim — time domain simulation of marine systems,” *Proceedings of the International Conference on Offshore Mechanics and Arctic Engineering - OMAE*, vol. 8, 2014.
- [32] P. C. Endresen, J. Birkevold, M. Føre, A. Fredheim, D. Kristiansen, and P. Lader, “Simulation and validation of a numerical model of a full aquaculture net-cage system,” *Proceedings of the International Conference on Offshore Mechanics and Arctic Engineering - OMAE*, vol. 7, 2014.
- [33] P. Li and O. Faltinsen, “Wave-induced vertical response of an elastic circular collar of a floating fish farm,” 2012.
- [34] O. M. Faltinsen, “Hydrodynamic aspects of a floating fish farm with circular collar,” in *The 26th International Workshop on Water Waves and Floating Bodies (IWWFB)*, Athens, Greece, 2011.
- [35] T. Kristiansen and O. Faltinsen, “Mooring loads of a circular net cage with elastic floater in waves and current,” in *6th International Conference on Hydroelasticity in Marine Technology*, 2012, pp. 183–191.
- [36] A. Tsarau and D. Kristiansen, “Application of fhsim for the analysis of environmental loads on a complete fish-farm system,” 2019.
- [37] H. Cheng, K. G. Aarsæther, L. Li, and M. C. Ong, “Numerical study of a single-point mooring gravity fish cage with different deformation suppression methods (under

- revision),” *Proceedings of the International Conference on Offshore Mechanics and Arctic Engineering - OMAE*, 2018.
- [38] R. Saetre, Ed., *The Norwegian coastal current*. Tapir academic press, Trondheim, 2007.
- [39] C. C. Huang, H. J. Tang, and J.-Y. Liu, “Effects of waves and currents on gravity-type cages in the open sea,” *Aquacultural Engineering*, vol. 38, 2008.
- [40] K. Bruserud and S. Haver, “Current conditions in the northern north sea,” *Ocean Engineering*, 2018.